NASA Technical Paper 1785

Tests of Graphite/Polyimide Sandwich Panels in Uniaxial Edgewise Compression

Charles J. Camarda

DECEMBER 1980

NASA

NASA Technical Paper 1785

Tests of Graphite/Polyimide Sandwich Panels in Uniaxial Edgewise Compression

Charles J. Camarda
Langley Research Center
Hampton, Virginia

NASA
National Aeronautics
and Space Administration

Scientific and Technical
Information Branch

1980

SUMMARY

An experimental and analytical investigation has been made of the local and general buckling behavior of graphite/polyimide (Gr/PI) sandwich panels simply supported along all four edges and loaded in uniaxial edgewise compression. Material properties of sandwich panel constituents (adhesive and facings) were determined from flatwise-tension and sandwich-beam-flexure tests. Results from the flatwise-tension tests established a suitable cure cycle for FM-34[1] polyimide film adhesive which was the adhesive used to fabricate the flatwise-tension, sandwich-beam, and buckling specimens. A cell-edge bonding technique using a liquid version of FM-34 polyimide adhesive was investigated and results indicated that a considerable mass savings may be possible using a cell-edge adhesive. Tensile and compressive material properties of the facings (quasi-isotropic, symmetric, laminates ($([0,+45,90,-45]_S$) of Celion[2]/PMR-15) were determined at 116 K, room temperature, and 589 K (-250°F, room temperature, and 600°F) using the sandwich-beam-flexure test method. Buckling specimens were 30.5 by 33 cm (12 by 13 in.), had quasi-isotropic, symmetric facings ($[0,\pm45,90]_S$), and a glass/polyimide honeycomb core (HRH-327[3]-3/8-4). Core thicknesses were varied (0.635, 1.27, 1.91, and 2.54 cm (0.25, 0.50, 0.75, and 1.00 in.)) and three panels of each thickness were tested at room temperature to investigate failure modes and corresponding buckling loads. Specimens 0.635 cm (0.25 in.) thick failed by overall buckling at loads close to the analytically predicted buckling load; all other panels failed by face wrinkling. Results of wrinkling tests indicated that several buckling formulas were unconservative and therefore not suitable for design purposes; a recommended wrinkling equation is presented.

INTRODUCTION

Preliminary structural studies of advanced space transportation systems using advanced composite structural materials of high-strength fibers and polyimide resin matrices indicate that a reduction of up to 25 percent in vehicle structural mass is obtained by the direct replacement of aluminum panels with graphite/polyimide (Gr/PI) panels (refs. 1 and 2). Furthermore, preliminary studies of the aft body flap of the Space Shuttle Orbiter (ref. 3) indicate that compression loads are the primary design condition for this structural component and because a biaxial state of stress exists in the cover panels a sandwich panel was chosen. The present study focuses on Gr/PI structural sandwich panels which may have application as cover skins on lightly loaded components such as the aft body flap of the Space Shuttle Orbiter. Based on the low magni-

---

[1]FM-34 film adhesive: manufactured by American Cyanamid Company, Bloomingdale Division.

[2]Celion: registered trademark of Celanese Corporation.

[3]HRH 327: registered trademark of Hexcel Products, Inc.

tude and biaxial nature of these loads, a minimum-gage, quasi-isotropic, symmetric Gr/PI laminate ($[0,\pm45,90]_s$) was chosen for the facings of these sandwich panels in the present study.

The purposes of the present study are to analytically and experimentally investigate the local and general buckling behavior of minimum-gage Gr/PI sandwich panels capable of use at temperatures ranging from 116 to 589 K (-250° to 600°F), to verify the fabrication method used in manufacture of the panels, and to determine the material properties of the $[0,\pm45,90]_s$ Gr/PI sandwich panel facings.

Buckling specimens 30.5 by 33.0 cm (12 by 13 in.) were designed and fabricated with various core thicknesses to study local and general instability failure modes. The buckling specimens were tested in uniaxial edgewise compression at room temperature (R.T.) and were simply supported along all four edges. Several analysis methods (refs. 4 to 8) were used to determine upper and lower bounds on critical stresses relating to intracellular buckling (dimpling), wrinkling, shear crimping, and general panel instability and are evaluated in this study for their capability in predicting buckling loads and modes of Gr/PI sandwich panels.

The panels were fabricated using a commercially available high-temperature film adhesive, FM-34, to bond the core to the facings. Flatwise-tensile tests were performed using the sandwich panel facing laminate orientation, core, and adhesive to determine a suitable fabrication cure cycle and the tensile adhesive bond strength in a core-to-facing bond situation. In addition, flatwise-tensile tests were used to evaluate BR-34, a liquid version of the FM-34 film adhesive, as a cell-edge adhesive.

Sandwich-beam-flexure tests were performed to determine modulus, strength, and Poisson's ratio of the facings. The flatwise-tensile tests and sandwich-beam-flexure tests were conducted at temperatures of 116 K, R.T., and 589 K (-250°F, R.T., and 600°F). Quality control standards for fabrication of all specimens were high to minimize scatter in the data. Results of the tests are presented in tabular and graphical form. Results of the beam tests were analyzed statistically and a best-fit third-order polynomial relating stress and strain was fit through the data.

Certain commercial materials are identified in this paper in order to specify adequately which materials were investigated in the research effort. In no case does such identification imply recommendation or endorsement of the product by NASA, nor does it imply that the materials are necessarily the only ones or the best ones available for the purpose. In many cases equivalent materials are available and would probably produce equivalent results.

SYMBOLS

Values are given in both SI and U.S. Customary Units. The measurements and calculations were made in U.S. Customary Units.

$[A],[B],[D]$	stiffness matrices of sandwich panel
b	width of plate
C_0,C_1,C_2,C_3	coefficients of polynomials used in regression analysis
$D_{F11},D_{F22},D_{F12},D_{F66}$	flexural stiffness of composite facings
D_{Q_x},D_{Q_y}	transverse shear stiffness of sandwich plate in x- and y-directions, respectively
D_x,D_y	flexural stiffness of orthotropic sandwich plate in x- and y-directions, respectively
D_{xy}	twisting stiffness of orthotropic sandwich plate
E	elastic modulus
E_{c_z}	modulus of core in z-direction
E_f	facing modulus
E_{f_x},E_{f_y}	facing modulus in x- and y-directions, respectively
E_T	tangent modulus
$\bar{E}_x,\bar{E}_y$	average elastic moduli of laminate in x- and y-directions, respectively
F_c	lower of flatwise core compressive or tensile strengths, or core-to-facing bond strength
F_{cu}	compressive ultimate strength
G	shear modulus
$G_{c_{xz}}$	core shear modulus in xz-plane
$G_{c_{yz}}$	core shear modulus in yz-plane
$G_{f_{xy}}$	facing shear modulus in xy-plane
j	total number of points in regression analysis
l	length of plate
m,n	number of half sine waves in x- and y-directions, respectively
N_x,N_y	resultant normal forces in x- and y-directions, respectively

P	load
$S_{\sigma/\varepsilon}$	standard error of estimate
s	honeycomb cell size
T_g	glass transition temperature
t	thickness
t_c	core thickness
t_f	average facing thickness
t_{f_1}	thickness of facing 1
t_{f_2}	thickness of facing 2
t_h	total sandwich panel thickness
V_f	fiber volume fraction
V_v	void volume fraction
x,y,z	rectangular coordinates
δ	initial panel waviness
ε	strain
μ	Poisson's ratio
μ_x,μ_y	Poisson's ratio of orthotropic plate associated with bending of plate in x- and y-directions, respectively
$\bar{\mu}_{xy},\bar{\mu}_{yx}$	average Poisson's ratios of orthotropic plate associated with extension of plate in x- and y-directions, respectively
ρ	density
σ	stress
σ_{crim}	critical stress associated with shear crimping
σ_{dim}	critical stress associated with dimpling
σ_{wr}	critical stress associated with wrinkling

Subscripts:

av	average

cr	critical
i	index of summation
max	maximum
ult	ultimate
x,y	coordinate directions
1,2	directions parallel and perpendicular to fiber direction, respectively

TEST SPECIMENS, APPARATUS, AND PROCEDURE

Graphite/Polyimide Materials

This program was conducted as part of the NASA program, Composites for Advanced Space Transportation (CASTS) (ref. 1). The CASTS effort focused on graphite/polyimide, and a significant part of the program included evaluating and characterizing various fiber and resin materials. As a result of these evaluations, the materials used in different phases of the present study varied as improved systems were identified. Specifically, for flatwise-tensile tests, the laminates were HTS[4]-1/PMR-15; for sandwich-beam-flexure tests, the laminates were Celion 6000/PMR-15; for buckling tests, the laminates were Celion 3000/PMR-15. The primary purpose of the flatwise-tensile tests was to evaluate adhesive tensile strengths and therefore the difference in facing materials was not critical. The thinnest gage prepreg, Celion 3000/PMR-15, was chosen over the Celion 6000/PMR-15 to minimize mass of the sandwich panels, and the Celion fiber was chosen over the HTS fiber because Celion exhibits less material property degradation than HTS at elevated temperatures.

Flatwise-Tensile Specimens

Forty-six 7.62 by 7.62-cm (3 by 3-in.) specimens were fabricated using precured $[0,\pm45,90]_s$ laminates of HTS-1/PMR-15 Gr/PI facings, glass/polyimide honeycomb core (HRH-327-3/16-6 or 8) and the desired adhesive. A schematic diagram of a typical specimen is shown in figure 1. Details of fabrication procedures and cure cycles are given in reference 9 and table I, respectively. Steel load blocks were bonded to the facings of the specimens and each block had a tapped hole for attaching a loading rod. Universal joints were attached between the testing machine and the loading rods to assure proper alignment of the fixture in the loading machine. The specimens were tested in a universal testing machine operating in a displacement control mode at a constant rate of 0.13 cm/min (0.05 in/min). Test temperatures other than room temperature were obtained using an environmental chamber positioned within the crossheads and posts of the testing machine. Specimens were held at desired test temperatures for 15 minutes prior to testing to insure thermal equilibrium. Maximum load was recorded for each test and converted to a normal tensile stress.

[4]HTS graphite fiber: product of Hercules Incorporated.

Sandwich-Beam-Flexure Tests

Specimens.- Sandwich-beam-flexure specimens consisted of Gr/PI facings and glass/polyimide honeycomb core as shown in figure 2. The honeycomb core was HRH 327-3/16-8 glass/polyimide and was cut into strips 2.54 cm (1.00 in.) wide by 55.88 cm (22.0 in.) long by 3.175 cm (1.25 in.) high. The test facing of the beam was a $[0,+45,90,-45]_S$ laminate of Celion 6000/PMR-15 and the opposite facing had a laminate orientation of $[0_2,+45,90,-45]_S$. The additional 0° layers of the non-test facing insured failure of the test facing. These laminate orientations were chosen to avoid microcracks in the laminate which are believed to occur when adjacent layers are stacked at an angle greater than or equal to 90° with respect to one another. The honeycomb core was filled with BR-34 liquid adhesive and glass beads throughout the length of the beams, except for the 7.62-cm (3.00-in.) test section in the center of the beams, to prevent premature adhesive failure. Details of the fabrication of the sandwich beam specimens are presented in reference 9.

Apparatus and instrumentation.- Each specimen was instrumented at the midspan of the beam with a high-temperature strain rosette (WK-03-060-WR-350) oriented at 0°, 45°, and 90° with the load axis and bonded to the test facing, and a single strain gage (WK-03-125-AD-350) oriented at 0° with the load axis and bonded to the non-test facing. These gages were manufactured by Micro-Measurements Division of Vishay Intertechnology, Inc. The strain gages were bonded to the outer surfaces of the beam using a polyimide adhesive (either M-Bond 610 or PLD-700 available from Micro-Measurements and BLH Electronics, respectively).

The sandwich beams were placed in a four-point bending test apparatus (fig. 3) which supported the beam on rollers 48.26 cm (19.00 in.) apart with flat sections 2.54 cm (1.00 in.) wide machined in them. Load was applied by a 222-kN (50-kip) capacity hydraulic testing machine which acted at two points on the top flange of the beam spaced 10.16 cm (4.00 in.) apart and symmetric about the beam's center. For testing at temperatures other than room temperature the specimen was instrumented with a thermocouple attached to the test facing and the test fixture and specimen were completely enclosed in an environmental chamber and either heated or cooled to the desired test temperature. Specimens were allowed to soak at the test temperature for 20 minutes to insure thermal equilibrium. A data handling system consisting of 40-channel scanner, digital voltmeter, plotter, printer, clock, and calculator was used to record and reduce data.

Procedure.- The load signals from the load cell on the hydraulic testing machine were input to one channel of the scanner. Strain signals were input to selected scanner channels and initally set to zero using Wheatstone bridge balance (for non-room-temperature tests, initial strain signals were set to zero after thermal equilibrium). Strains were corrected for transverse sensitivity of the gages and nonlinearity of the bridge circuit. Thermocouples were connected to the scanner through a 273 K (32°F) cold-junction reference.

Beams were tested to failure during the test, load was applied at a rate of 80 N/sec (20 lbf/sec), data were recorded every 3 seconds, and a stress-strain

curve was plotted in real time. Quantities were stored in volts and engineering units on magnetic tape and printed during each test. A data reduction program used the longitudinal stresses and strains of replicate tests as input to a regression analysis to determine the coefficients of a best fit, in the least-squares sense, of a third-order polynomial relating stress and strain according to the polynomial equation:

$$\sigma = C_0 + C_1\varepsilon + C_2\varepsilon^2 + C_3\varepsilon^3 \tag{1}$$

A more detailed explanation of the analysis is given in reference 10.

To assess the magnitude of scatter of experimental points about the regression equation, the standard error of estimate $S_{\sigma/\varepsilon}$, which is a measure of the mean deviation of the sample points from the regression line, is determined as follows:

$$S_{\sigma/\varepsilon} = \left(\frac{\sum_{i=1}^{j} \sigma_i^2 - C_0 \sum_{i=1}^{j} \sigma_i - C_1 \sum_{i=1}^{j} \varepsilon_i\sigma_i - C_2 \sum_{i=1}^{j} \varepsilon_i^2\sigma_i - C_3 \sum_{i=1}^{j} \varepsilon_i^3\sigma_i}{j - 4} \right)^{1/2} \tag{2}$$

This method of statistical analysis is similar to that presented in reference 10.

Buckling Tests

Specimens.- Design considerations of the buckling specimens are given in appendix A. Specimens were 30.5 by 33.0 cm (12 by 13 in.) with core thicknesses of 0.635, 1.27, 1.91, and 2.54 cm (0.25, 0.50, 0.75, and 1.00 in.). Facings of all sandwich panels were similar and were symmetric quasi-isotropic 8-ply laminates of Celion/PMR-15 $[0,\pm45,90]_S$. Figure 4 shows a completed buckling specimen; details on specimen manufacture are given in reference 9; details of significant panel parameters are listed in table II. Quality-control standards (refs. 1, 2, and 9) for fabrication of the panels were very high to minimize scatter in experimental data.

Apparatus and instrumentation.- Simply supporting the edges of the test panels was considered to be a realistic representation of the boundary conditions that actual panels on the shuttle body flap will experience. A test fixture, similar to that of reference 4, was fabricated to simply support all four edges of the sandwich panel and allow adjustments to be made during loading which would align the specimen and thus maintain a uniform strain distribution across the panel. Details of the simple supports are shown in

figures 5(a) and (b). The stainless-steel alignment sheet embedded in each of the potted ends of the panel fit into stainless-steel knife edges which fit into steel V-groove load blocks as shown in figure 5(a). The load blocks fit into adjustable end loading heads which were attached to the hydraulic load machine. The end loading heads contained a flat stainless-steel bar which, together with the aligning screws, was used to obtain a uniform longitudinal strain across the specimen. Figure 6 shows the buckling specimen in the test fixture. The sides of the panel were simply supported by knife edges which were supported by Z-section steel beams as shown in figure 5(b). The side supports maintained a relatively snug fit against the panel because of the high degree of flatness of the panels. However, because of the raised scalloped doublers the side supports could not extend the complete length of the panel. The Z-section beams were braced so that motion of the side supports was restrained. The knife edges of the side supports were bolted snugly in place at two locations on two sides as shown in the schematic of figure 5(b) and as partially shown in figure 6. The side supports were positioned 1.27 cm (0.5 in.) from each side edge, making the test section width 30.5 cm (12 in.).

A 222-kN (50-kip) hydraulic load machine was used to compress the panels. A mercury-vapor light source was used in conjunction with a photographic line grid having a pitch of 19.7 lines/cm (50 lines/in.) to determine out-of-plane displacements and mode shapes using the grid-shadow Moiré technique as discussed in references 11 and 12. A camera was positioned perpendicular to the sandwich panel and the light source formed an angle of 30° with that perpendicular.

Each panel was instrumented with 12 single, foil-type strain gages and 2 45° strain rosettes, Micro-Measurements WK-03-125-AD-350 and WK-03-060-WR-350, respectively, as shown schematically in figure 7. The positioning of the gages allowed measurement of longitudinal strain distributions on each facing across the panel length and width. Back-to-back longitudinal strain gages were positioned at five points on the panel (four corner points and a centrally located one). The purpose of the back-to-back gages was to detect bending of the panel and to determine the general buckling load and possibly the wrinkling load. The data acquisition system used to reduce and store data is identical to that mentioned earlier for the sandwich beams.

Procedure.- During each test, the hydraulic testing machine was operated in a displacement control mode at a rate of approximately 0.020 cm/sec (0.008 in/sec), strain gages were scanned approximately every 3 seconds, and the specimen was loaded to failure. Raw data were converted to engineering units, printed in real time, and stored on a disk. Stresses were calculated by dividing the load by the combined cross-sectional area of the two facings. Gages were balanced prior to testing using Wheatstone bridge circuits as discussed earlier. Prior to tesing, panels were loaded up to approximately 50 percent of failure load and were aligned using the adjustable screws shown in figure 6. The panel was then unloaded and the Moire' grid positioned in front of the specimen. Strain gages were then zeroed and load was applied to the specimen until failure.

TEST RESULTS

Flatwise Tensile Tests

Preliminary tests indicated that significant improvements of bond strengths could be obtained by abrasively cleaning the edges of the honeycomb and by dipping the core in primer instead of brush or roller coating it on the core. (See ref. 9.)

A series of flatwise tensile tests of specimens, bonded with FM-34 using various cure cycles, aided in the selection of a suitable cure cycle. Two specimens were tested at room temperature for each cure-cycle variation listed in table I. Specimen failures occurred by either adhesive bondline rupture or facing delamination; figures 8 and 9 show the two modes of failure. Results of those tests, listed in table III, indicate that cure cycles 1 and 5 produced the strongest bonds, with failures occurring in the facing. Delamination of the facings also occurred with cure cycle 4 but because the bond cure temperature of 616 K (650°F) was greater than the facing cure temperature of 603 K (625°F) the interlaminar shear strength of the facing was degraded and failure loads were lower. Bonding one face of the specimen at a time, with the face to be bonded positioned under the core (cure cycle 3), provided good filleting between the face and core but did not enhance the strength of the bond. Instead, bond strengths were lower and failures occurred in the second of the two bonds. Six specimens were tested at 589 K (600°F); two specimens were fabricated at each of three cure cycles 1, 5, and cure cycle 1 with a higher cure temperature (603 K (625°F)). It was hoped that the higher cure temperature would improve the elevated temperature bond strength.

Cure cycle 1 with the elevated cure temperature was chosen because of the higher bond strengths at elevated temperature and because maintaining a vacuum during cure would help eliminate volatiles produced during the cure of the FM-34 adhesive. Although trapped volatiles did not degrade the strengths of the 7.62 by 7.62 cm (3 by 3 in.) specimens, it would be more difficult to vent the volatiles in larger panels.

Sixteen flatwise-tension specimens were fabricated using cure cycle 1 with a cure temperature of 603 K (625°F). Test results from these specimens are presented in table IV. Flatwise-tensile strengths at room temperature and 116 K (-250°F) increased from 1.6 MPa (230 psi) to an average value of 3.2 (470 psi) when the edges of the honeycomb were cleaned and primed as mentioned earlier. Failures at this stress level were usually by facing delamination as shown in figure 9. Flatwise-tensile strengths at 589 K (600°F) were generally higher than 1.4 MPa (200 psi) with failures occurring in the bondline, similar to the room-temperature test shown in figure 8.

Flatwise-tensile test results at room temperature of specimens bonded using BR-34 as a cell-edge adhesive are presented in table IV(b). Most of these specimens failed by facing delamination. However, for these specimens the facings

delaminated locally about each cell edge as shown in figure 10 and usually resulted in slightly lower strengths. When local facing delamination did not occur, strengths were similar to results of the FM-34 film adhesive. Flatwise tensile strengths using BR-34 were much higher than results presented in reference 13. The mass of the BR-34 adhesive was 0.244 kg/m^2 (0.05 lbm/ft^2) which is a 59-percent reduction in mass compared with FM-34 film adhesive having a mass of 0.586 kg/m^2 (0.12 lbm/ft^2). The use of BR-34 would result in a mass savings equivalent to 10 percent of the total sandwich panel mass for a panel consisting of 8-ply Gr/PI facings and a 1.27-cm (0.50-in.) thick core having a density of 64 kg/m^3 (4 lbm/ft^3).

Results of the bond study indicate that a liquid cell-edge adhesive can result in considerable mass savings without necessarily sacrificing bond strength and that further research in this area is warranted. However, since flatwise-tensile strengths with BR-34 were not consistent, FM-34 film adhesive was used to fabricate the sandwich beam and buckling specimens.

Sandwich-Beam-Flexure Tests

Results of the sandwich beam flexure tests are presented in tables V and VI and in figures 11 to 16. As shown in table V, the scatter of test data, as determined by the standard error of estimate, was lowest for the room temperature and 116 K (-250°F) tensile tests. Maximum scatter occurred for the elevated and room temperature compression tests in which the standard errors of estimates $S_{\sigma/\varepsilon}$ were 10.67 MPa (1547 psi) and 11.10 MPa (1610 psi) as compared to respective average ultimate strengths of 567.7 MPa (82.34 ksi) and 334.0 MPa (48.44 ksi) (see table VI). The average compression ultimate strain was 1.38 percent at room temperature and 0.657 percent at 589 K (600°F). Average ultimate strengths of the laminate were slightly higher in compression than tension for each test temperature. Ultimate strengths of the Celion 6000/PMR-15 $[0,+45,90,-45]_S$ laminates were higher than results for HTS/PMR-15 as reported in references 10 and 14 except for tensile strength at 589 K (600°F) reported in reference 14. Average room temperature tensile and compressive ultimate strengths for the HTS/PMR-15 laminates were 450.6 and 532.4 MPa (65.36 and 77.23 ksi), respectively, as compared with 565.2 and 567.7 MPa (81.98 and 82.34 ksi) for Celion 6000/PMR-15. Average tensile ultimate strengths at 116 K (-250°F) increased by 8.5 percent over room temperature values while strengths at 589 K (600°F) decreased by 43 percent. Average compressive ultimate strengths at 116 K (-250°F) and 589 K (600°F) increased and decreased, respectively, by 13.8 and 41.2 percent from room-temperature values.

Modulus values of the Celion 6000/PMR-15 laminates were higher for all test temperatures than values reported in references 10 and 14 for HTS/PMR-15 laminates. This difference is probably due to the higher fiber volume fraction, 72 percent for the Celion/PI laminates of the present study compared with 43 to 55 percent for the HTS/PMR-15 laminates of references 10 and 14. Modulus values at 0.2 percent strain and 116 K (-250°F) were about 10 percent higher than values at room temperature. Modulus values at 589 K (600°F) were about the same as room-temperature values. Stress and tangent modulus as a function of strain for various temperatures are presented in figures 11 to 16. Table V

lists the coefficients of the regression equation, used in the reduction of the experimental data. The data points in the figures represent experimental values all replicate tests; the solid line in the figures is the best-fit third-order polynomial obtained from the regression analysis. Tangent modulus as a function of strain was calculated by differentiation of the third-order polynomial (eq. (1)). Tensile modulus values were fairly linear throughout the usable strain region ($\varepsilon \leqq 0.35$ percent) as shown by figures 11, 13, and 15. Compressive modulus values tended to be nonlinear at room temperature and became linear at 589 K (600°F) as shown by figures 14 and 16.

Representative tensile and compressive failures are shown in figures 17 and 18, respectively. Most compressive failures occurred near the edge of the potted section of the honeycomb next to the load tabs.

Buckling Tests

Two modes of panel failure were discernable from experimental results: wrinkling and overall buckling. Specimens with a core thickness t_c of approximately 0.635 cm (0.25 in.) failed by overall buckling, and all other specimens, having nominal core thicknesses of 1.27, 1.91, and 2.54 cm (0.5, 0.75, and 1.00 in.), failed by wrinkling. None of the panels tested failed by laminate yield, dimpling, or shear crimping. The shadow Moiré method was useful in determining mode shapes of the overall buckling specimens but was not able to determine wrinkling mode shapes because of the high stiffness and brittle nature of the Gr/PI facings and, hence, the relatively small out-of-plane displacements. The use of a finer Moiré line grid would increase the sensitivity of the optical technique and possibly enable the determination of local buckling modes.

Wrinkling specimens.- Results of longitudinal strain uniformity across specimen width are presented in figures 19(a) and (b) for two values of applied load and two different panels. The adjustable test fixture was useful in eliminating large strain variations caused by misalignment, similar to test fixtures used in reference 4. Strains were fairly uniform across the width of the panel as shown in figures 19(a) and (b). However, slightly higher strains and strain variations do occur at the edges of the panels as was noted in reference 4. Trends in strain distributions at the low load level, 44.48 kN (10 000 lbf), were similar to trends at the higher load level of 88.96 kN (20 000 lbf). There were no consistent trends in strain distributions from panel to panel. However, most of the wrinkling specimens did fail near the end of the side simple supports where slightly higher strains were recorded.

Longitudinal strains as a function of stress were calculated for each strain-gage position on the panel. Results of several tests (panel numbers BT-5 and BT-6) are presented in figures 20(a) and (b). Back-to-back strain variation was usually lowest in the center of the panels ($x = y = 0$). Irregularities in slopes were noted in some specimens as shown in figure 20(b) for panel number BT-6. These irregularities in slope occur at too low a load to be an indication of wrinkling or some form of local instability as mentioned in reference 4. The irregularities in the present study were possibly caused by some interference or interaction of the test fixture. Material behavior was slightly nonlinear to failure, similar to results of the four-point flexure tests as noted earlier.

Back-to-back stress-strain data did not predict the onset of local buckling (wrinkling) and the use of the force stiffness method of reference 15 to predict wrinkling was unsuccessful. All panel failures were abrupt with no indication of local instability. It would probably be necessary to extensively instrument both sides of a facing to calculate facing bending strains and predict local buckling. Modulus values at 0.2 percent strain, maximum back-to-back strain variation at 0.6 percent strain, theoretical wrinkling stress, and experimental ultimate stress and strain values of each panel are presented in table VII. Maximum back-to-back strain variation was fairly low, considering the size and complexity of the sandwich panels. Compressive modulus values at 0.2 percent strain of the sandwich panels which used Celion 3000 material were slightly higher than results of beam tests which used the Celion 6000 material; the average modulus of all wrinkling specimens is 53.9 GPa (7.82×10^6 psi) as compared to 48.95 GPa (7.10×10^6 psi) obtained using the four-point beam flexure test method. Since the fiber volume fraction V_f of the beam specimens was higher than that of the buckling specimens (72 percent compared with approximately 61 percent) it appears that the thinner gage Celion 3000 material did not experience any degradation in modulus. Results of replicate tests indicate that scatter was low. Scatter in critical wrinkling stress ranged from a minimum of 7.6 MPa (1.1 ksi) for the 1.27 cm (0.5 in.) specimens to a maximum of 89 MPa (13 ksi) for the 2.54 cm (1.00 in.) specimens. This amounts to a range from minimum to maximum of 1.7 to 29 percent, respectively, when compared to average critical stress values. From tables II and VII some trends in results are evident:

1. Average failure stresses of the wrinkling specimens decrease as core height t_c increases. This is characteristic of a wrinkling or local buckling type of instability. Average failure stresses were 452, 354, and 311 MPa (65.6, 51.4, and 45.1 ksi) for the 1.27-, 1.91-, and 2.54-cm (0.50-, 0.75-, and 1.00-in.) thick cores, respectively.

2. Average failure strains were 0.87, 0.71, and 0.63 percent for the 1.27-, 1.91-, and 2.54-cm (0.50-, 0.75-, and 1.00-in.) thick cores, respectively.

3. Specimens with higher total facing thicknesses had higher failure loads; however, these specimens did not necessarily have higher failure stresses. This is because the thicker facings had a lower fiber volume fraction V_f because not enough resin was removed during the consolidation phase of laminate fabrication.

4. Panels with the largest value of initial waviness δ_{max} had the lowest ultimate load.

5. Ultimate strains of the wrinkling specimens were well below ultimate laminate strain results from the beam tests.

As mentioned earlier, most of the wrinkling specimens failed close to the end of one of the side simple supports. Failure of a 1.27-cm (0.50-in.) panel is illustrated in figures 21(a) and (b); the failure extends across the panel to the top of the left-side simple support. The failures were nearly perpendicular to the direction of load. Wrinkling failure was most noticeable in the 1.27-cm (0.50-in.) specimens in which the facings separated from the core due to a ten-

sile failure of the adhesive. Failed panel BT-4 (fig. 22(a)) illustrates the outward buckling of the facing; the panel was cut along the dashed line in that figure to further illustrate the tensile failure of the adhesive which was precipitated by wrinkling (fig. 22(b)). Figure 23 is a side view of two different panels (t_c = 1.27 cm (0.50 in.)). It is not conclusive from the side views whether the failures were symmetric or antisymmetric; however, laminate failures on either facing were similar which suggests that failures were symmetric. This agrees with results of references 4 and 16 which indicate that for honeycomb cores, where the modulus of the core in the direction of the load is much less than the modulus of the core in the direction perpendicular to the facings, symmetric wrinkling will occur at a lower load than that for antisymmetric wrinkling.

Overall buckling specimens.- Experimental results of overall buckling specimens are presented in table VIII and figures 24(a), (b), and (c). The experimental critical overall buckling stress was determined from the applied load associated with the reversal of extreme fiber strain on the convex side of the buckled panel. The specimens exhibited a very short postbuckling region as evidenced by the experimental results of P_{cr} and P_{ult} as shown in table VIII. Average values of P_{cr}, P_{ult}, σ_{cr}, and σ_{ult} are 101.9 kN (22 903 lbf), 106.3 kN (23 897 lbf), 264.1 MPa (38.3 ksi), and 275.5 MPa (39.96 ksi), respectively, and corresponding scatter is 21, 20, 21, and 20 percent.

Similar to results of reference 4, all the overall buckling specimens failed on the concave side of the specimen in a typical compressive failure mode. Most of the specimens failed in the center, all the failures were perpendicular to the direction of load as shown in figure 25. The Moiré method was useful in visualizing the deflected mode shapes of the specimens and determining the effectiveness of the simple supports. Panel number BT-2 was the only specimen which failed near a simple support. Photographs of Moiré fringe patterns of panel BT-2 indicated that it did not deform symmetrically in half sine waves in the length and width directions as expected. The out-of-plane deformation of panel BT-2 with increasing load is illustrated in figures 26(a), (b), and (c). As shown, the peak out-of-plane deformation occurs in the upper right-hand portion of the specimen. This panel eventually failed near the lower left-hand simple support. All other specimens failed in the center. Moiré fringe patterns of a typical buckling specimen are shown in figures 27(a) to (d) for increasing load. As shown, the maximum out-of-plane displacement does occur in the center of the panel. Displacements seem to be symmetric in the longitudinal direction; however, nonzero displacements appear to occur near the right-hand simple support. Displacements do occur at the corners of the panel since the simple supports do not extend the total panel length. As the panel approaches failure, mode shapes tend to be nonsymmetric (fig. 27(d)). As mentioned in reference 4, it is very difficult to simulate true simply supported boundaries when the buckled mode shape occurs at $m = n = 1$ or the buckled shape is a half sine wave in the length and width direction.

Comparison of analytical and experimental results.- The analysis assumes the room-temperature unidirectional properties and dimensions listed in table IX.

From laminate theory $\bar{E}_x = \bar{E}_y = E_f = 51.97$ GPa (7.538×10^6 psi) and $\bar{\mu}_{xy} = 0.3075$. These results agree with experimental results from the sandwich beam flexure tests in which the average modulus, $\bar{E}_x = 48.95$ GPa (7.1×10^6 psi) and $\bar{\mu}_{xy} = 0.347$. Since laminates were quasi-isotropic, symmetric ($[0,\pm45,90]_s$), A_{16} and A_{26} coupling terms of the sandwich were identically zero, and the D_{16} and D_{26} coupling terms were negligible. Analytical results, assuming a lamina thickness of 0.0076 cm (0.003 in.), are presented and compared with experimental results in tables VII and VIII and in figure 28. The overall buckling analysis described in reference 7, which included the core shear flexibility, agreed well with experimental overall buckling results. Local and general buckling formulas used in the present analysis are presented in appendix B.

The average experimental overall buckling stress was 264 MPa (38.3 ksi) and compared exactly with the analytically predicted overall buckling stress. From experimental wrinkling results it appears that equations (B5), (B6) and (B8) were unconservative and impractical to use from a design standpoint. Equation (B4), however, was conservative in its prediction of symmetric wrinkling loads and is useful for design purposes. Wrinkling results obtained by using equation (B6) and assuming $\delta_{max} = 0.01$ cm (0.004 in.) were 7, 26, and 32 percent higher than experimental results for the 1.27-, 1.91-, and 2.54-cm (0.50-, 0.75-, and 1.00-in.) thick cores, respectively. The equation for overall buckling is equation (B11) and, as explained earlier, when core shear flexibility is accounted for, the results using this equation agree exactly with average experimental values of σ_{cr}.

CONCLUDING REMARKS

The purpose of the present study was to investigate the buckling behavior, local and general, of graphite/polyimide (Gr/PI) sandwich panels capable of use at temperatures ranging from 116 to 589 K (-250 to 600°F) as the sandwich skin of the space shuttle body flap. The adhesive and facing material properties were investigated and buckling formulas for predicting local and general sandwich panel instabilities were evaluated. Results of a bond study include a fabrication technique for adhesively bonding sandwich structures and a cure cycle for FM-34 film adhesive which produced flatwise tensile strengths in excess of 3.4 MPa (500 psi) at 116 K and R.T. (-250°F and R.T.) in 1.4 MPa (200 psi) at 589 K (600°F). Results also indicate that a liquid cell-edge adhesive (BR-34) can result in considerable panel mass savings (10 percent) without necessarily sacrificing bond strength; however, further research is necessary since flatwise-tensile strengths using BR-34 were not consistent. Material property tests of quasi-isotropic, symmetric laminates ($[0,\pm45,90]_s$) of Celion 6000/PMR-15 Gr/PI material indicate that it maintains suitable structural properties for short-term use at temperatures from 116 to 589 K (-250° to 600°F).

Experimental results of flat rectangular honeycomb sandwich panels which were simply supported along all four edges and tested in uniaxial edgewise compression indicate that two modes of panel failure, wrinkling or overall buckling, can occur depending on the core thickness. As predicted analytically, specimens with a core thickness of 0.635 cm (0.25 in.) failed by overall buckling and all other specimens, having nominal core thicknesses of 1.27, 1.91,

and 2.54 cm (0.50 , 0.75, and 1.00 in.), failed by wrinkling. The shadow Moiré method was useful in determining mode shapes of the overall buckling specimens but was not able to detect wrinkling.

Results of the wrinkling tests indicated that several analytical methods were unconservative and therefore not suitable for design purposes. Most of the wrinkling specimens failed near the side simple supports. The failure mode appeared to be symmetric wrinkling with failures occurring because of tensile rupture of the adhesive. Some trends in wrinkling results are:

1. Average failure stresses of the wrinkling specimens decrease as core thickness increases and are 452, 354, and 311 MPa (65.6, 51.4, and 45.1 ksi) for the 1.27-, 1.91-, and 2.54-cm (0.50-, 0.75-, and 1.00-in.) thick cores, respectively.

2. Average failure strains were 0.87, 0.71, and 0.63 percent for the 1.27-, 1.91-, and 2.54-cm (0.50-, 0.75-, and 1.00-in.) thick cores, respectively.

3. Panels with the largest value of initial waviness had the lowest ultimate load.

The average experimental overall buckling stress of the 0.635-cm (0.25-in.) thick specimens was 264 MPa (38.3 ksi) and compared exactly with the analytically predicted overall buckling stress. All the overall buckling specimens except one failed in the center on the concave facing by compression.

Langley Research Center
National Aeronautics and Space Administration
Hampton, VA 23665
December 2, 1980

APPENDIX A

DESIGN CONSIDERATIONS FOR BUCKLING SPECIMENS

Preliminary studies of structural loads on the shuttle body flap (ref. 3) indicate that compression loads are the primary design condition and that a biaxial state of stress is present. For this reason a sandwich panel design was chosen. Furthermore, based on the low magnitude and biaxial nature of stresses, minimum-gage symmetric laminates of $[0,\pm45,90]_S$ Gr/PI were chosen for the facings of the sandwich skin of the body flap. Therefore, buckling specimens similar to the sandwich skin of the body flap are examined in the present study.

Only symmetric laminates were considered in the present investigation to prevent laminate warpage during the cure cycle caused by bending-stretching coupling terms (nonzero [B] matrix of the material). If nonsymmetric laminates such as [0,±45,90] could be fabricated and forced flat and bonded symmetrically with respect to the center line of the core, this would reduce the mass of the panel and may be sufficient to accommodate the low loads predicted for the body flap. However, analysis techniques would have to be generalized to include anisotropic facings as was done in reference 4. Because of these fabrication uncertainties, however, nonsymmetric laminates were not considered for the experimental study.

Thin-gage Celion 3000 material was chosen because it would present a substantial mass savings over the thicker gage Celion 6000 material. Average thickness per ply of the Celion 3000 laminates were 0.007 cm (0.0028 in.) as compared to 0.0165 cm (0.0065 in.) for Celion 6000.

The lowest density commercially available core which can function structurally at 589 K (600°F) is either Hexcel HRH-327-3/16-4 or HRH-327-3/8-4 glass/PI which has a density of 64 kg/m^3 (4 lbm/ft^3) and either a 0.5 cm (3/16 in.) or a 0.95 cm (3/8 in.) cell size, respectively. Both of these cases were examined in the analytical investigation.

Simply supported boundary conditions and uniaxial edgewise compression loading were chosen at test conditions because they closely represent conditions actual shuttle body flap panels will experience. Both overall and local panel buckling modes were considered in the analysis. Elements of the [A] and [D] matrices were calculated for the quasi-isotropic, symmetric Gr/PI sandwich based on laminate theory presented in references 9, 17, and 18. Overall buckling equations (ref. 7) were minimized with respect to m and n, to predict overall panel buckling load (assuming both infinite and finite core shear stiffness); the local instability equations of reference 8 were used to predict local instability modes and associated loads. The local and general buckling equations are also presented in appendix B. Buckling loads were computed for various ply thicknesses, core thicknesses, and operating temperatures.

Unidirectional laminate material properties used in the design of the buckling specimens were obtained from references 19 and 20. Honeycomb core material properties were obtained from reference 5. Some of the material properties used in the present analysis are presented in table IX. Various cores and core

thicknesses (0.635 to 2.54 cm (0.25 to 1.00 in.)) and panel lengths and widths (10.2 to 122 cm (4.0 to 48.0 in.)) were analytically investigated at various temperatures (room temperature to 589 K (600°F)), and design envelopes, typified by figure 28, were determined. Since the laminate orientation of the facings is quasi-isotropic and symmetric, the average elastic modulus $\bar{E}_x$ or $\bar{E}_y$ was used for the facing-modulus E_f equations in appendix B. Results of critical stress as a function of core thickness for an assumed ply thickness of 0.0076 cm (0.003 in.) are shown in figure 28.

The design envelope curves in figure 28 indicate that either overall buckling, dimpling, laminate strength, or wrinkling could be critical failure modes depending on scatter in material properties and different analysis techniques. Since it is desirable to verify as many analytical predictions for various failure modes as possible, the honeycomb core with the larger cell size (0.95 cm (3/8 in.)) was chosen because it lowers the dimpling stress to values closer to the other critical stresses. A panel size of 30.5 by 30.5 cm (12 by 12 in.) was adequate to investigate several failure modes.

The honeycomb core near the loaded ends of the specimens was potted with BR-34 liquid polyimide adhesive, and tapered end tabs of $[\pm 45]_s$ glass/PI were bonded at each end to prevent local end failures such as core crushing or end brooming; scalloped doublers were bonded beneath the end tabs to enhance load diffusion into the panel and help reduce stress concentrations. A stainless-steel sheet was embedded in the BR-34 potting at each end to align the specimens in the knife edges. Laminates were bonded to the core and end tabs and doublers were secondary bonded using FM-34 film adhesive. Significant panel parameters, related to the fabrication and quality of the wrinkling and overall buckling specimens such as fiber and void volume fractions and the glass transition temperature, are presented in table II. Facing and total sandwich panel thickness measurements were made at various panel locations and initial panel waviness δ was measured as explained in reference 9. Because of good fabrication and quality control procedures the panels were consistent in dimensional and material properties. Average thickness per ply of all wrinkling specimens was 0.0071 cm (0.0028 in.) with maximum variations in total laminate (8 plies) thicknesses averaging only 0.00451 cm (0.00178 in.); average variation in total sandwich panel thicknesses was only 0.0059 cm (0.0023 in.). Maximum panel waviness δ_{max} averaged only 0.0097 cm (0.0038 in.).

APPENDIX B

BUCKLING FORMULAS USED IN THE PRESENT STUDY

There are several instability modes which can cause failure of a sandwich structure; as shown in figure 29 they are: intracellular buckling (face dimpling), face wrinkling (either symmetric or antisymmetric), and shear crimping. Intracellular buckling is a localized mode of instability which occurs only when the core is not continuous, as in the case of honeycomb or corrugated cores. As shown in figure 29(a), the facings buckle in a platelike fashion directly above core cells, with cell edges acting as edge supports. These buckles can deform sufficiently to cause permanent, plastic deformations and can eventually lead to the face wrinkling instability mode (fig. 29(b)). The face wrinkling mode is a localized buckling of the facings in which the wavelength of the buckles is of the same order as the thickness of the core. Depending on the nature of the material properties of the core the facings can buckle symmetrically or antisymmetrically. For the honeycomb cores, in which the elastic modulus parallel to the facings is very low compared with the modulus in the direction perpendicular to the facings, failure is usually by symmetric wrinkling (ref. 16).

Shear crimping (fig. 29(c)) is considered to be a special form of general instability for which the buckle wavelength is very short due to a low transverse shear modulus of the core. This mode occurs suddenly and usually causes the core to fail in shear; however, it may also cause a shear failure in the core-to-facing bond.

Overall buckling was calculated using the method of reference 7 which assumes simply supported boundary conditions and includes consideration of core shear flexibility.

There are many references concerning the analysis and prediction of local instability modes of failure of sandwich structures (refs. 4, 6, 8, and 21 to 24). Formulas for predicting local instability vary among references and for that reason several methods were used to predict local failure loads. An upper and a lower bound were calculated for various failure modes and sandwich panel thicknesses. The formulas for local buckling of a sandwich panel subject to uniaxial compression and appropriate references are given as follows:

Dimpling:

From references 8 and 22 to 24, for isotropic facings

$$\sigma_{dim} = \frac{2E_f}{(1 - \mu^2)} \left(\frac{t_f}{s}\right)^2 \tag{B1}$$

where E_f is the facing modulus, t_f is the facing thickness, and s is the honeycomb cell size.

APPENDIX B

From reference 4

$$\sigma_{dim} = 3E_f \left(\frac{t_f}{s}\right)^2 \tag{B2}$$

From reference 4, assuming orthotropic faces

$$\sigma_{dim} = 0.825 \frac{\pi^2}{3} \left[\frac{2\sqrt{E_{f_x} E_{f_y}} + \bar{\mu}_{yx} E_{f_x} + \bar{\mu}_{xy} E_{f_y}}{4(1 - \bar{\mu}_{xy}\bar{\mu}_{yx})} + G_{f_{xy}} \right] \left(\frac{t_f}{s}\right)^2 \tag{B3}$$

where E_{f_x} and E_{f_y} are the facing moduli in the x- and y-direction, respectively, and $G_{f_{xy}}$ is the facing shear modulus in the xy-plane.

For isotropic faces, equation (B3) reduces to

$$\sigma_{dim} = 0.825 \frac{\pi^2}{3} \left[\frac{E_f(1 + \mu)}{2(1 - \mu^2)} + G_{f_{xy}} \right] \left(\frac{t_f}{s}\right)^2$$

Facing wrinkling (symmetric):

From references 11 and 23, the lower bound on wrinkling stress is

$$\sigma_{wr} = 0.33E_f \left(\frac{E_{c_z} t_f}{E_f t_c}\right)^{1/2} \tag{B4}$$

and the upper bound is

$$\sigma_{wr} = 0.82E_f \left(\frac{E_{c_z} t_f}{E_f t_c}\right)^{1/2} \tag{B5}$$

where E_{c_z} is the modulus of the core in the direction normal to the facings and t_c is the thickness of the core,

From reference 23, accounting for initial facing imperfections

APPENDIX B

$$\sigma_{wr} = \frac{0.82E_f\left(\frac{E_{C_z}t_f}{E_f t_c}\right)^{1/2}}{1 + 0.64\delta\left(\frac{E_{C_z}}{t_c F_c}\right)} \tag{B6}$$

where F_c is the flatwise sandwich strength and δ is the amplitude of initial waviness in the facings.

From reference 8, for $\frac{t_c}{t_f} < 50$

$$\sigma_{wr} = 0.5\left(G_{C_{xz}}E_{C_z}E_f\right)^{1/3}$$

and for $\frac{t_c}{t_f} > 50$

$$\sigma_{wr} = 0.76\left(G_{C_{xz}}E_{C_z}E_f\right)^{1/3} \tag{B7}$$

From reference 4

$$\sigma_{wr} = \frac{\pi 2}{t_f l^2}\left\{D_{F_{11}}m^2 + 2\left(D_{F_{12}} + 2D_{F_{66}}\right)\left(\frac{l}{b}\right)^2 + \frac{D_{F_{22}}}{m^2}\left(\frac{l}{b}\right)^4\right\} + \frac{2E_{C_z}l^2}{t_f m^2 \pi^2 (t_c + t_f)} \tag{B8}$$

Shear crimping:

From reference 8

$$\sigma_{crim} = \frac{\left(t_c + t_f\right)^2}{2t_f t_c} G_{C_{xz}} \tag{B9}$$

and from reference 22,

$$\sigma_{crim} = \left(\frac{t_c}{2t_f}\right) G_{c_{xz}} \tag{B10}$$

Overall buckling:

From reference 7

$$N_x\left(\frac{m\pi}{l}\right)^2 = W_{11} - \frac{W_{22}W_{13}^2 + W_{33}W_{12}^2 - 2W_{12}W_{13}W_{23}}{W_{22}W_{33} - W_{23}^2} \tag{B11}$$

where

$$\left.\begin{aligned}
W_{11} &= \bar{D}_x\left(\frac{m\pi}{l}\right)^4 + D_{12}\left(\frac{m\pi}{l}\right)^2\left(\frac{n\pi}{b}\right)^2 + \bar{D}_y\left(\frac{n\pi}{b}\right)^4 \\
W_{12} &= \bar{D}_y\left(\frac{n\pi}{b}\right)^3 + \frac{D_{12}}{2}\left(\frac{m\pi}{l}\right)^2\left(\frac{n\pi}{b}\right) \\
W_{13} &= \bar{D}_x\left(\frac{m\pi}{l}\right)^3 + \frac{D_{12}}{2}\left(\frac{m\pi}{l}\right)\left(\frac{n\pi}{b}\right)^2 \\
W_{22} &= D_{Q_y} + \bar{D}_y\left(\frac{n\pi}{b}\right)^2 + \frac{D_{xy}}{2}\left(\frac{m\pi}{l}\right)^2 \\
W_{23} &= \frac{D_{12} - D_{xy}}{2}\left(\frac{m\pi}{l}\right)\left(\frac{n\pi}{b}\right) \\
W_{33} &= D_{Q_x} + \bar{D}_x\left(\frac{m\pi}{l}\right)^2 + \frac{D_{xy}}{2}\left(\frac{n\pi}{b}\right)^2
\end{aligned}\right\} \tag{B12}$$

and

$$D_{12} = 2D_{xy} + \mu_x\bar{D}_y + \mu_y\bar{D}_x \tag{B13}$$

$$\bar{D}_x = \frac{D_x}{1 - \mu_x\mu_y} \qquad \bar{D}_y = \frac{D_y}{1 - \mu_x\mu_y} \tag{B14}$$

The buckling load of the sandwich is obtained from equations (B11) to (B14) by minimizing with respect to m and n, the number of half-waves in the buckle pattern in the length and width directions of the plate, respectively. The smallest n consistent with the assumption of simply supported plates is $n = 1$.

REFERENCES

1. Davis, John G., Jr., compiler: Composites for Advanced Space Transportation Systems - (CASTS). NASA TM-80038, 1979.

2. Dexter, H. Benson; and Davis, John G., Jr., eds.: Graphite/Polyimide Composites. NASA CP-2079, 1979.

3. Design and Test Requirements for the Application of Composites to Space Shuttle Orbiter. Volume I. Summary. SD 75-SA-0178-1, Space Div., Rockwell International Corp., Dec. 3, 1975.

4. Pearce, T. R. A.: The Stability of Simply-Supported Sandwich Panels With Fibre Reinforced Faceplates. Ph. D. Thesis, Univ. of Bristol, 1973.

5. Mechanical Properties of Hexcel Honeycomb Materials. TSB 120, Hexcel Corp., c.1975.

6. Plantema, Frederik J.: Sandwich Construction. The Bending and Buckling of Sandwich Beams, Plates, and Shells. John Wiley & Sons, Inc., c.1966.

7. Peterson, James P.: Plastic Buckling of Plates and Shells Under Biaxial Loading. NASA TN D-4706, 1968.

8. Sullins, R. T.; Smith, G. W.; and Spier, E. E.: Manual for Structural Stability Analysis of Sandwich Plates and Shells. NASA CR-1457, 1969.

9. Camarda, Charles J.: Experimental Investigation of Graphite/Polyimide Sandwich Panels in Edgewise Compression. NASA TM-81895, 1980.

10. Raju, B. Basava; Camarda, Charles J.; and Cooper, Paul A.: Elevated-Temperature Application of the IITRI Compression Test Fixture for Graphite/Polyimide Filamentary Composites. NASA TP-1496, 1979.

11. Dykes, B. C.: Analysis of Displacements in Large Plates by the Grid-Shadow Moiré Technique. Experimental Stress Analysis and Its Influence on Design, M. L. Meyer, ed., Inst. Mech. Eng., c.1971, pp. 125-134.

12. Chiang, Fu-Pen: Moiré Methods of Strain Analysis. Exp. Mech., vol. 19, no. 8, Aug. 1979, pp. 290-308.

13. Poesch, Jon G.: Development of Lightweight Graphite/Polyimide Sandwich Panels. Non-Metallic Materials, Volume 4 of National SAMPE Technical Conference Series, Soc. Aerosp. Mater. & Process Eng., c.1972, pp. 605-614.

14. Shuart, Mark J.; and Herakovich, Carl T.: An Evaluation of the Sandwich Beam in Four-Point Bending as a Compressive Test Method for Composites. NASA TM-78783, 1978.

15. Jones, Robert E.; and Greene, Bruce E.: The Force/Stiffness Technique for Nondestructive Buckling Testing. A Collection of Technical Papers - AIAA/ASME/SAE 15th Structures, Structural Dynamics and Materials Conference, Apr. 1974. (Available as AIAA Paper 74-351.)

16. Norris, Charles B.; Ericksen, Wilhelm S.; March, H. W.; Smith, C. B.; and Boller, Kenneth H.: Wrinkling of the Facings of Sandwich Constructions Subjected to Edgewise Compression. Rep. No. 1810, Forest Prod. Lab., U.S. Dep. Agr., Nov. 1949.

17. Jones, Robert M.: Mechanics of Composite Materials. McGraw-Hill Book Co., c.1975.

18. Ashton, J. E.; Halpin, J. C.; and Petit, P. H.: Primer on Composite Materials: Analysis. Technomic Pub. Co., Inc., c.1969.

19. Hanson, Morgan P.; and Chamis, Christos C.: Graphite-Polyimide Composite for Application to Aircraft Engines. NASA TN D-7698, 1974.

20. Advanced Composites Design Guide. Volume IV - Materials. Third ed., Air Force Materials Lab., U.S. Air Force, Jan. 1973. (Available from DTIC as AD 916 682L.)

21. Allen, Howard G.: Analysis and Design of Structural Sandwich Panels. Pergamon Press, 1969.

22. Sandwich Construction for Aircraft. ANC-23, Pts. I and II, Air Force-Navy-Civil Subcommittee on Aircraft Design Criteria, 1951.
Part I - Fabrication, Inspection, Durability and Repair.
Part II - Materials Properties and Design Criteria.

23. Honeycomb and Prepreg in Sandwich Construction. TSB 100, Hexcel Corp., c.1974.

24. Military Standardization Handbook - Structural Sandwich Composites. MIL-HDBK-23A, Dec. 30, 1968.

TABLE I.- CURE CYCLES OF FLATWISE-TENSILE SPECIMENS

Cure cycle	Description
1	Vacuum + 0.34 MPa (50 psi) at R.T. Cure to 589 K (600°F) at 5 K/min (9°F/min) and hold for 2 hours No post cure
2	Vacuum + 0.34 MPa (50 psi) at R.T. Cure to 450 K (350°F) at 5 K/min (9°F/min) and hold for 2 hours Post cure at 589 K (600°F) and hold at temperature for 2 hours with clamps
3	Same as cure cycle 1 but bond top and bottom facings separately with facings to be bonded on bottom
4	Vacuum + 0.34 MPa (50 psi) at R.T. Cure to 616 K (650°F) at 5 K/min (9°F/min) and hold for 1.5 hours
5	Same as cure cycle 1 but don't apply vacuum

TABLE II.- SIGNIFICANT PANEL PARAMETERS

[Values in parentheses are averages of replicate specimens]

(a) SI Units

Panel	V_f, percent	V_v, percent	T_g, K	t_h, cm	t_c, cm	t_{f_1}, cm	t_{f_2}, cm	$t_{f_1} + t_{f_2}$, cm	t_{av} per ply, cm	δ_{max}, cm	Δt_f, cm	Δt_h, cm
BT-1	61.2	0.3	592	0.78344	0.66632	0.05955	0.05757	0.11712	0.00732	0.00940	0.0025	0.003
BT-2	60.7	.1	605	.78260	.66576	.05814	.05870	.11684	.00732	.00813	.0051	.005
BT-3	60.3	0	611	.78402	.66751	.05786	.05870	.1166	.00729	.0109	.0025	.005
	(61.1)	(1.175)	(605)	(.78184)	(.66726)	(.05729)	(.11456)	(.0940)	(.00716)	(.00940)	(.00381)	(.004)
BT-4	63.6	2.5	601	1.3984	1.2923	0.05362	0.05249	0.10612	0.00663	0.00711	0.0025	0.005
BT-5	58.4	2.4	589	1.4087	1.2969	.05701	.05475	.11176	.00699	.00711	.0051	.013
BT-6	63.9	1.9	606	1.4052	1.2972	.05390	.05419	.10809	.00676	.01190	.0051	.005
	(62)	(2.27)	(599)	(1.4041)	(1.2954)	(.05433)	(.05433)	(.10866)	(.00653)	(.00864)	(.00592)	(.008)
BT-7	61	0.2	614	2.0368	1.9208	0.05786	0.05814	0.11600	0.00724	--------	0.0025	0.005
BT-8	59.3	.4	607	2.0360	1.9174	.05926	.05926	.11852	.00742	--------	.0025	.005
BT-9	63.1	.9	611	2.0317	1.9169	.05842	.05644	.11486	.00719	0.01118	.0051	.005
	(61.1)	(.5)	(611)	(2.0348)	(1.9184)	(.05824)	(.05824)	(.11646)	(.00728)	(.01118)	(.00338)	(.005)
BT-10	59.5	0.4	612	2.6883	2.5719	0.05814	0.05842	0.11656	0.00728	0.00711	0.0051	0.005
BT-11	60.6	0	600	2.6838	2.5686	.05786	.05729	.11514	.00720	.00940	.0025	.005
BT-12	63.5	.2	622	2.6839	2.6839	.05786	.05842	.11628	.00727	.01067	.0051	.005
	(61.2)	(.2)	(611)	(2.6465)	(2.5694)	(.05795)	(.05804)	(.00724)	(.00724)	(.00914)	(.0042)	(.005)

TABLE II.- Concluded

(b) U.S. Customary Units

Panel	V_f, percent	V_v, percent	T_g, °F	t_h, in.	t_c, in.	t_{f_1}, in.	t_{f_2}, in.	$t_{f_1} + t_{f_2}$, in.	t_{av} per ply, in.	δ_{max}, in.	Δt_f, in.	Δt_h, in.
BT-1	61.2	0.3	606	0.30844	0.26233	0.02344	0.02267	0.04611	0.00288	0.0037	0.001	0.001
BT-2	60.7	.1	630	.308111	.26211	.02289	.02311	.04600	.00288	.0032	.002	.002
BT-3	60.3	0	640	.30867	.26280	.02278	.02311	.04589	.00287	.0043	.001	.002
	(61.1)	(1.175)	(629)	(.30781)	(.26270)	(.02256)	(.02256)	(.04510)	(.00282)	(.0037)	(.0015)	(.0015)
BT-4	63.6	2.5	622	0.55056	0.50878	0.02111	0.02067	0.041778	0.002611	0.0028	0.001	0.002
BT-5	58.4	2.4	600	.55460	.51060	.02244	.02156	.04406	.00275	.0028	.002	.005
BT-6	63.9	1.9	631	.55322	.51070	.02122	.02133	.042556	.00266	.0047	.002	.002
	(62)	(2.27)	(618)	(.55280)	(.510)	(.02139)	(.02139)	(.042778)	(.00257)	(.0034)	(.00233)	(.003)
BT-7	61	0.2	646	0.80189	0.75622	0.02278	0.02289	0.04567	0.00285	-------	0.001	0.002
BT-8	59.3	.4	633	.80156	.75489	.02333	.02333	.04666	.00292	-------	.001	.002
BT-9	63.1	.9	640	.7999	.57467	.02300	.02222	.04522	.00283	.0044	.002	.002
	(61.1)	(.5)	(640)	(.80112)	(.02293)	(.02293)	(.02293)	(.04585)	(.002867)	(.0044)	(.00133)	(.002)
BT-10	59.5	0.4	642	1.0584	1.01256	0.02289	0.02300	0.04589	0.002868	0.0028	0.002	0.002
BT-11	60.6	0	621	1.0566	1.01127	.02278	.02256	.04533	.002833	.0037	.001	.002
BT-12	63.5	.2	660	1.05667	1.05667	.02278	.02300	.04578	.002861	.0042	.002	.002
	(61.2)	(.2)	(641)	(1.0572)	(1.01158)	(.022815)	(.022852)	(.04567)	(.00285)	(.0036)	(.00167)	(.002)

TABLE III.- FLATWISE-TENSILE TEST RESULTS OF CURE-CYCLE BOND STUDY

[FM-34 film adhesive; Core density = 96 kg/m^3 (6 lbm/ft^3)]

Specimen	Cure cycle	P_{ult}, kN (lbf)	σ_{ult}, MPa (psi)	Description of failure
Tests at room temperature				
FTT-1	1	18.90 (4250)	3.25 (472)	Failed between facing and core. Facing delaminated also.
FTT-2	1	23.35 (5250)	4.02 (583)	Failed between facing and core. Facing delaminated.
FTT-3	2	16.24 (3650)	2.80 (406)	Facing delamination.
FTT-4	2	19.79 (4450)	3.41 (494)	Failed between facing and core.
FTT-5	4	13.57 (3050)	2.34 (339)	Facing delamination.
FTT-6	4	17.70 (3980)	3.05 (442)	Facing delamination.
FTT-7	5	21.13 (4750)	3.64 (528)	Failed between facing and core.
FTT-8	5	23.22 (5220)	4.00 (580)	Facing delamination.
FTT-9	3	16.90 (3800)	2.91 (422)	Failed second bond between facing and core.
FTT-10	3	16.01 (3600)	2.76 (400)	Failed second bond between facing and core.
Tests at 589 K (600°F)				
FTT-11	1	7.918 (1780)	1.37 (198)	Failed between facing and core.
FTT-12	1	8.363 (1880)	1.44 (209)	Failed between facing and core.
FTT-13	[a]1	11.23 (2525)	1.94 (281)	Failed between facing and core.
FTT-14	[a]1	7.451 (1675)	1.28 (186)	Failed between facing and core.
FTT-15	5	4.938 (1110)	0.848 (123)	Failed between facing and core.
FTT-16	5	6.139 (1380)	1.06 (153)	Failed between facing and core.

[a]Same as cure cycle 1 but cured to 603 K (625°F).

TABLE IV.- FLATWISE-TENSILE TEST RESULTS

(a) FM-34 film adhesive; Cure cycle 1 with cure temperature = 603 K (625°F); ρ = 0.586 kg/m^2 (0.12 lbm/ft^2)

Specimen	Temperature, K (°F)	Core density, kg/m^3 (lbm/ft^3)	P_{ult}, kN (lbm)	σ_{ult}, MPa (psi)	Description of failure
FTT-17	R.T.	96 (6)	13.12 (2950)	2.26 (328)	Facing delamination.
FTT-18	R.T.	96 (6)	21.80 (4900)	3.75 (544)	Facing delamination.
FTT-19	589 (600)	96 (6)	8.807 (1980)	1.52 (220)	Failed between facing and core.
FTT-20	589 (600)	96 (6)	7.784 (1750)	1.33 (194)	Failed between facing and core.
FTT-21	589 (600)	96 (6)	3.38 (760)	0.58 (84)	Failed between end-block and facing.
FTT-22	116 (-250)	96 (6)	1.11 (250)	1.92 (278)	Failed between end-block and facing.
FTT-23	116 (-250)	96 (6)	4.448 (1000)	0.765 (111)	Facing delamination.
FTT-24	R.T.	128 (8)	18.24 (4100)	3.14 (456)	Failed between facing and core.
FTT-25	116 (-250)	128 (8)	18.46 (4150)	3.18 (461)	Facing delamination.
FTT-26	R.T.	128 (8)	13.34 (3000)	2.30 (333)	Failed between facing and core.
FTT-27	R.T.	128 (8)	22.24 (5000)	3.83 (556)	Facing delamination.
FTT-28	589 (600)	128 (8)	7.651 (1720)	1.32 (191)	Failed between facing and core.
FTT-29	589 (600)	128 (8)	8.451 (1900)	1.46 (211)	Failed between facing and core.
FTT-30	589(600)	128 (8)	8.051 (1810)	1.39 (201)	Failed between facing and core.
FTT-31	116 (-250)	128 (8)	18.90 (4250)	3.25 (472)	Facing delamination.
FTT-32	116 (-250)	128 (8)	24.24 (5450)	4.18 (606)	Failed between facing and core.

TABLE IV.- Concluded

(b) Br-34 cell-edge adhesive; Cure cycle 1 with cure temperature = 603 K (625°F); R.T.; ρ = 0.244 kg/m^2 (0.05 lbm/ft^2)

Specimen	Core density, kg/m^3 (lbm/ft^3)	P_{ult}, kN (lbm)	σ_{ult}, MPa (psi)	Description of failure
FTT-33	96 (6)	9.186 (2065)	1.58 (229)	Failed between block and facing.
FTT-34	96 (6)	5.627 (1265)	0.97 (141)	Failed between block and facing.
FTT-35	96 (6)	5.783 (1300)	0.99 (144)	Failed between block and facing.
FTT-36	96 (6)	11.30 (2540)	1.94 (282)	Facing delamination (localized around cell edges).
FTT-37	96 (6)	3.09 (695)	0.53 (77)	Facing delamination (localized around cell edges).
FTT-38	96 (6)	11.23 (2525)	1.94 (281)	Facing delamination (localized around cell edges).
FTT-39	96 (6)	12.41 (2790)	2.14 (310)	Facing delamination (localized around cell edges).
FTT-40	96 (6)	12.86 (2890)	2.21 (321)	Facing delamination (localized around cell edges.)
FTT-41	96 (6)	17.68 (3975)	3.05 (442)	Failed between facing and core.
FTT-42	128 (8)	16.22 (3647)	2.79 (405)	Facing delamination (not localized).
FTT-43	128 (8)	----------	----------	Failed immediately at very low load between block and facing.
FTT-44	128 (8)	----------	----------	Failed immediately at very low load between block and facing.
FTT-45	128 (8)	20.68 (4650)	3.57 (517)	Facing delamination.
FTT-46	96 (6)	19.48 (4380)	3.31 (487)	Facing delamination.

TABLE V.- COEFFICIENTS OF POLYNOMIALS USED TO CURVE-FIT DATA

$$[\sigma = C_0 + C_1\varepsilon + C_2\varepsilon^2 + C_3\varepsilon^3]$$

Test conditions	C_0, Pa (psi)	C_1, Pa (psi)	C_2, Pa (psi)	C_3, Pa (psi)	Standard error of estimate	
					psi	MPa
Room temperature tension (1 to 4)	-3.695E+4 (-5.359E+0)	5.012E+10 (7.269E+6)	2.293E+12 (3.325E+8)	-2.327+14 (-3.375E+10)	792.187	5.46
Room temperature compression (5 to 8)	1.964E+6 (2.848E+2)	5.047E+10 (7.320E+6)	-2.900E+11 (-4.200E+7)	-3.330E+13 (-4.830E+9)	1609.543	11.10
Low temperature tension (9 to 12)	-2.944E+5 (-4.270E+1)	6.194E+10 (8.983E+6)	3.924E+10 (5.692E+6)	-7.619E+13 (-1.105E+10)	980.474	6.76
Low temperature compression (13 to 16)	-2.450E+6 (-3.533E+2)	5.887E+10 (8.538E+6)	-5.273E+11 (-7.648E+7)	-1.549E+13 (-2.247E+9)	1271.968	8.77
High temperature tension (17 to 20)	-4.360E+5 (-6.324E+1)	5.291E+10 (7.674E+6)	8.894E+11 (1.290E+8)	-1.430E+14 (-2.074E+10)	1399.392	9.65
High temperature compression (21 to 24)	4.613E+6 (-6.691E+2)	4.648E+10 (6.741E+6)	7.660E+11 (1.111E+8)	-2.372E+13 (-3.441E+9)	1546.977	10.67

TABLE VI.- SUMMARY OF SANDWICH-BEAM-FLEXURE TESTS OF $[0,+45,90,-45]_s$

Celion 6000/PMR-15

(a) SI Units

Specimen	Test condition	Temperature, K	σ_{ult}, MPa	$\sigma_{ult_{av}}$, MPa	ε_{ult}, percent	$\varepsilon_{ult_{av}}$, percent	E at ε = 0.002, GPa	μ at ε = 0.002	μ_{av} at ε = 0.002
BTF-1	Tension	R.T.	539.2	565.2	(a)	(a)	56.54	0.343	0.333
BTF-2		↓	569.2		↓			.312	
BTF-3			595.9					.354	
BTF-4			556.6					.322	
BTF-5	Compression	R.T.	599.0	567.7	-1.391	-1.381	48.95	0.350	0.347
BTF-6		↓	590.5		-1.579			.313	
BTF-7			557.9		-1.328			.356	
BTF-8			523.3		-1.227			.368	
BTF-9	Tension	116	579.1	613.5	(a)	(a)	61.36	(a)	0.329
BTF-10		↓	(a)		↓			0.343	
BTF-11			661.3					.332	
BTF-12			600.0					.312	
BTF-13	Compression	91.5	666.1	646.2	-1.368	-1.285	56.54	0.334	0.337
BTF-14		136	618.9		-1.249			.345	
BTF-15		116	679.2		(a)			.313	
BTF-16		116	620.5		-1.237			.356	
BTF-17	Tension	589	318.7	322.8	0.626	0.608	54.47	0.289	0.344
BTF-18		↓	317.5		.580			.366	
BTF-19			346.2		.653			.354	
BTF-20		597	308.7		.573			.367	
BTF-21	Compression	589	296.5	334.0	-0.644	-0.657	48.95	0.388	0.382
BTF-22		↓	423.0		-.690			.376	
BTF-23			338.4		-.696			.376	
BTF-24			278.0		-.657			.388	

[a]Gage malfunction.

TABLE VI.- Concluded

(b) U.S. Customary Units

Specimen	Test condition	Temperature, °F	σ_{ult}, psi	$\sigma_{ult_{av}}$, psi	ε_{ult}, percent	$\varepsilon_{ult_{av}}$, percent	E at ε = 0.002, psi	μ at ε = 0.002	μ_{av} at ε = 0.002
BTF-1	Tension	R.T.	78.20	81.98	(a)	(a)	8.2×10^6	0.343	0.333
BTF-2		↓	82.55		↓			.312	
BTF-3			86.42					.354	
BTF-4			80.73					.322	
BTF-5	Compression	R.T.	86.87	82.34	-1.392	-1.381	7.1×10^6	0.350	0.347
BTF-6		↓	85.65		-1.579			.313	
BTF-7			80.92		-1.328			.356	
BTF-8			75.90		-1.227			.368	
BTF-9	Tension	-250	83.99	88.97	(a)	(a)	8.9×10^6	(a)	0.329
BTF-10		↓	(a)		↓			0.343	
BTF-11			95.91					.332	
BTF-12			87.02					.312	
BTF-13	Compression	-295	96.60	93.72	-1.368	-1.285	8.2×10^6	0.334	0.337
BTF-14		-215	89.77		-1.249			.345	
BTF-15		-250	98.51		(a)			.313	
BTF-16		250	90.00		-1.237			.356	
BTF-17	Tension	600	46.22	46.81	0.626	0.608	7.9×10^6	0.289	0.344
BTF-18		↓	46.05		.580			.366	
BTF-19			50.21		.653			.354	
BTF-20		615	44.77		.573			.367	
BTF-21	Compression	600	43.00	48.44	-0.644	-0.657	7.1×10^6	0.388	0.382
BTF-22		↓	61.35		-.690			.376	
BTF-23			49.08		-.696			.376	
BTF-24			40.33		-.599			.388	

[a]Gage malfunction.

TABLE VII.- SUMMARY OF ROOM-TEMPERATURE WRINKLING PANEL RESULTS[a]

[$[0,\pm45,90]_s$ Celion 3000/PMR-15 facings and HRH-327-3/8-4 Glass/PI core]

Panel	Core thickness, t_c, cm (in.)	E at ε = 0.002, GPa (psi)	Max. back-to-back strain variation $\left(\frac{\Delta\varepsilon}{\varepsilon}\right)_{\varepsilon = 0.006}$, percent	Theoretical wrinkling stress, MPa (ksi), from equation -			Experimental		
				(B4)	(B5)	(B6)	σ_{ult}, MPa (ksi)	ε_{ult}, percent	P_{ult}, kN (lbf)
BT-4	1.27 (0.50)	53.4 (7.75×10^6)	16.7	292.3 (42.4)	723.9 (105.)	484.0 (70.2)	454.7 (65.95)	0.89	159.3 (35 820)
BT-5	↓	54.0 (7.83×10^6)	11.0	↓	↓	↓	447.5 (64.90)	.88	165.1 (37 120)
BT-6	↓	58.6 (8.5×10^6)	15.0	↓	↓	↓	455.1 (66.00)	.83	161.3 (36 270)
BT-7	1.91 (0.75)	52.9 (7.67×10^6)	25.0	240.6 (34.9)	597.1 (86.6)	446.1 (64.7)	356.1 (51.66)	0.70	136.4 (30 670)
BT-8	↓	52.9 (7.67×10^6)	16.7	↓	↓	↓	374.6 (54.33)	.78	146.6 (32 960)
BT-9	↓	53.8 (8.00×10^6)	20.0	↓	↓	↓	332.2 (48.18)	.66	126.0 (28 320)
BT-10	2.54 (1.00)	50.5 (7.33×10^6)	18.0	207.5 (30.1)	515.7 (74.8)	411.6 (59.7)	365.8 (53.06)	0.77	141.0 (31 650)
BT-11	↓	54.0 (7.83×10^6)	40.0	↓	↓	↓	276.5 (40.11)	.54	105.1 (23 640)
BT-12	↓	54.0 (7.83×10^6)	27.0	↓	↓	↓	289.9 (42.05)	.57	111.3 (25 020)

[a]Theoretical dimpling stress range: 409.7 MPa (59.42 ksi) to 641.2 MPa (93.0 ksi).
Laminate strength: 576 MPa (82.3 ksi).
Ultimate strength: 1.4 percent.

TABLE VIII.- SUMMARY OF ROOM-TEMPERATURE RESULTS OF OVERALL BUCKLING PANELS

[t_c = 0.635 cm (0.25 in.)]

Panel	Experimental results				Theoretical
	P_{cr}, kN (lb)	P_{ult}, kN (lb)	σ_{cr}, MPa (ksi)	σ_{ult}, MPa (ksi)	σ_{cr}, MPa (ksi)
BT-1	93.33 (20 981)	97.64 (21 950)	241.3 (35.00)	252.5 (36.62)	264.7 (38.39)
BT-2	114.38 (25 714)	118.76 (26 700)	296.5 (43.00)	307.8 (44.65)	↓
BT-3	97.92 (22 013)	102.50 (23 040)	254.4 (36.90)	266.3 (38.63)	

TABLE IX.- PROPERTIES USED IN BUCKLING ANALYSIS

E_{11} = 133 GPa (19.3×10^6 psi)

E_{22} = 9.10 GPa (1.32×10^6 psi)

μ_{12} = 0.37

μ_{21} = 0.025

G_{12} = 5.58 GPa (0.81×10^6 psi)

E_{c_z} = 0.345 GPa (50×10^3 psi)

$G_{c_{xz}}$ = 0.200 GPa (29×10^3 psi)

$G_{c_{yz}}$ = 0.083 GPa (12×10^3 psi)

F_c = 3.45 MPa (500 psi)

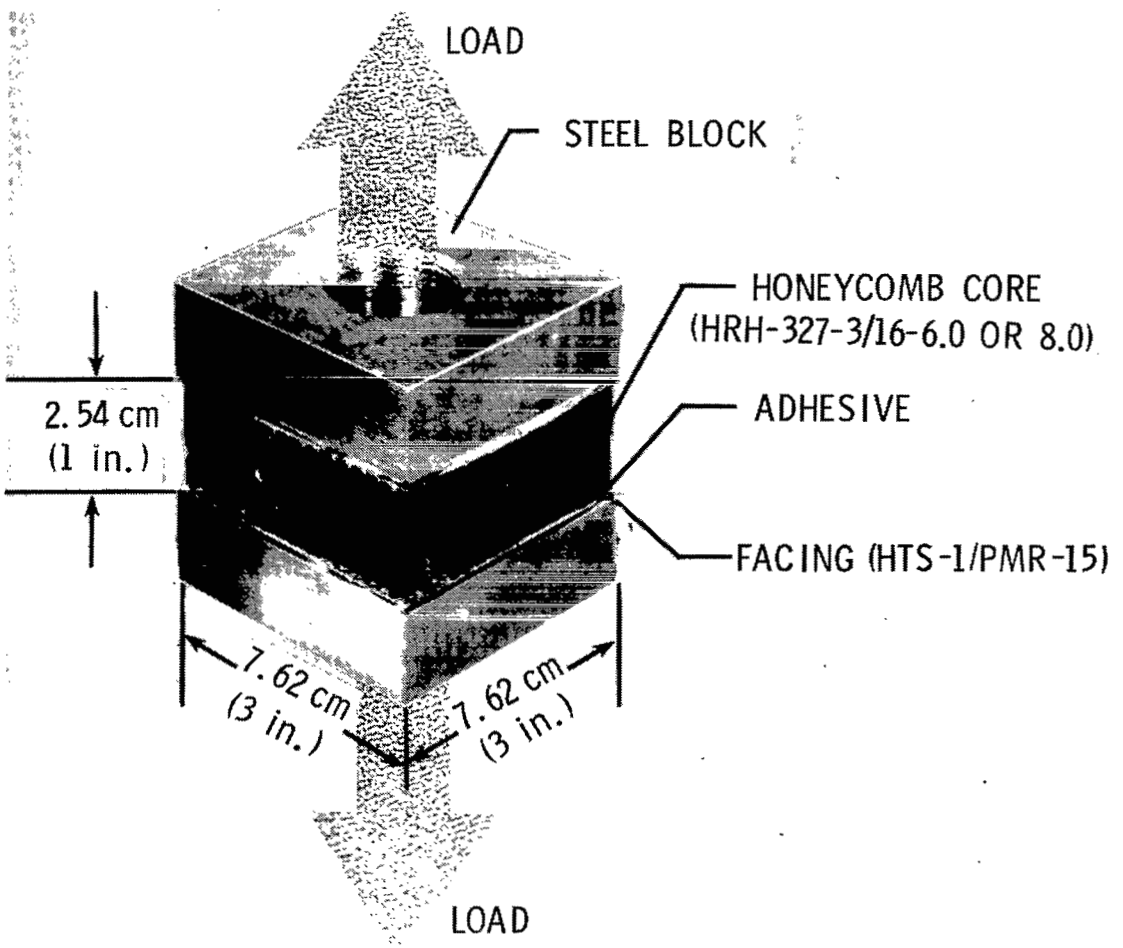

L-80-229

Figure 1.- Schematic diagram of flatwise-tensile specimen.

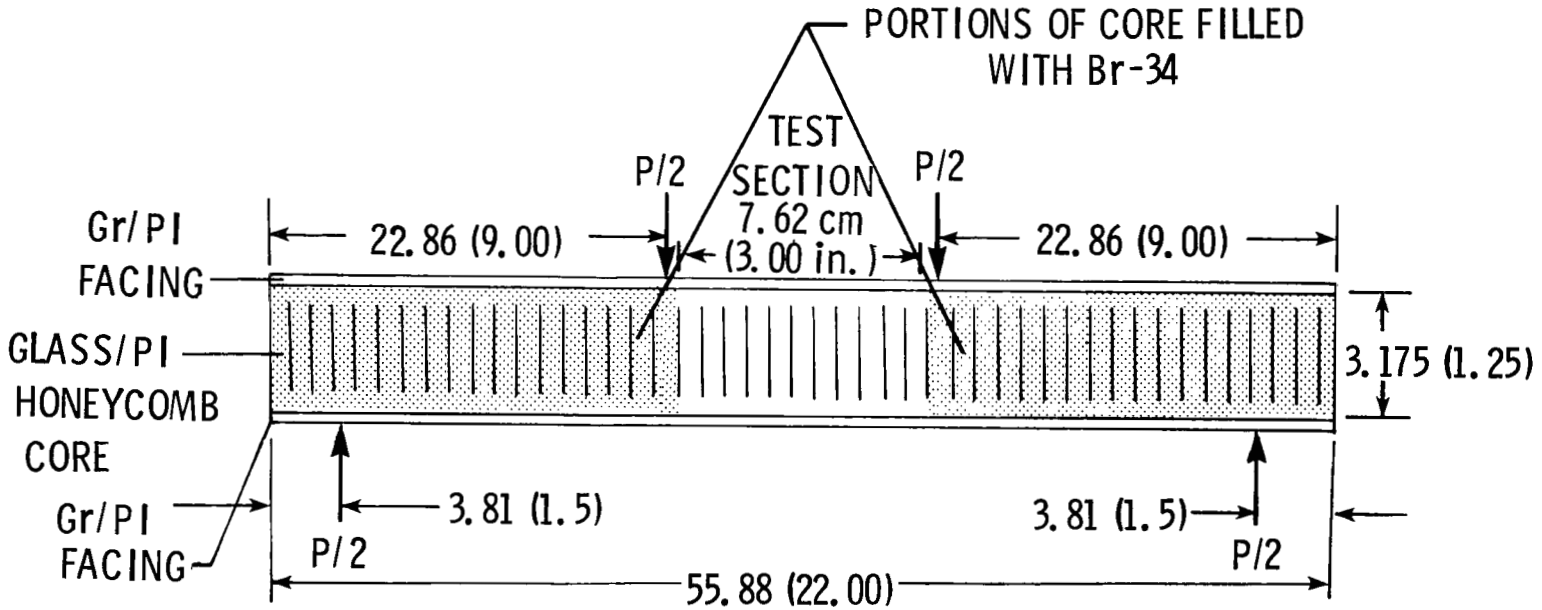

Figure 2.- Sandwich beam in four-point bending. All dimensions are in centimeters (inches).

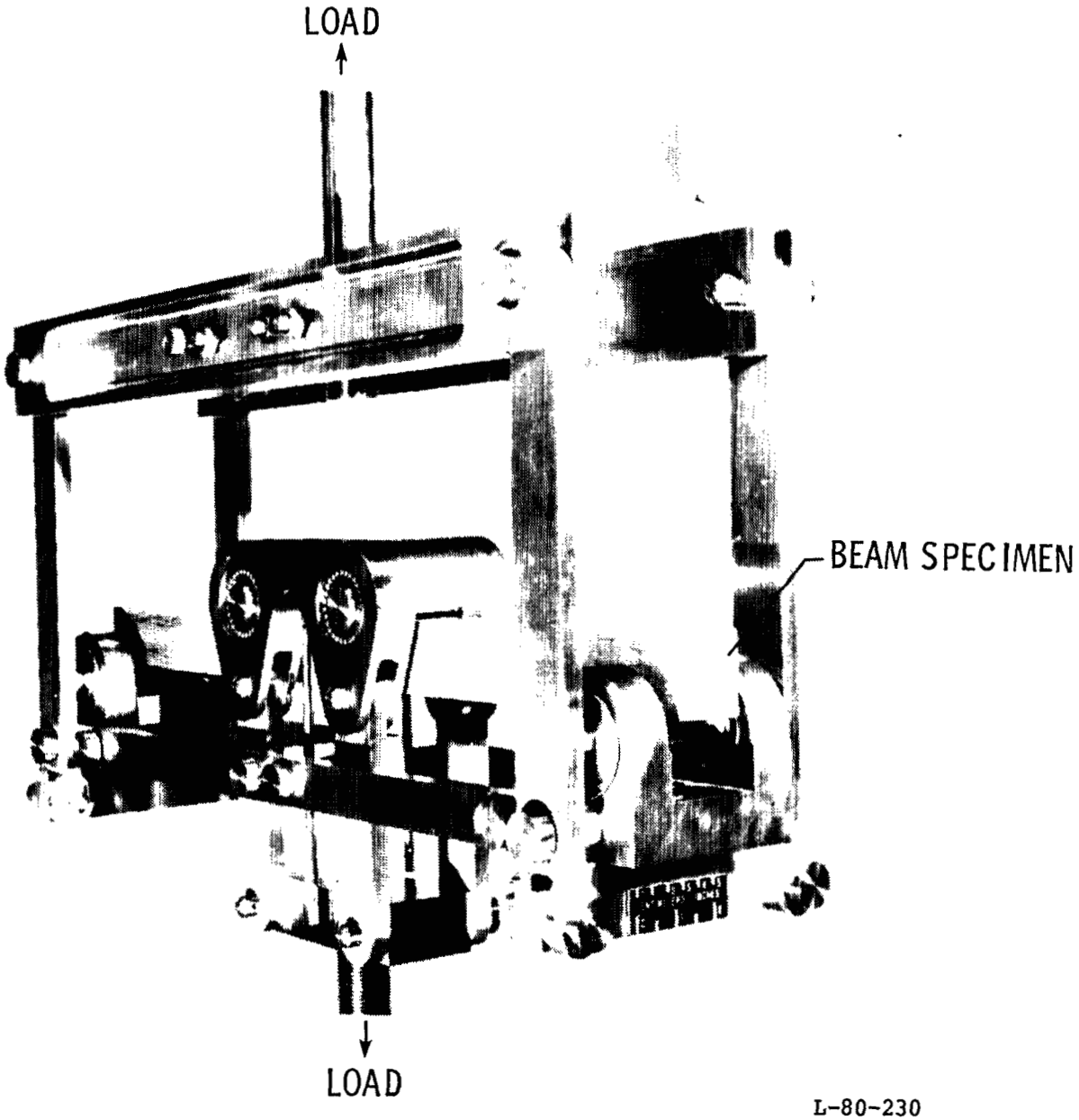

Figure 3.- Four-point bending test apparatus.

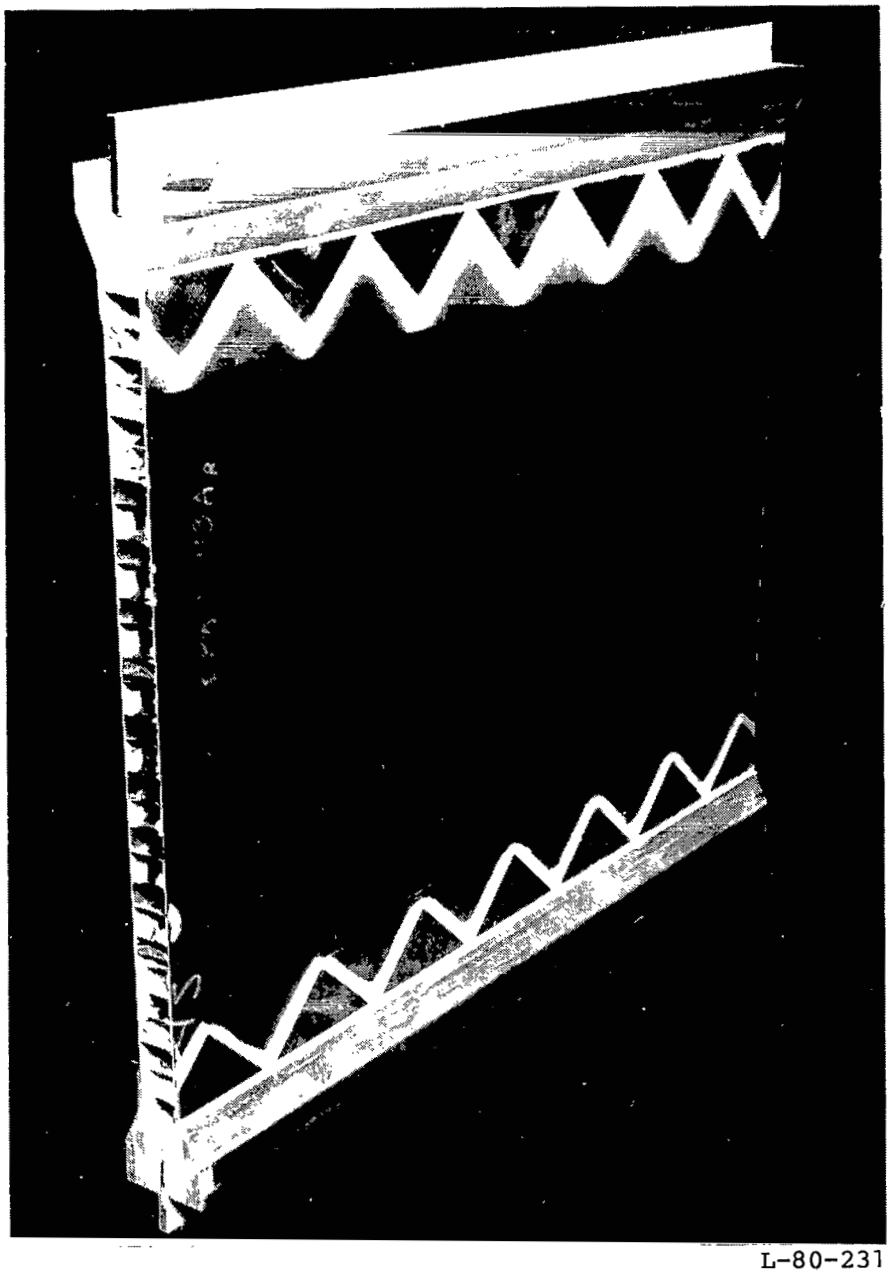

L-80-231

Figure 4.- Buckling specimen.

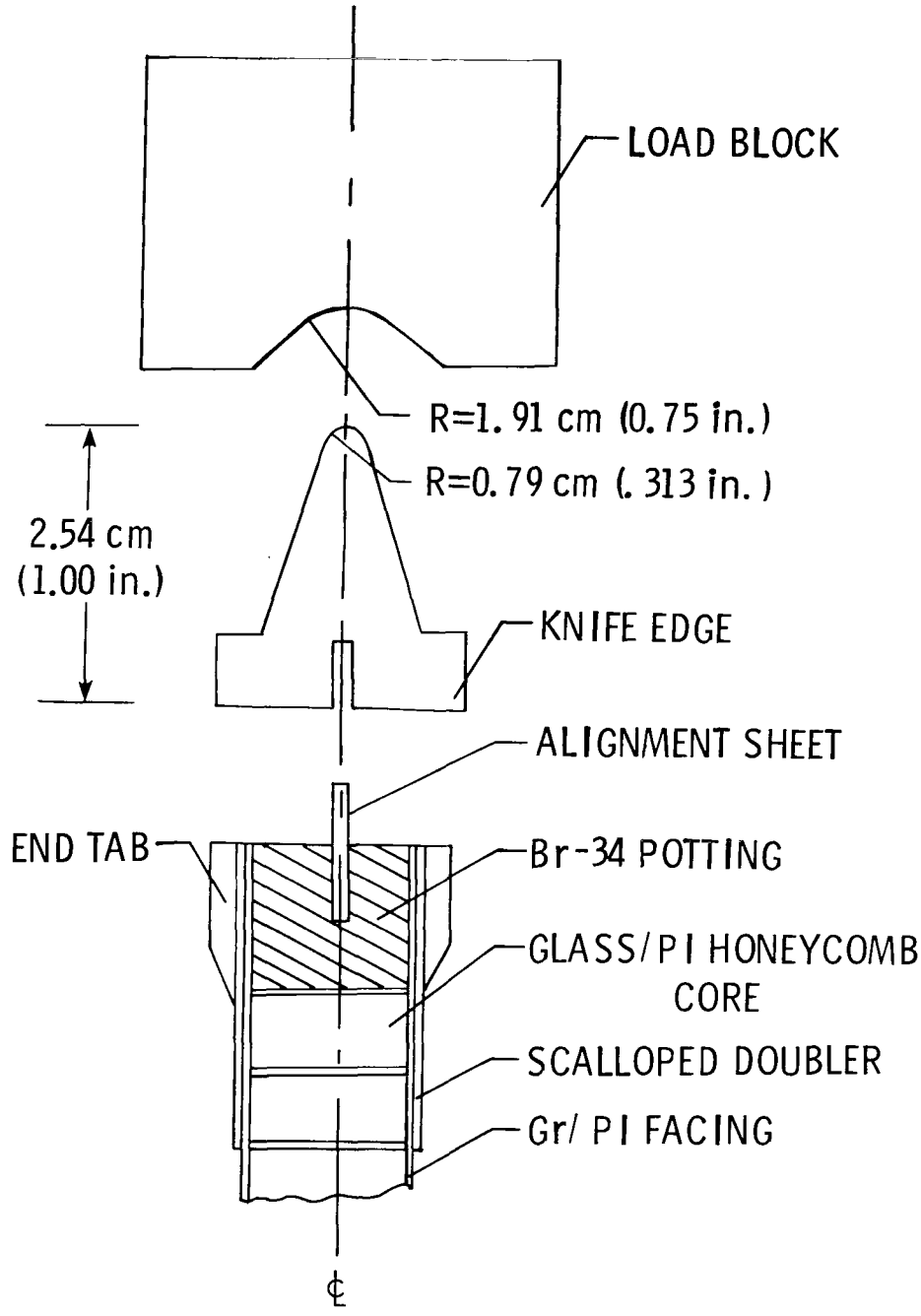

(a) End supports.

Figure 5.- Technique for simply supporting panel.

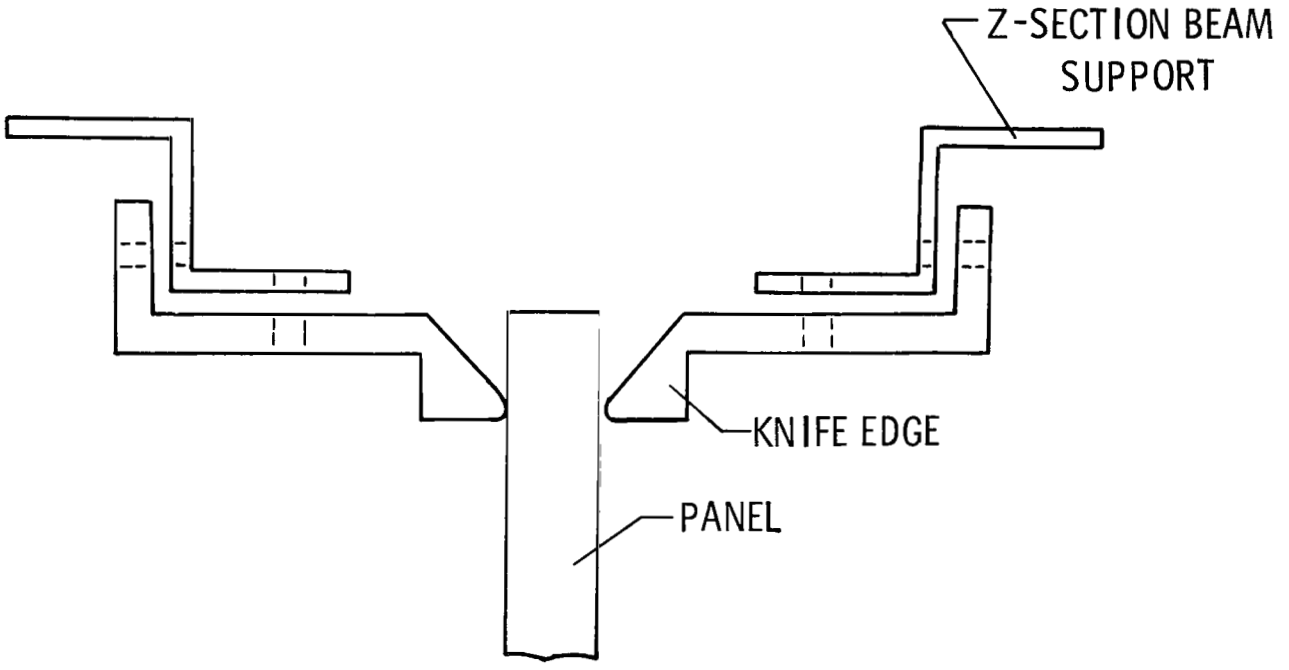

(b) Side supports.

Figure 5.- Concluded.

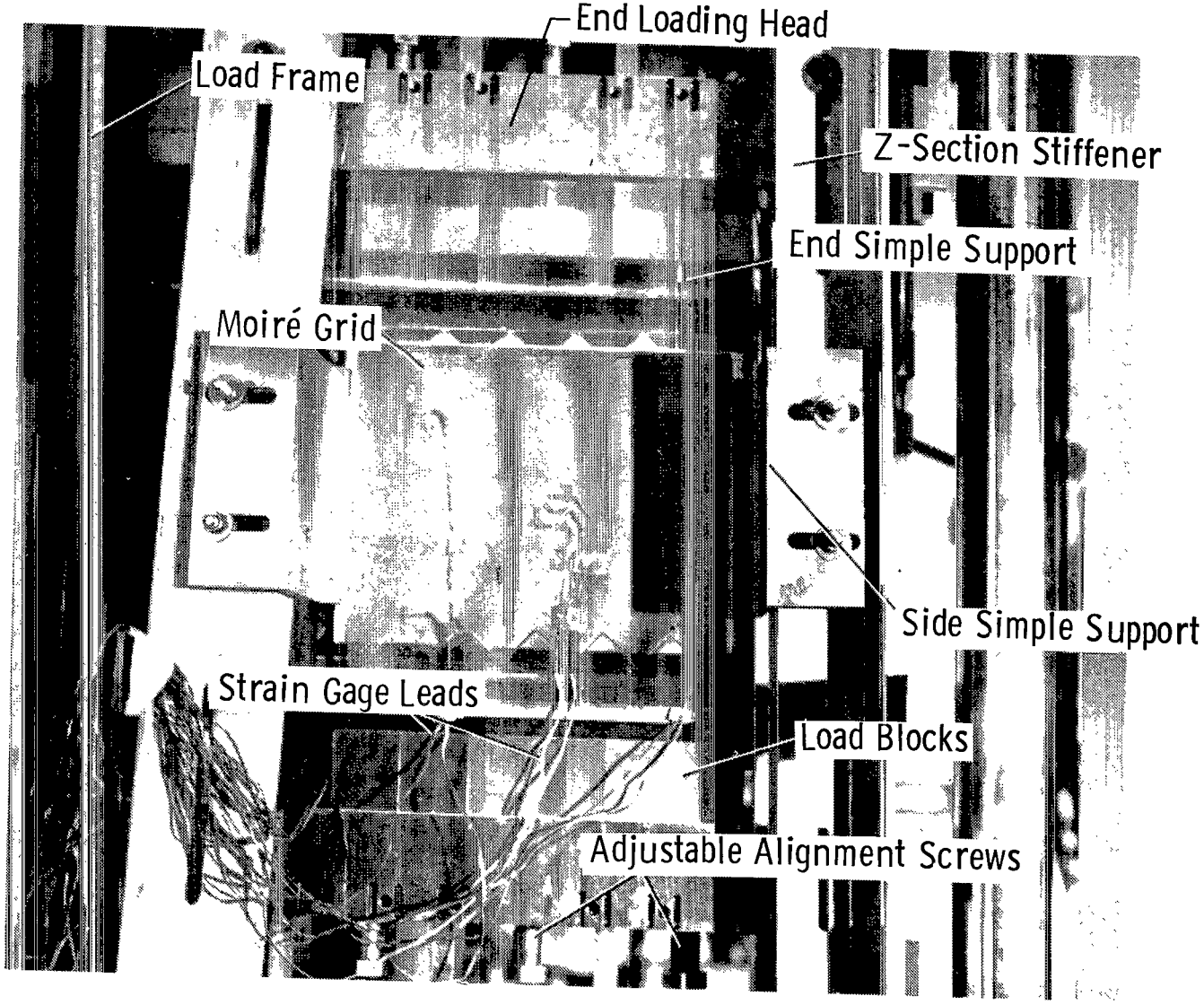

Figure 6.- Buckling specimen in test fixture.

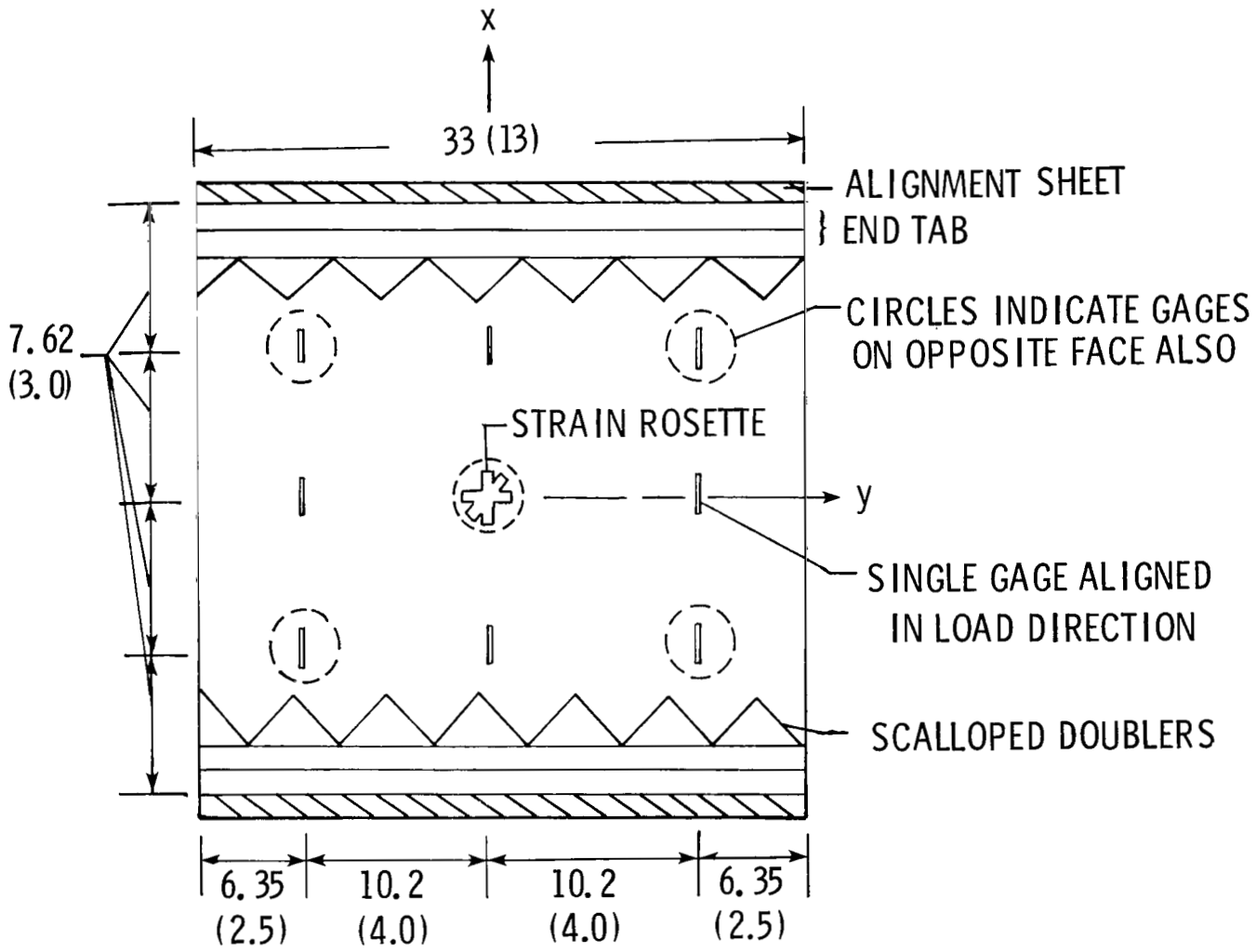

Figure 7.- Schematic diagram of strain-gage locations on buckling specimens. Dimensions are in centimeters (inches).

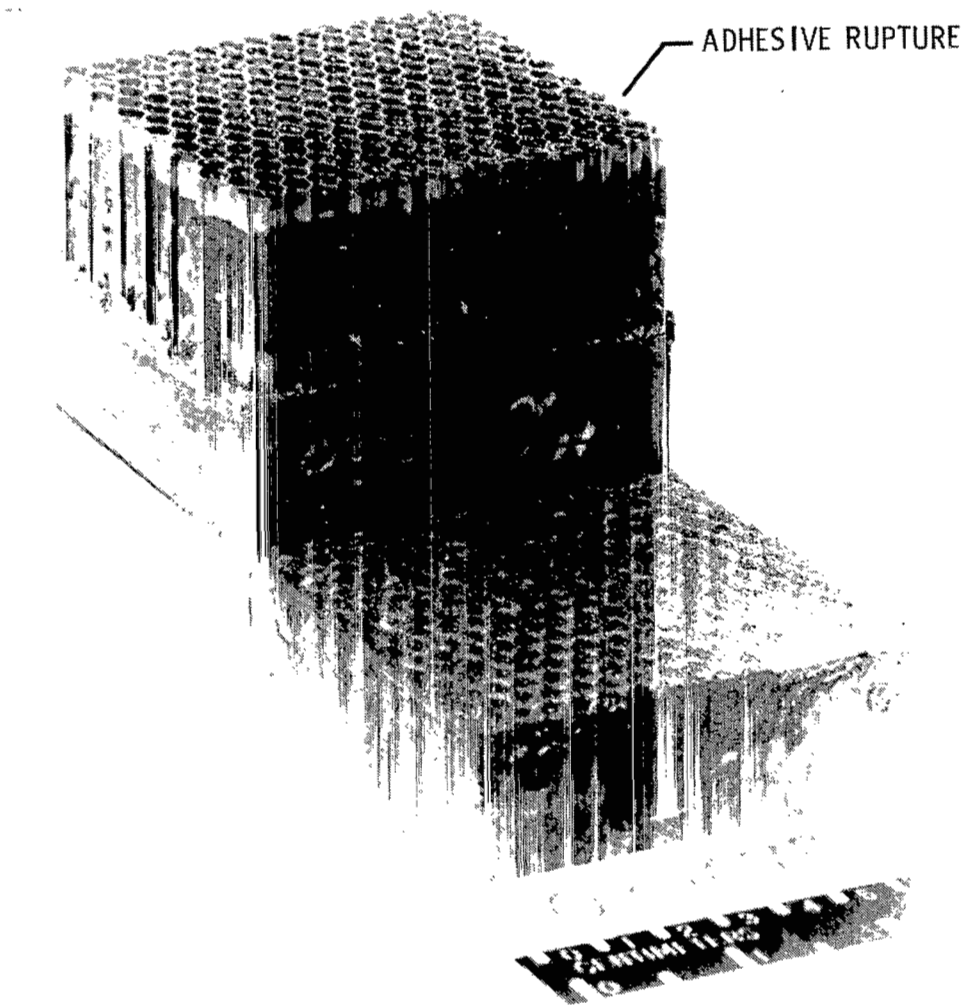

L-80-233

Figure 8.- Failed flatwise-tensile specimen (failure at bondline). Room temperature; σ_{cr} = 4.02 MPa (583 psi); FM-34 film adhesive.

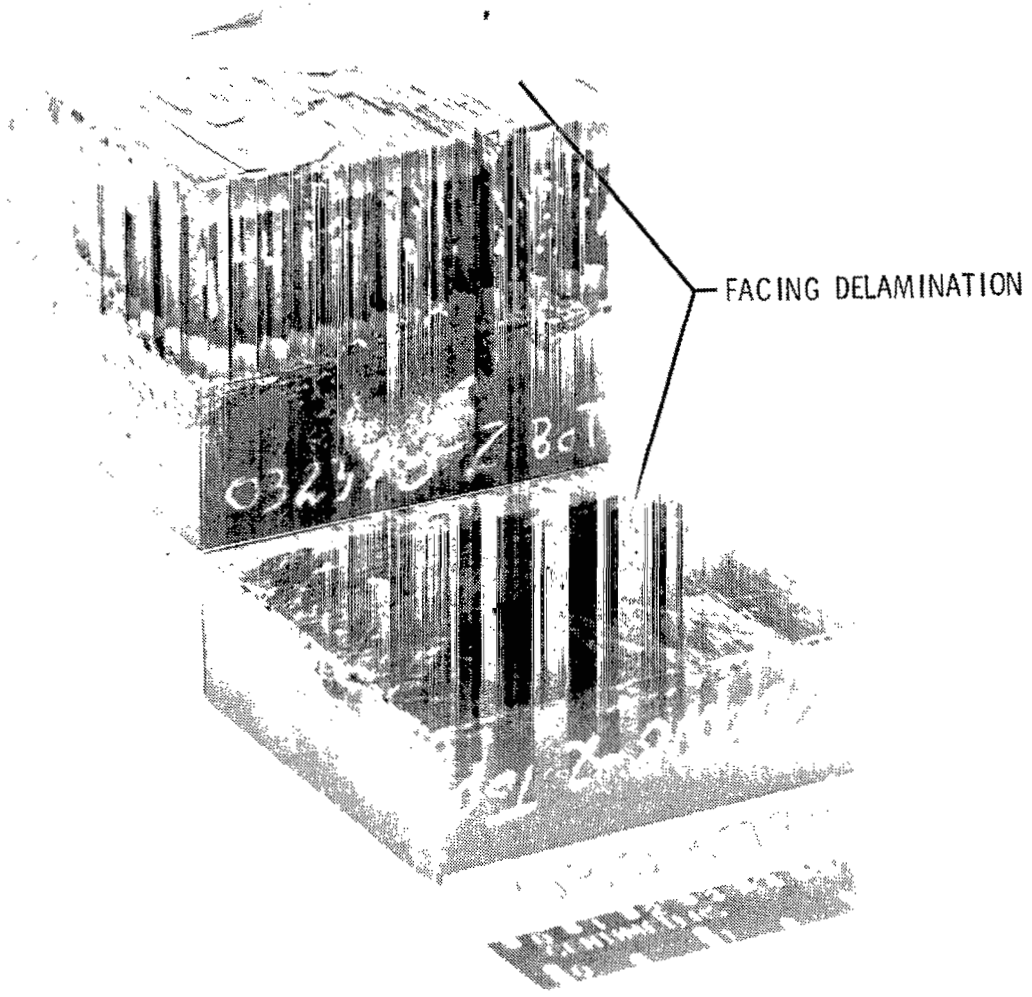

L-80-234

Figure 9.- Failed flatwise-tensile specimen (failure by facing delamination). Room temperature; σ_{cr} = 4.00 MPa (580 psi); FM-34 film adhesive.

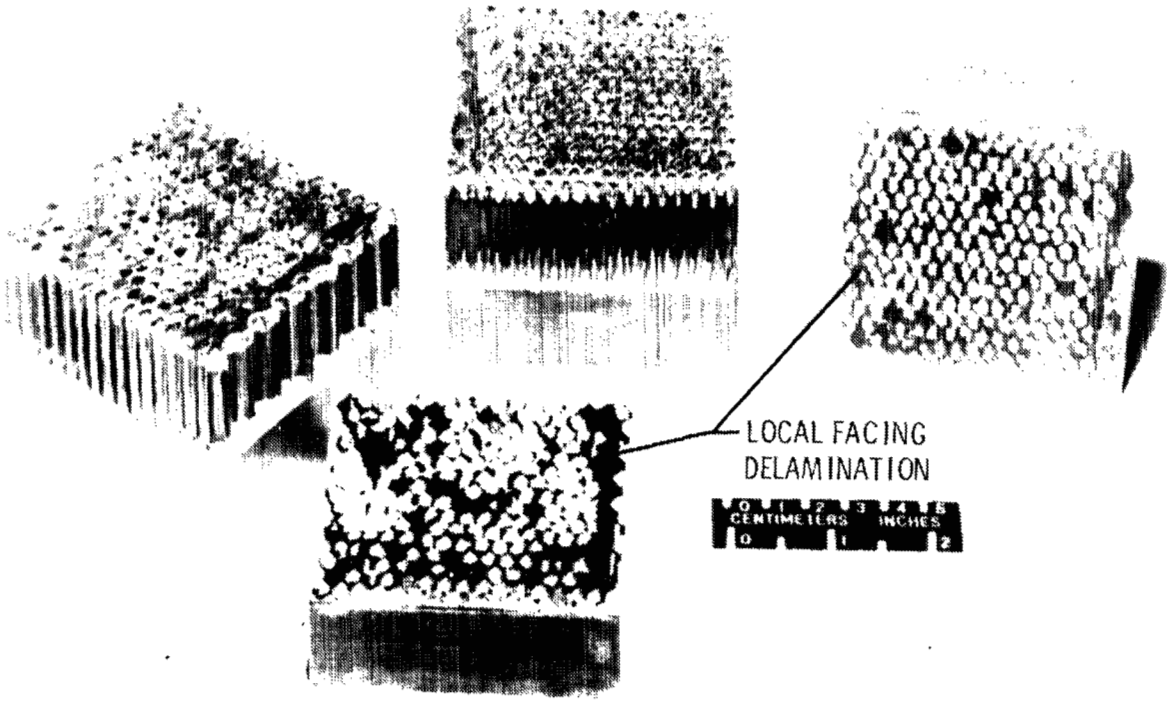

L-80-235

Figure 10.- Failed flatwise-tensile specimens. Room temperature; BR-34 liquid cell-edge adhesive.

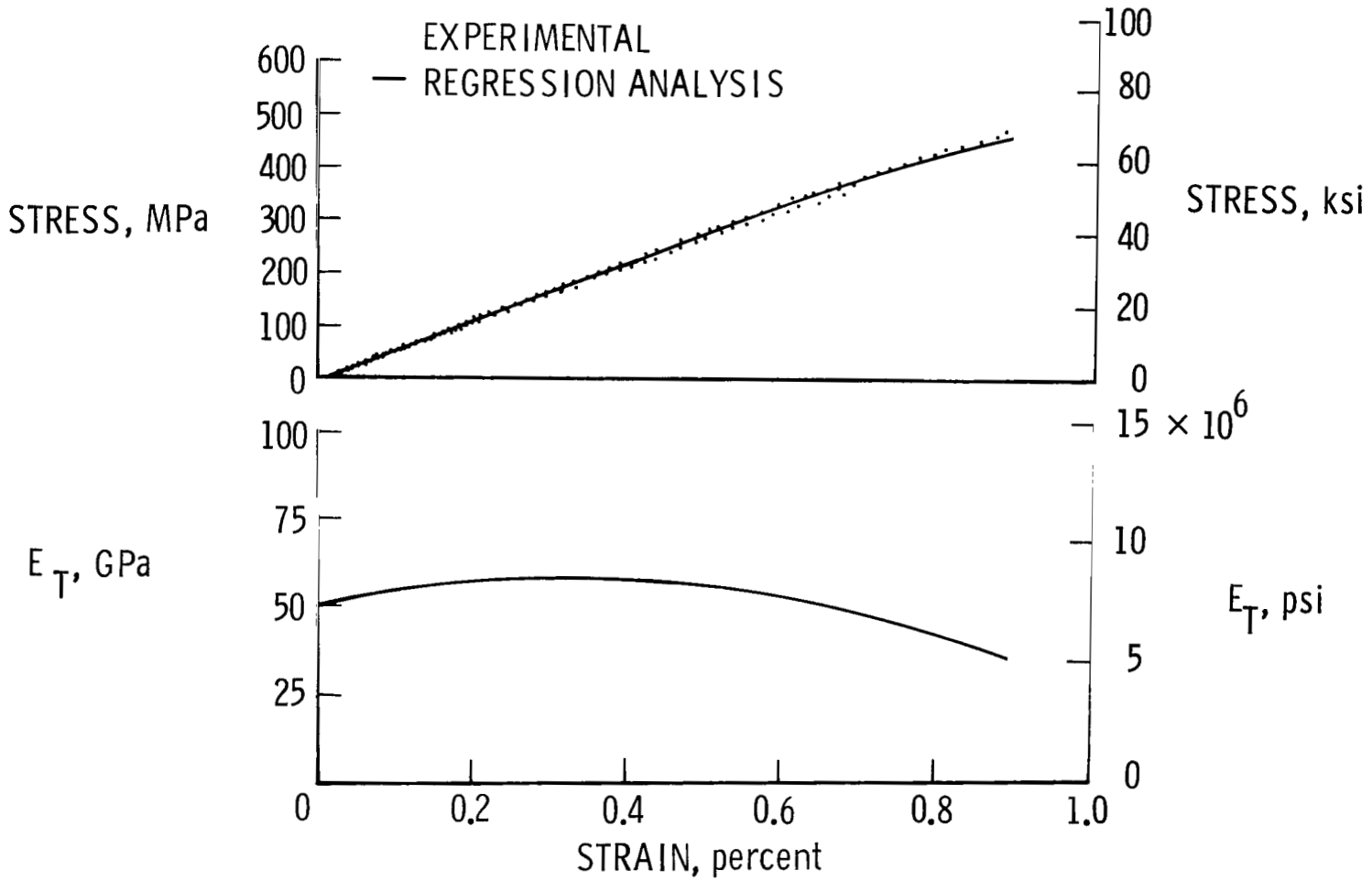

Figure 11.- Tensile stress and tangent modulus behavior of $[0,+45,90,-45]_s$ Celion 6000/PMR-15 at room temperature. Tests 1 to 4.

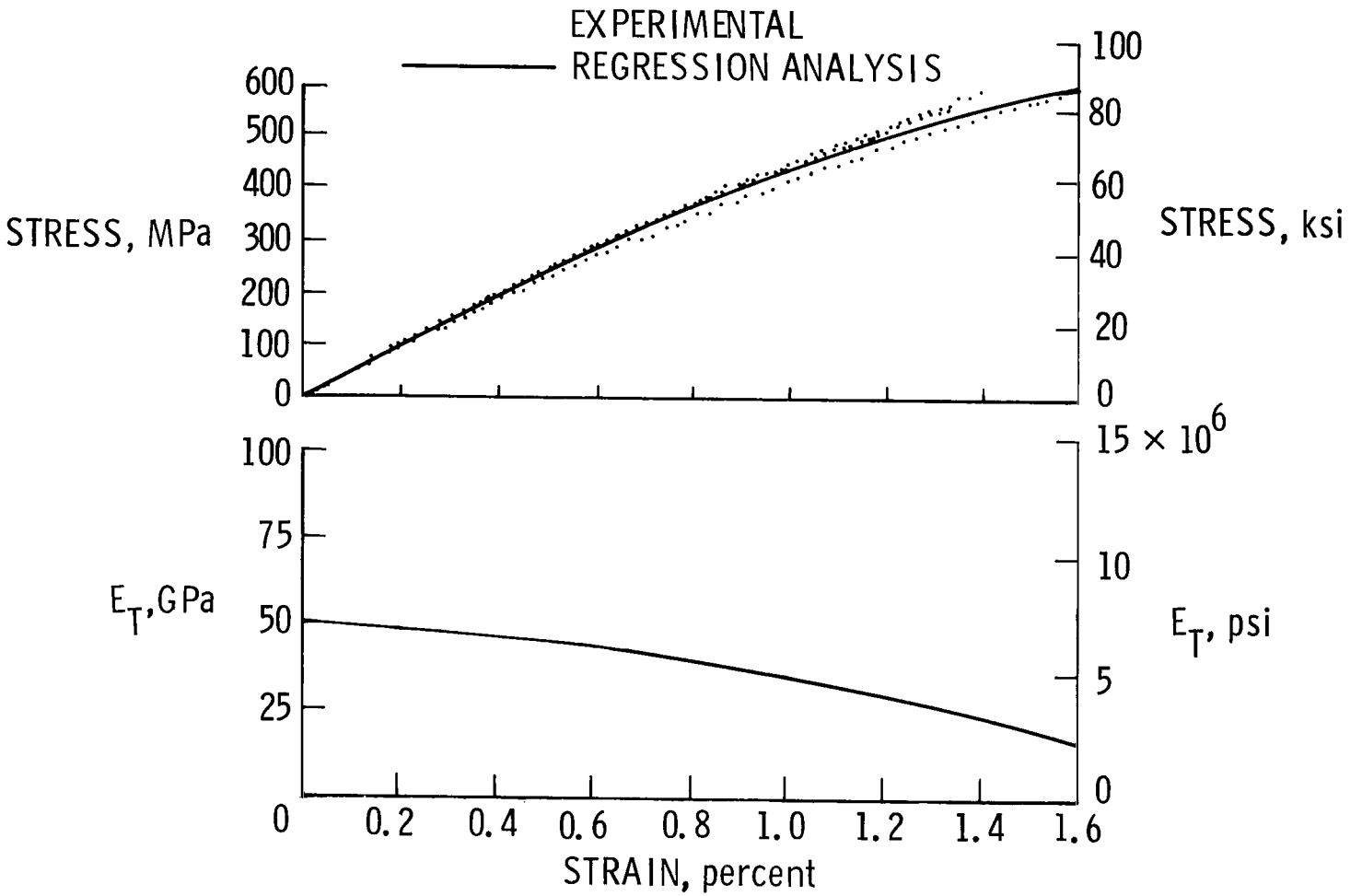

Figure 12.- Compressive stress and tangent modulus behavior of $[0,+45,90,-45]_s$ Celion 6000/PMR-15 at room temperature. Tests 5 to 8.

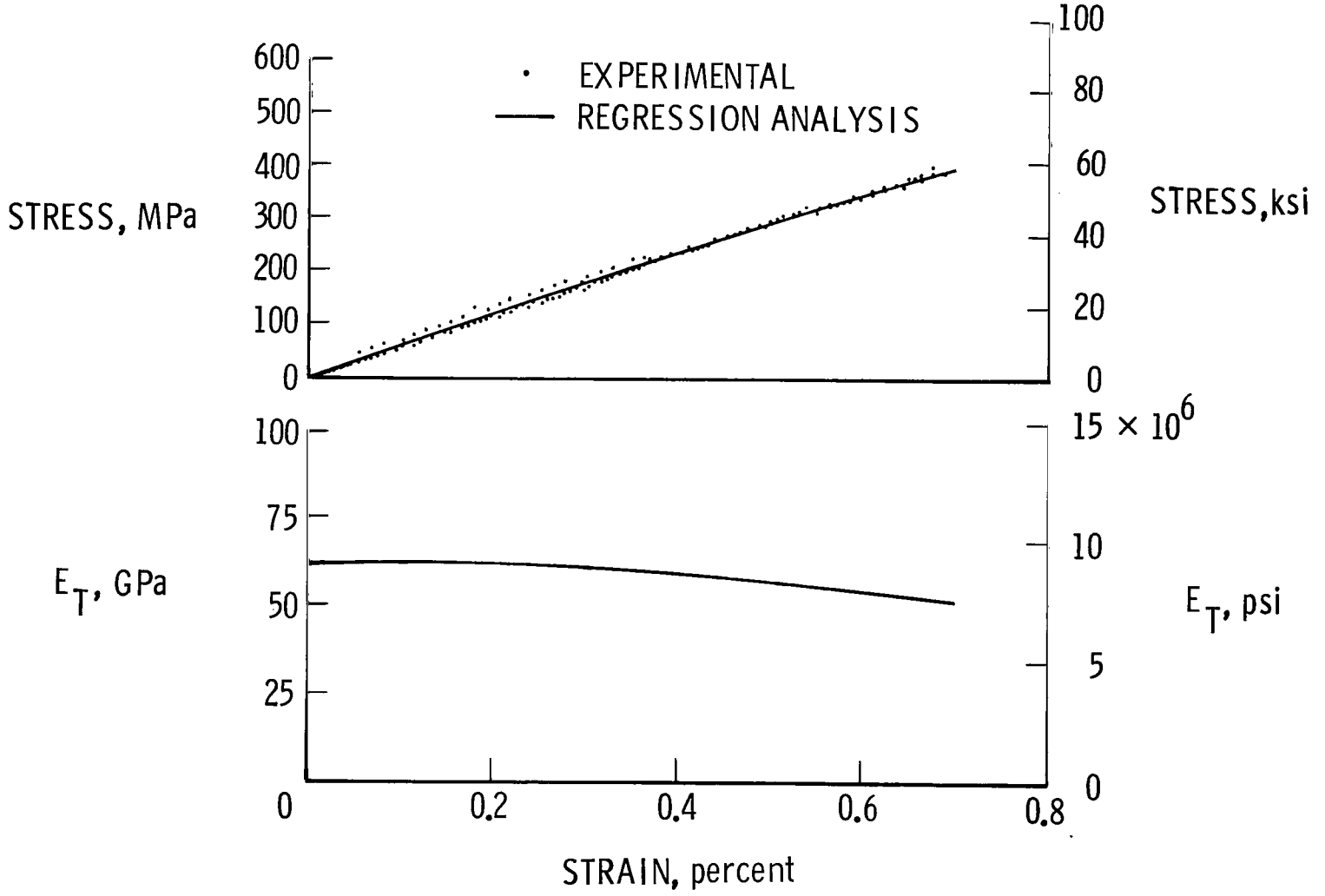

Figure 13.- Tensile stress and tangent modulus behavior of $[0,+45,90,-45]_s$ Celion 6000/PMR-15 at 116 K (-250°F). Tests 9 to 12.

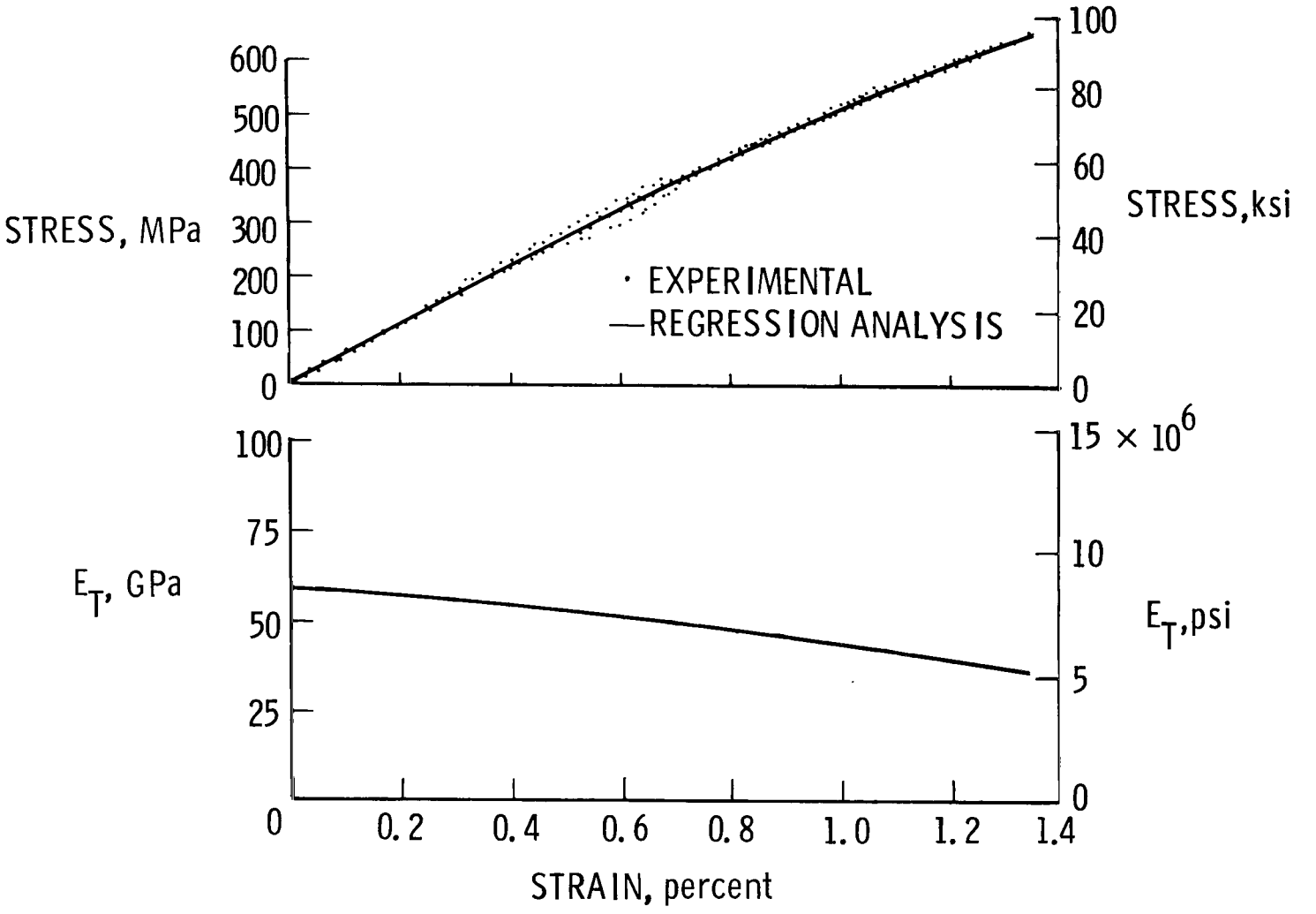

Figure 14.- Compressive stress and tangent modulus behavior of $[0,+45,90,-45]_s$ Celion 6000/PMR-15 at 116 K (-250°F). Tests 13 to 16.

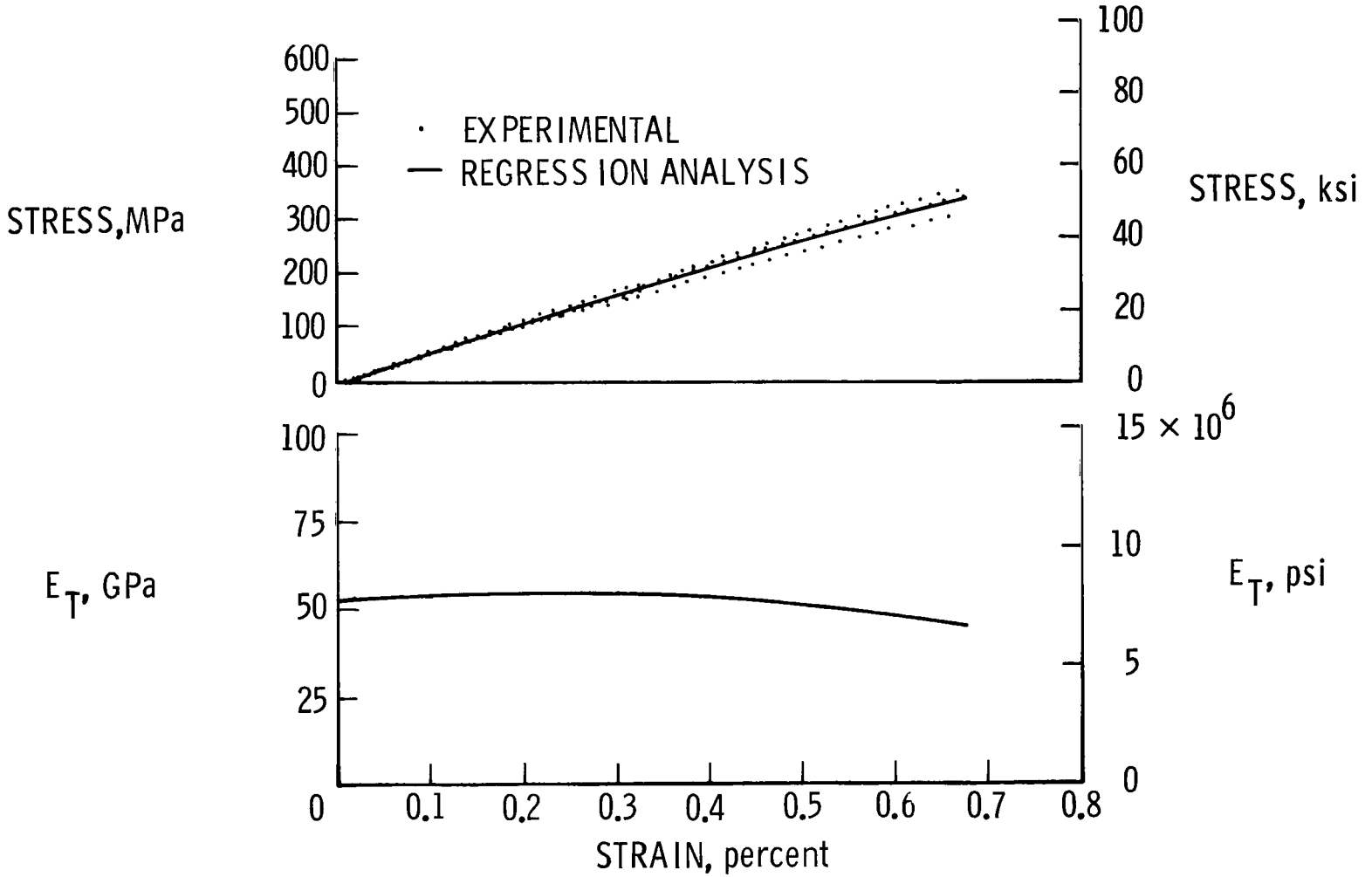

Figure 15.- Tensile stress and tangent modulus behavior of $[0,+45,90,-45]_s$ Celion 6000/PMR-15 at 589 K (600°F). Tests 17 to 20.

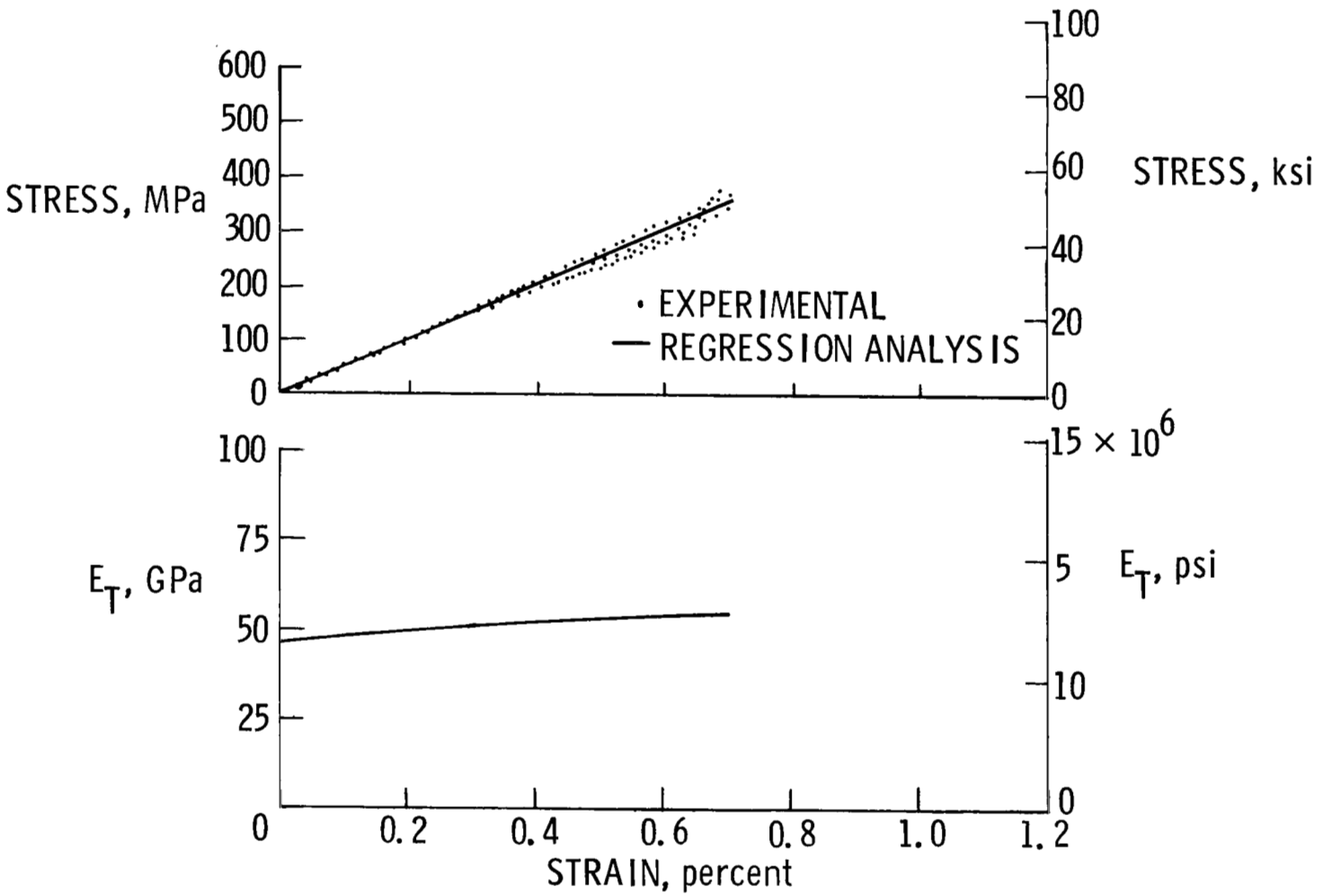

Figure 16.- Compressive stress and tangent modulus behavior of $[0,+45,90,-45]_s$ Celion 6000/PMR-15 at 589 K (600°F). Tests 21 to 24.

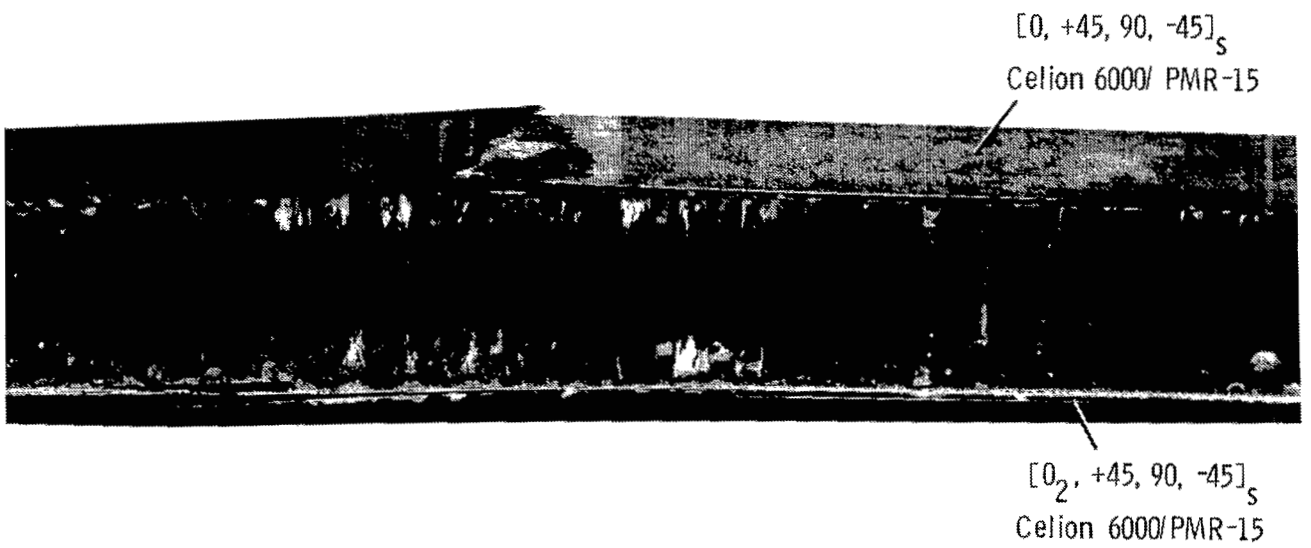

L-80-236

Figure 17.- Failed sandwich-beam-flexure specimen; tensile test.

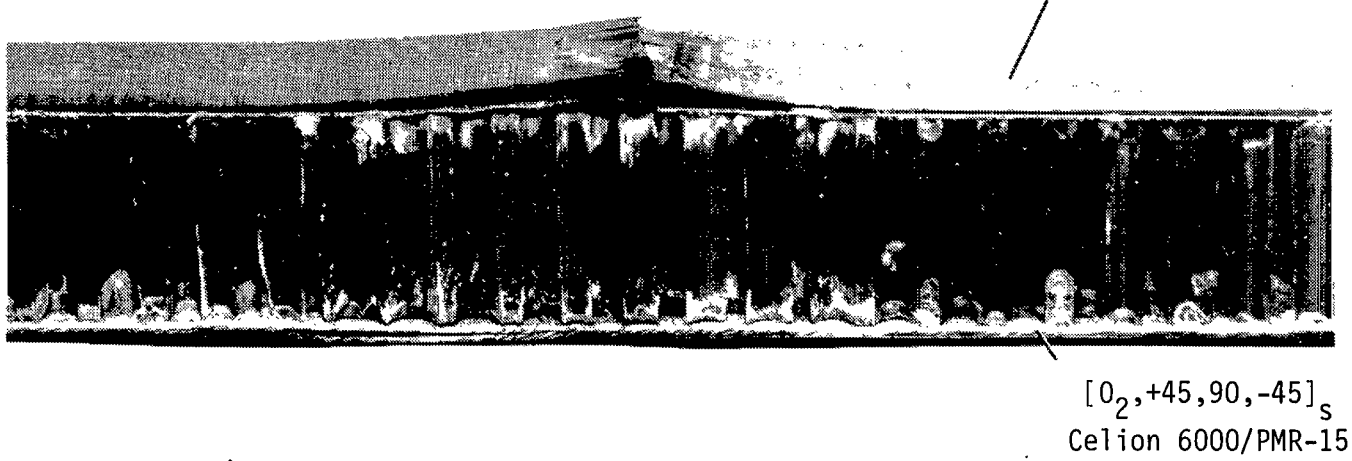

L-80-237

Figure 18.- Failed sandwich-beam-flexure specimen; compressive test.

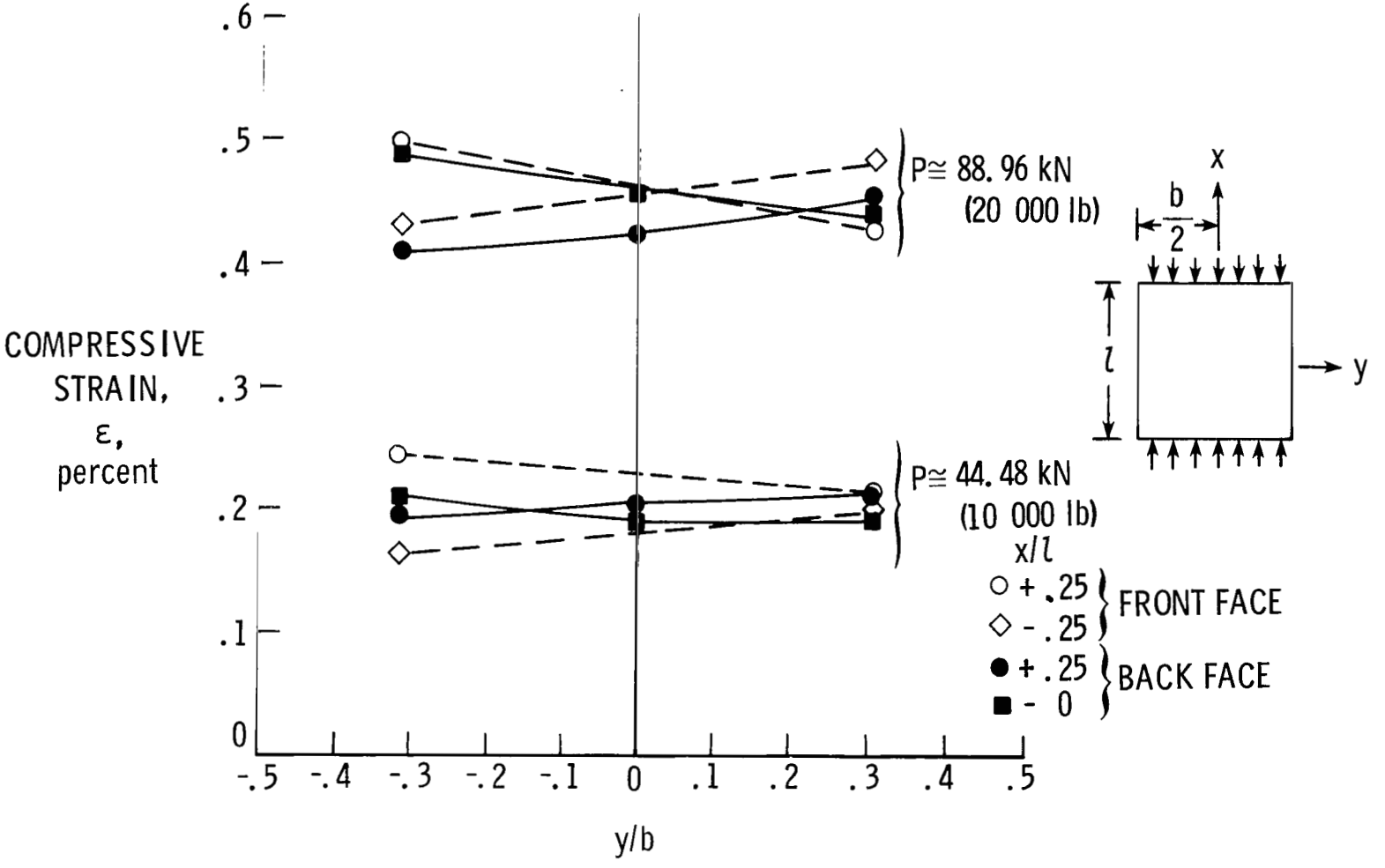

(a) Panel BT-9.

Figure 19.- Strain variation across panel width during loading.

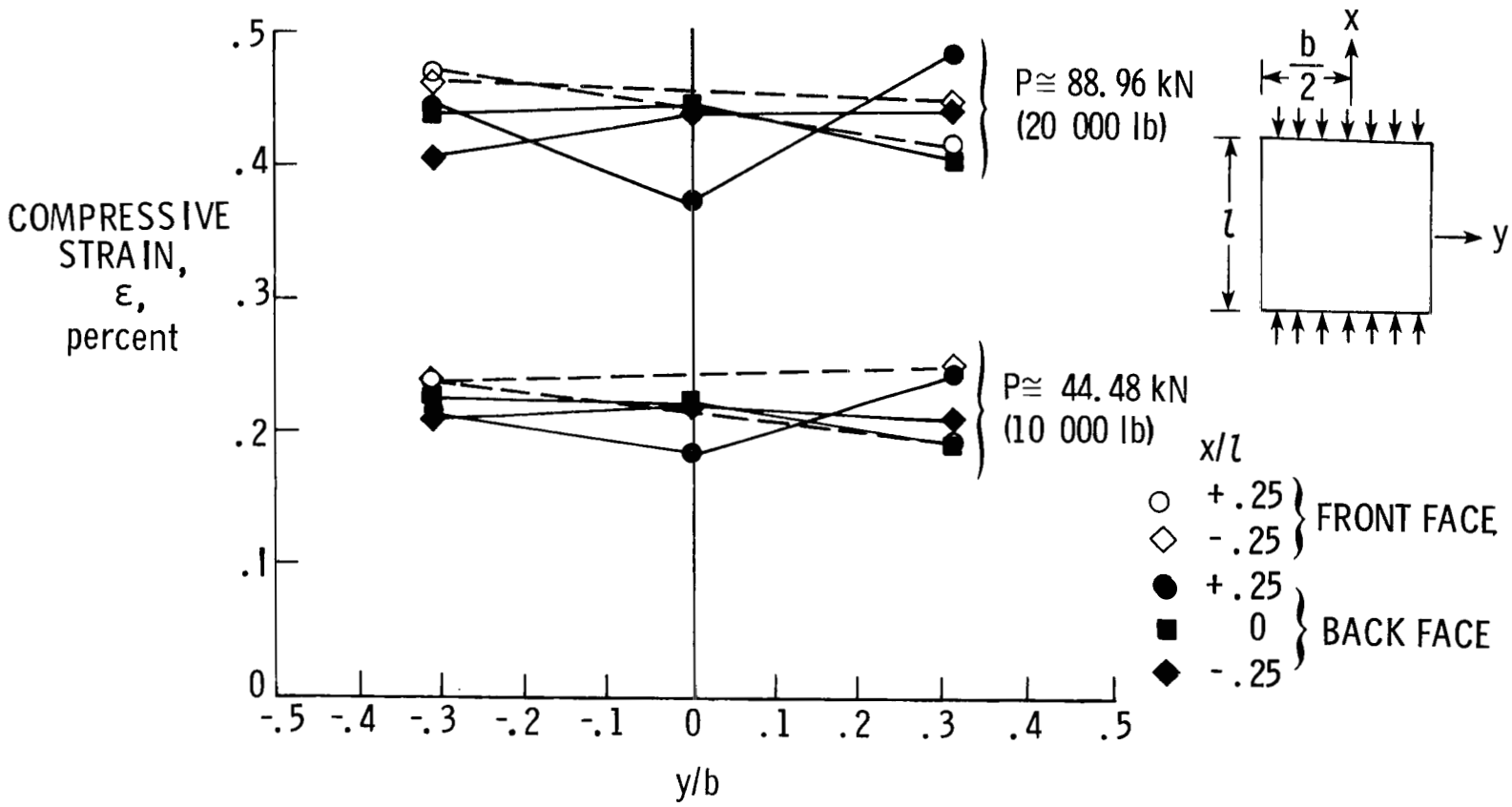

(b) Panel BT-8.

Figure 19.- Concluded.

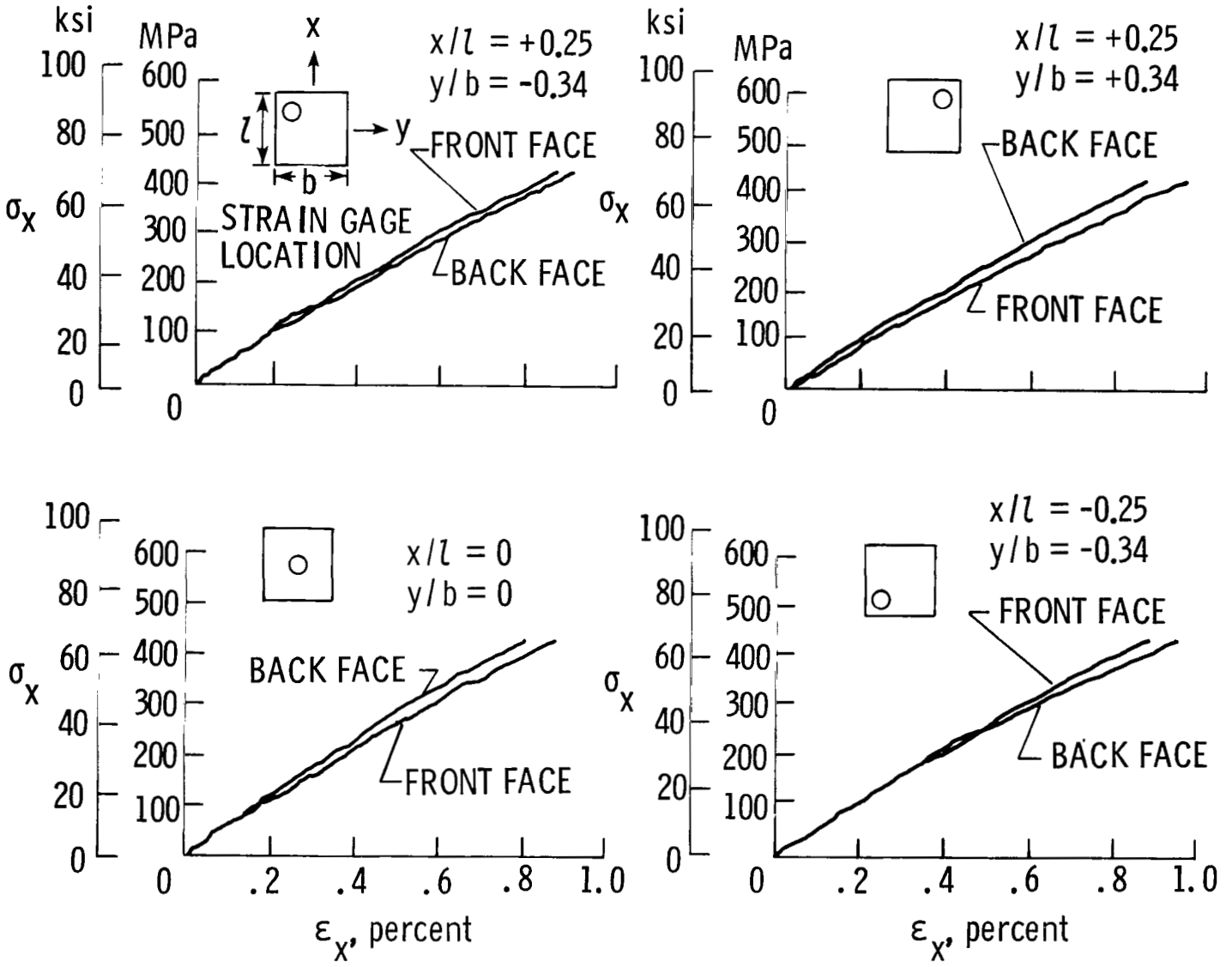

(a) Panel BT-5.

Figure 20.- Back-to-back stress-strain results at four locations on wrinkling specimens.

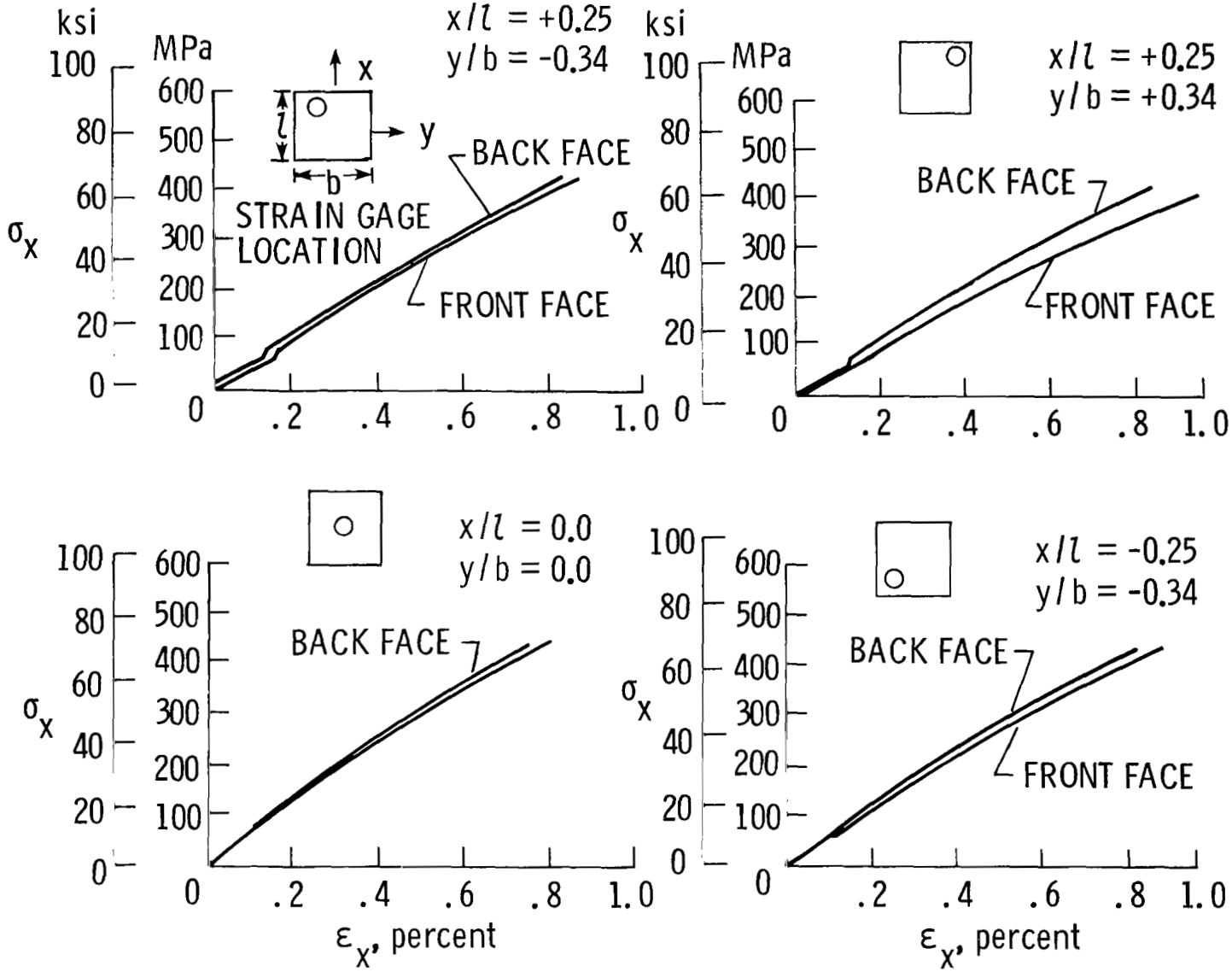

(b) Panel BT-6.

Figure 20.- Concluded.

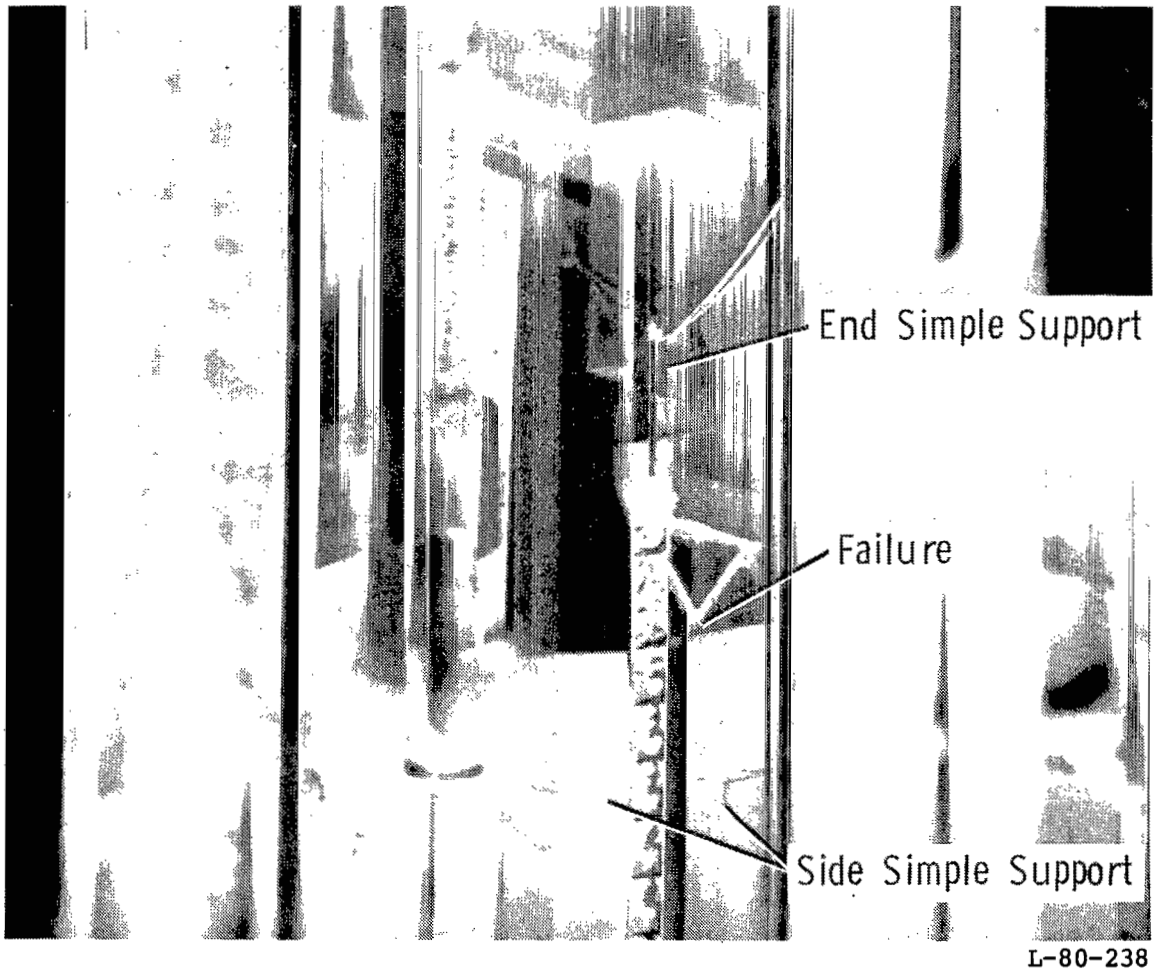

(a) Side view.

Figure 21.- Failure near side simple support. Wrinkling specimen; t_c = 1.27 cm (0.50 in.).

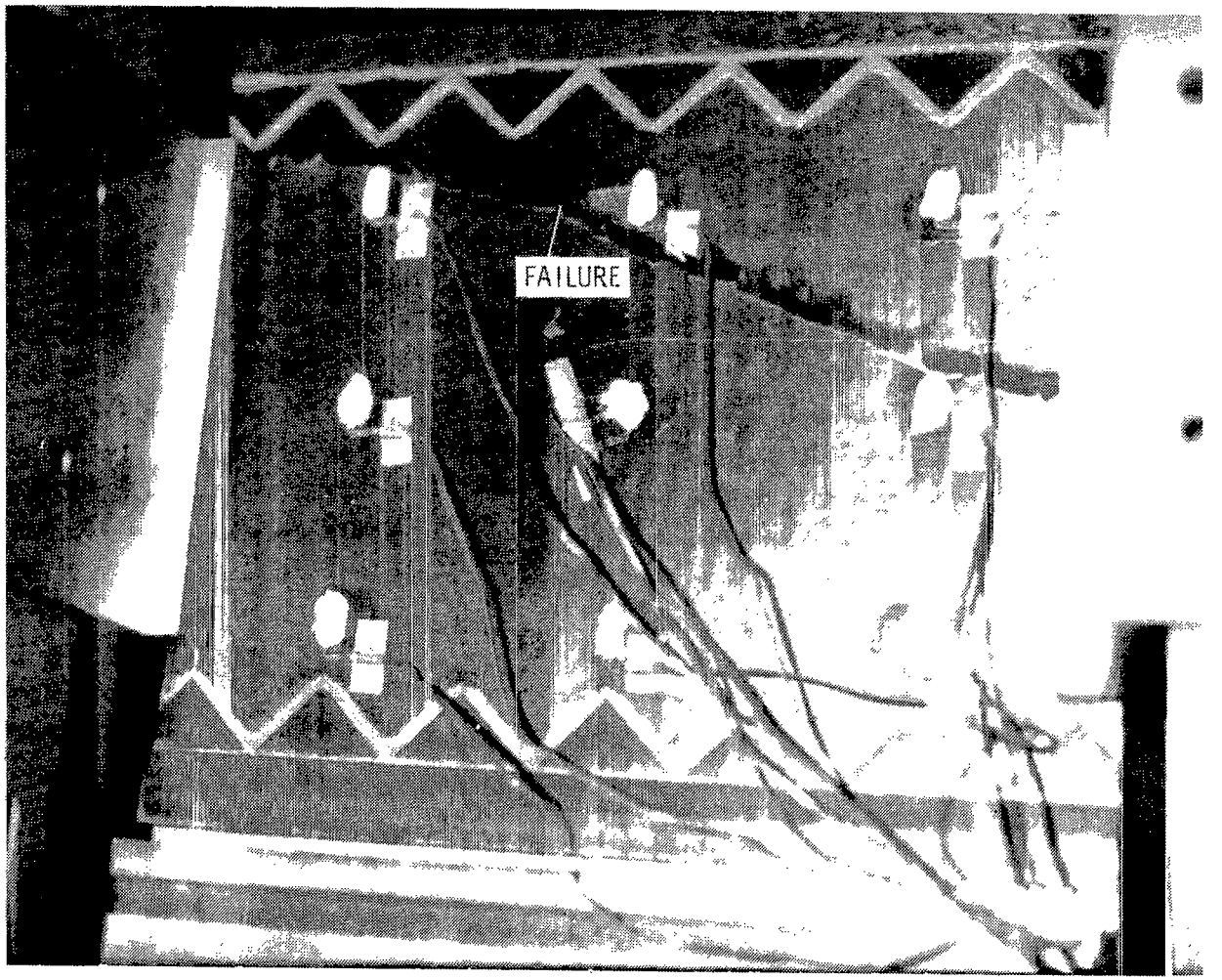

L-80-239

(b) Rear view.

Figure 21.- Concluded.

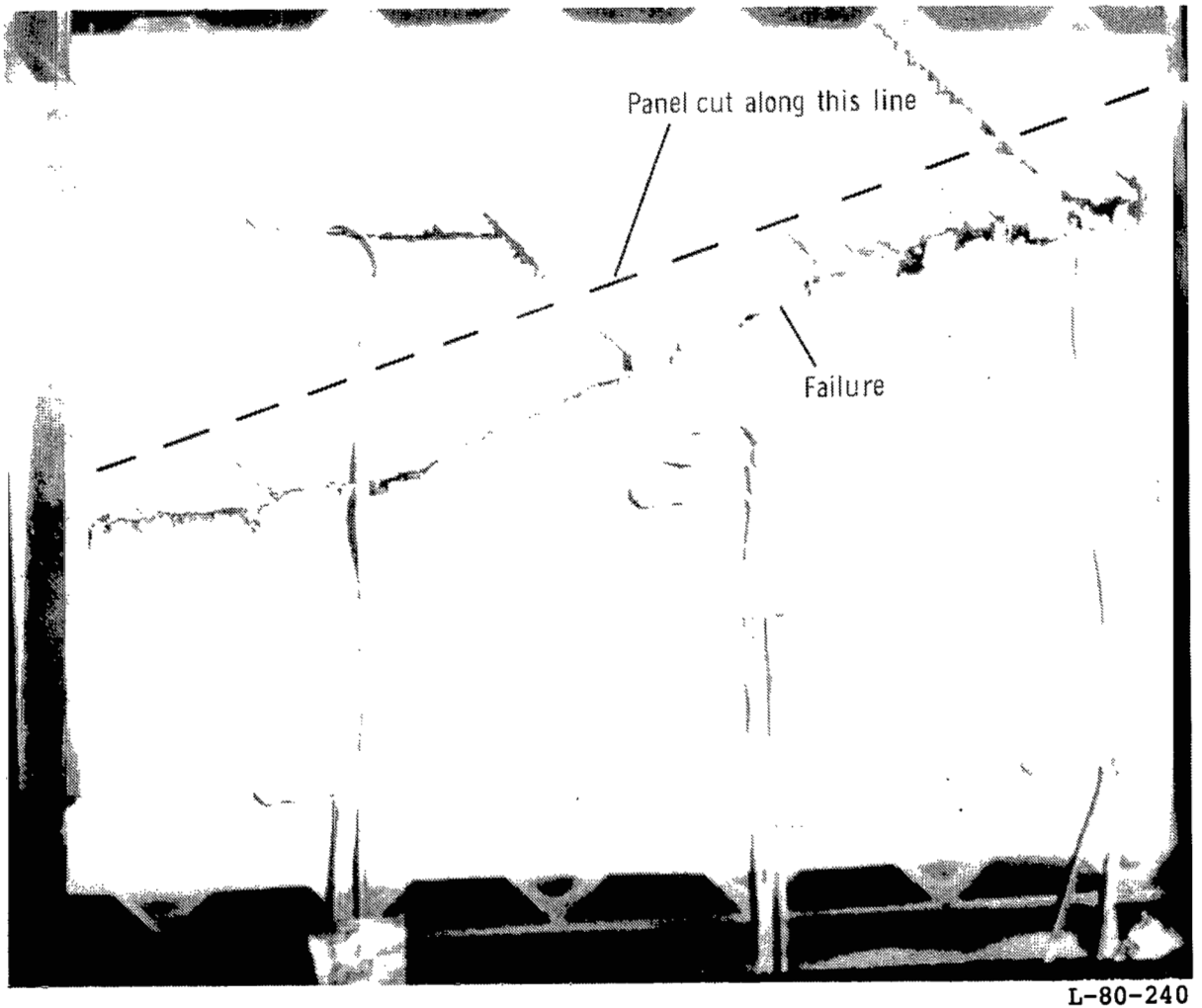

(a) Front view.

Figure 22.- Failed wrinkling specimen (panel BT-4).

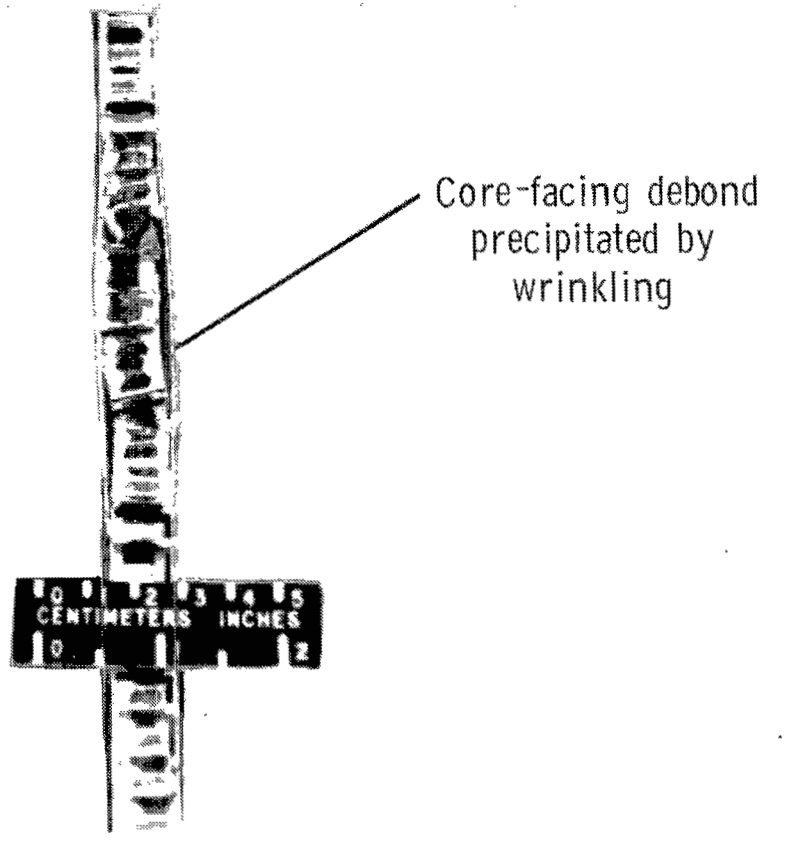

L-80-241

(b) Cutaway view of buckled region.

Figure 22.- Concluded.

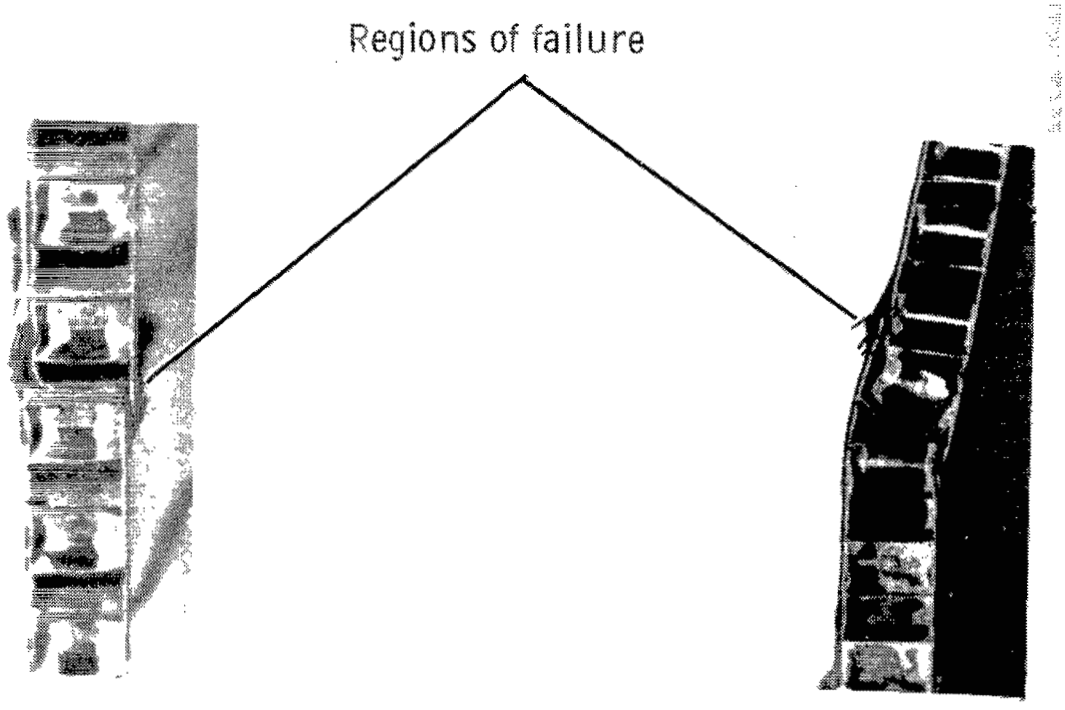

L-80-242

Figure 23.- Side view of two failed wrinkling specimens.
t_c = 1.27 cm (0.50 in.).

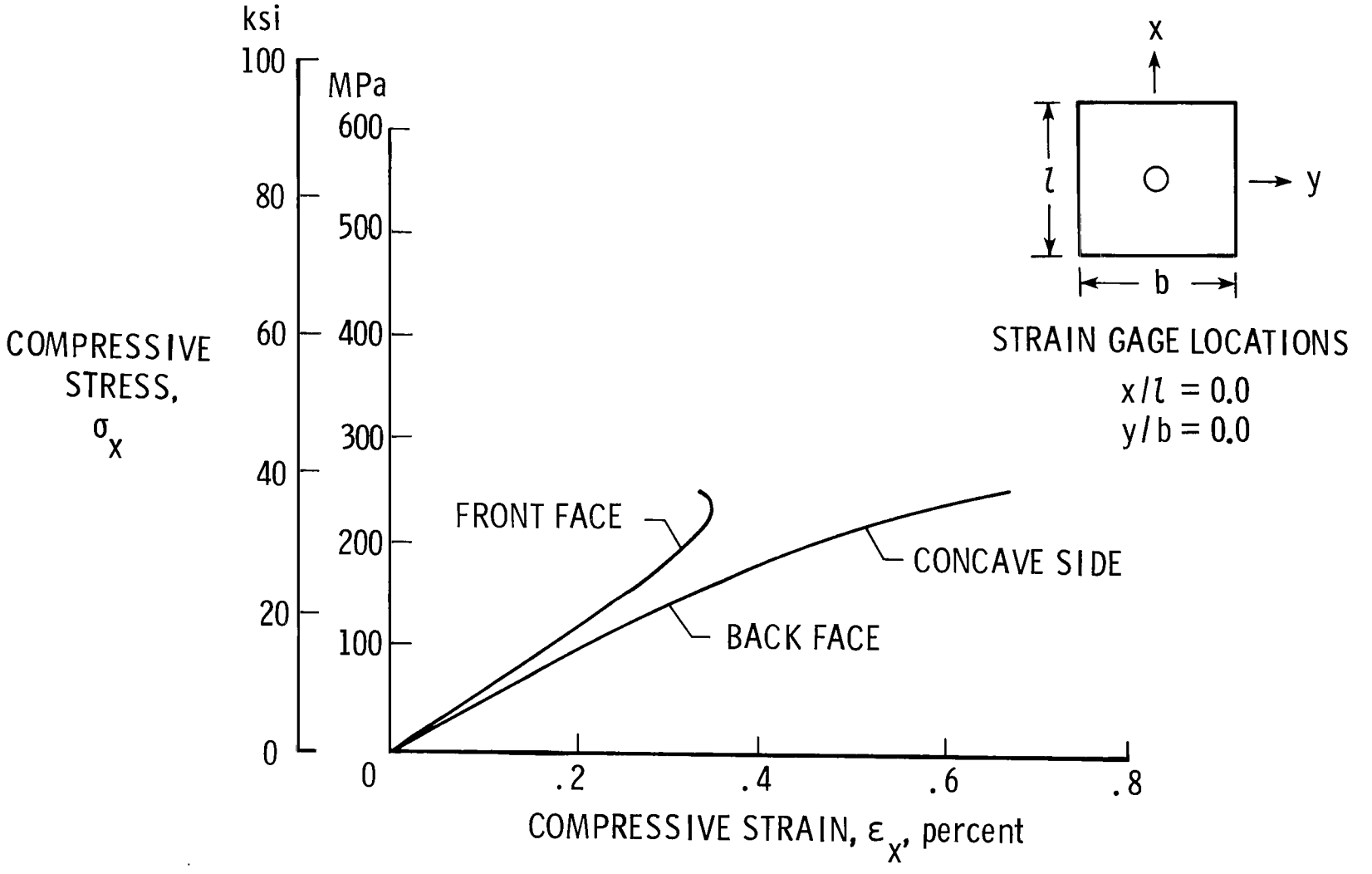

(a) Panel BT-1.

Figure 24.- Back-to-back stress-strain results of overall buckling specimens.

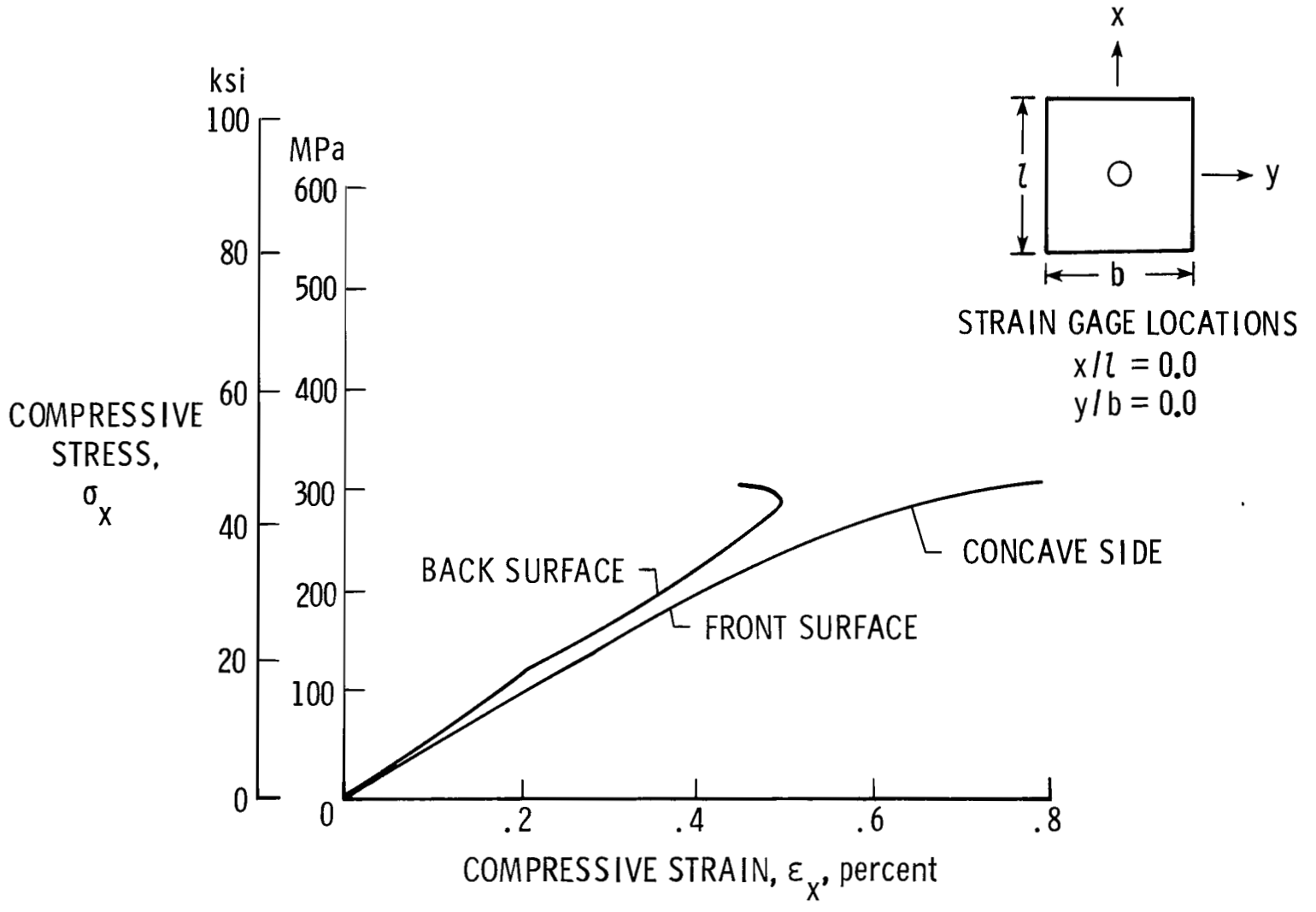

(b) Panel BT-2.

Figure 24.- Continued.

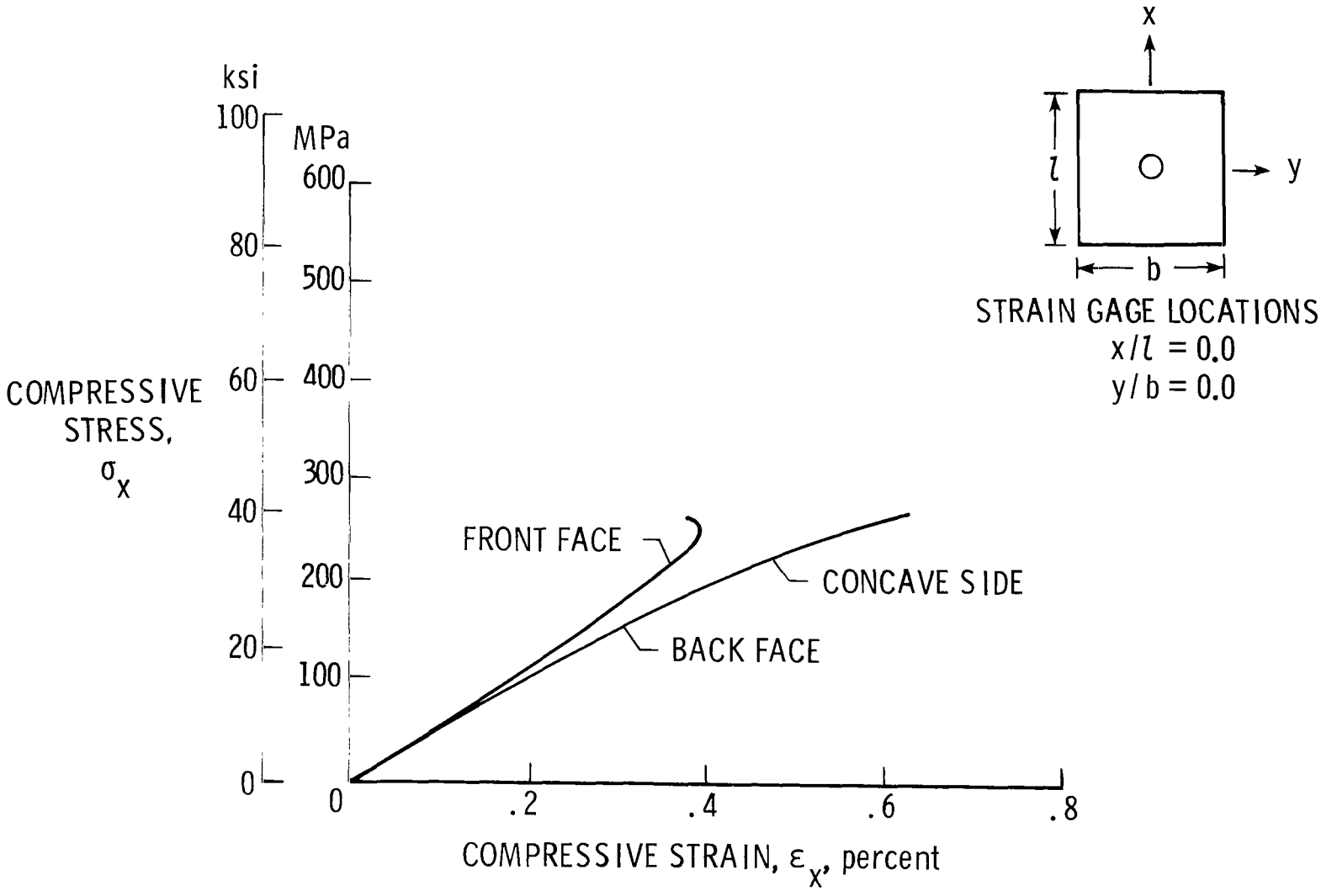

(c) Panel BT-3.

Figure 24.- Concluded.

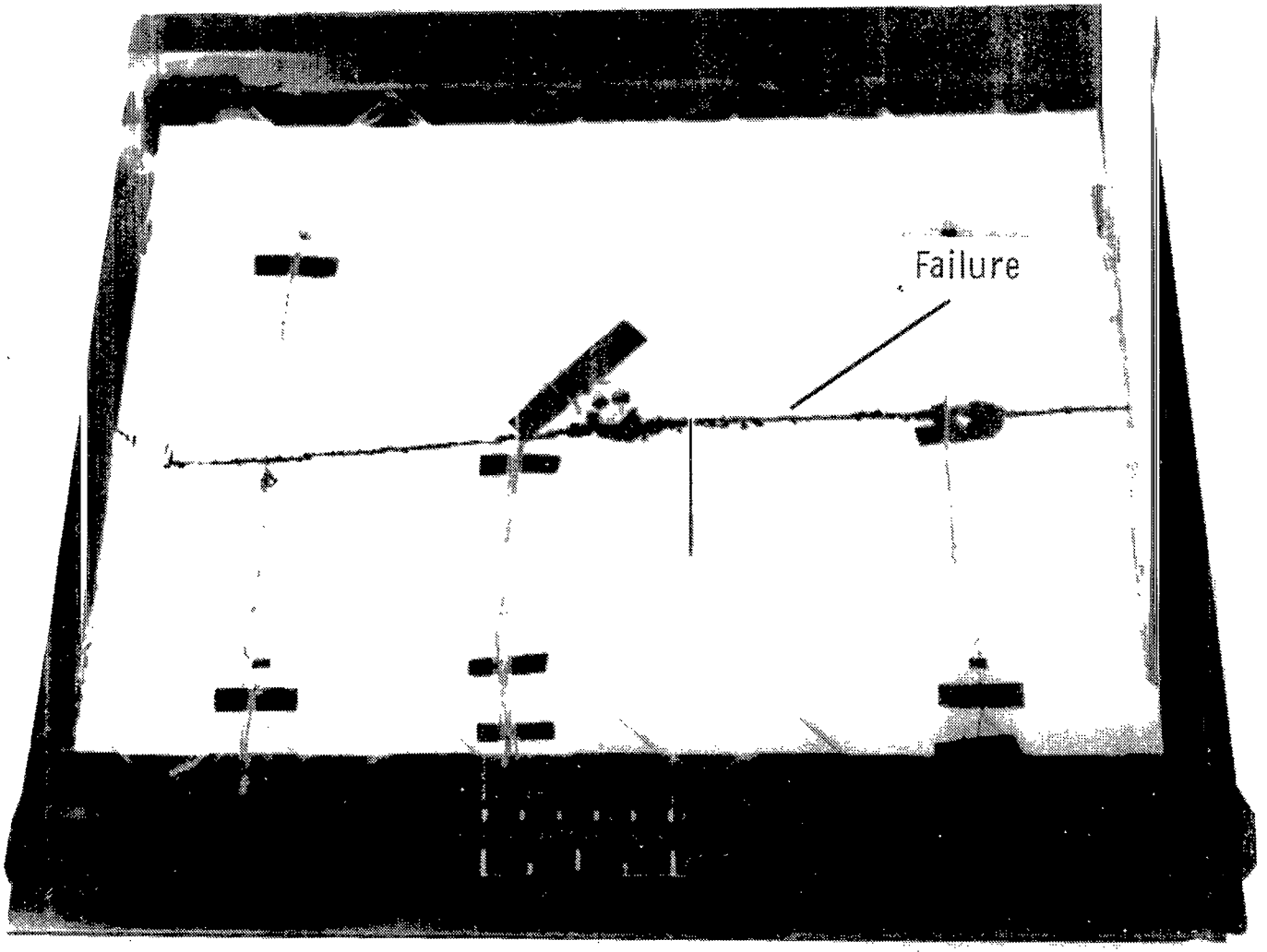

L-80-243

Figure 25.- Failed overall buckling specimen.

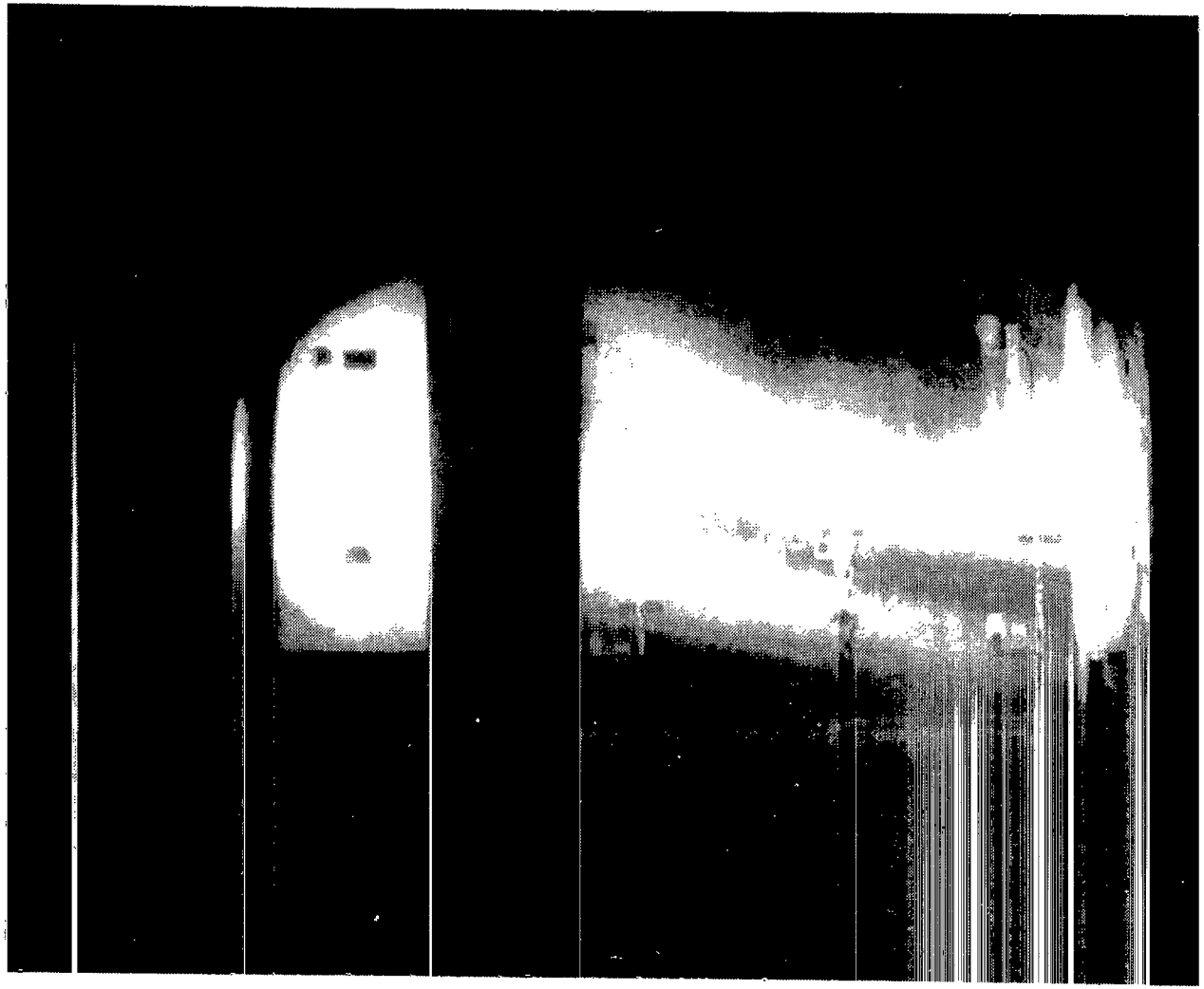

L-80-244

(a) $P/P_{ult} = 0.89$.

Figure 26.- Moiré fringe patterns of overall buckling specimen. Panel BT-2.

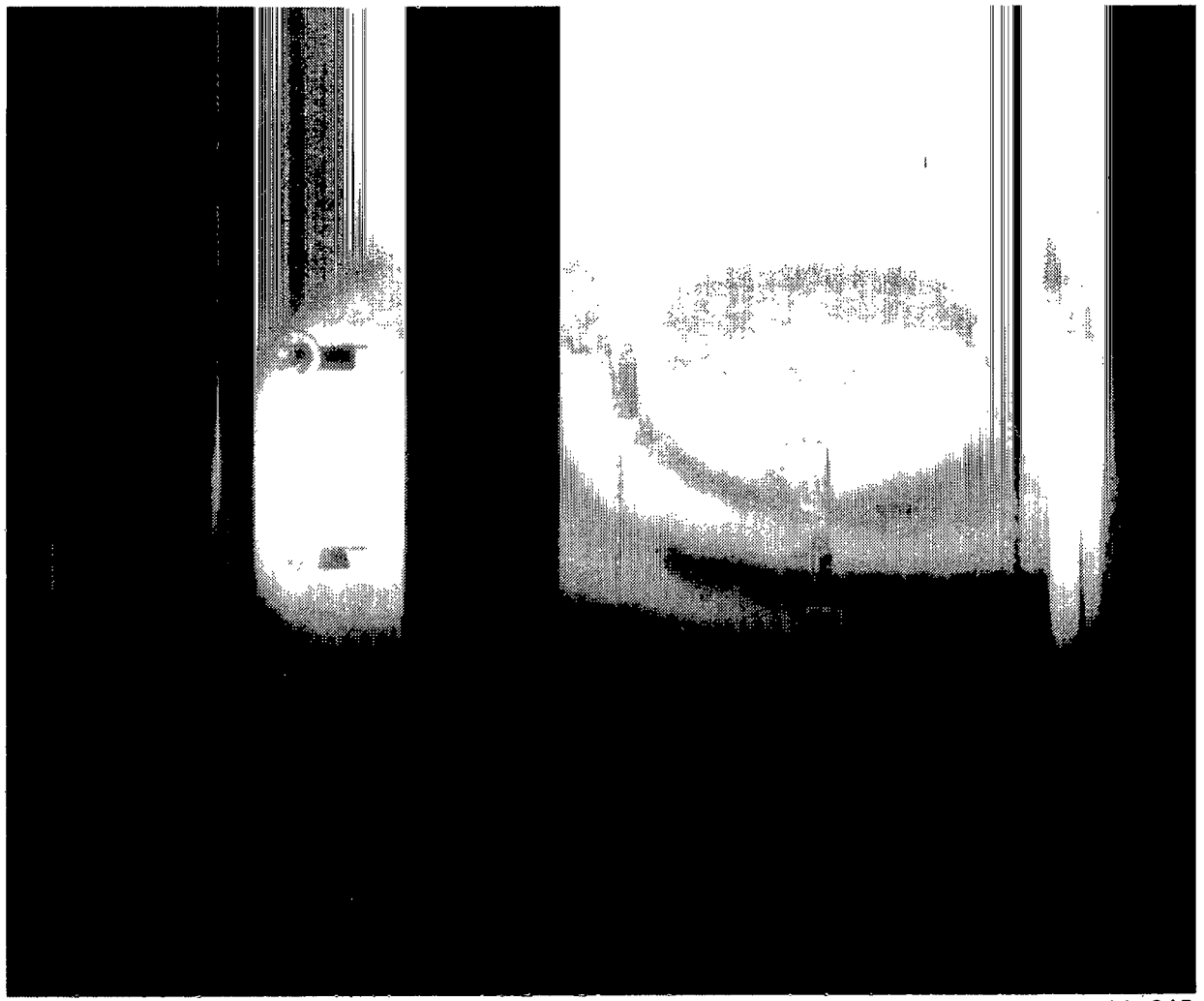

L-80-245

(b) $P/P_{ult} = 0.94$.

Figure 26.- Continued.

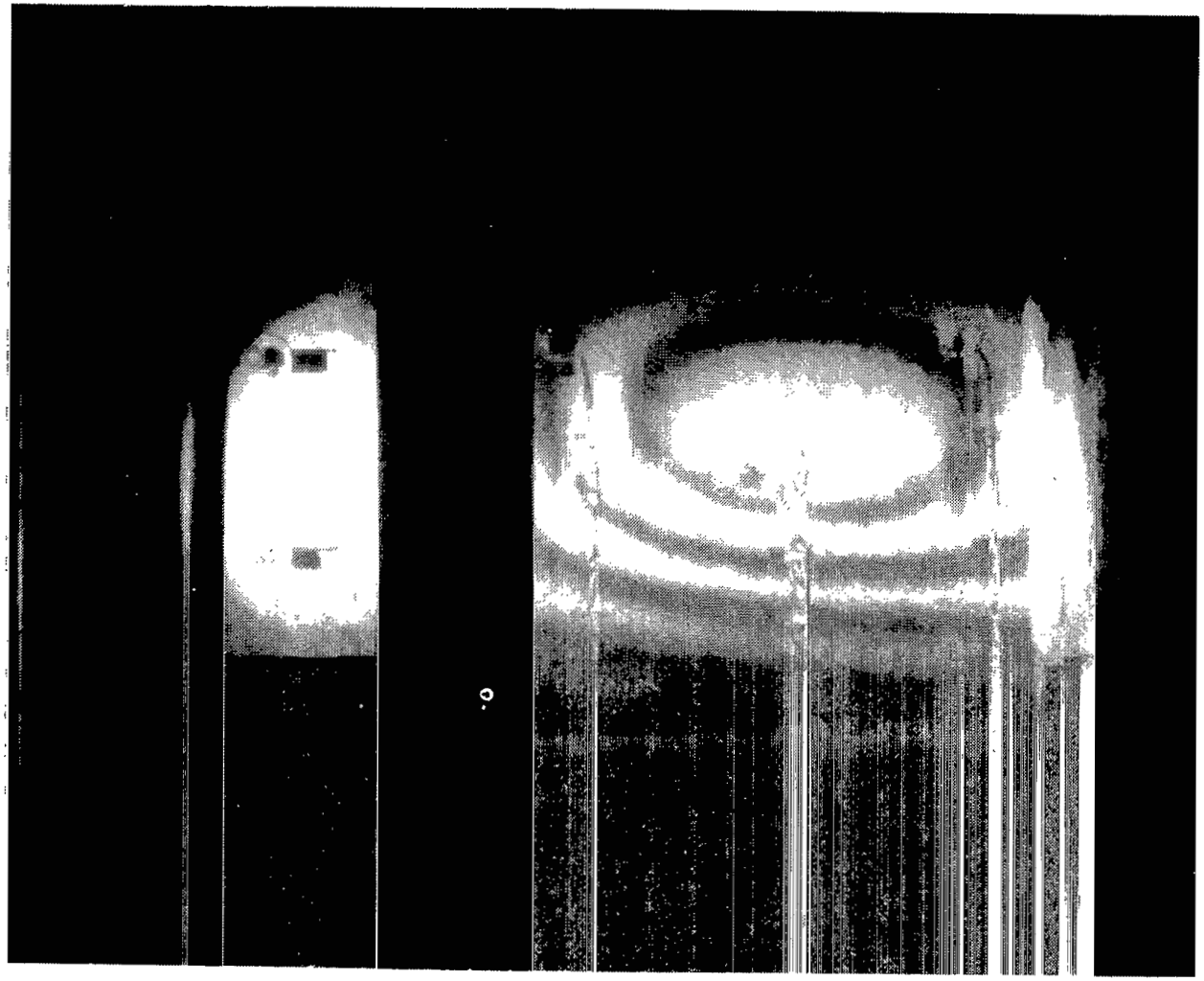

L-80-246

(c) $P/P_{ult} = 1.0$.

Figure 26.- Concluded.

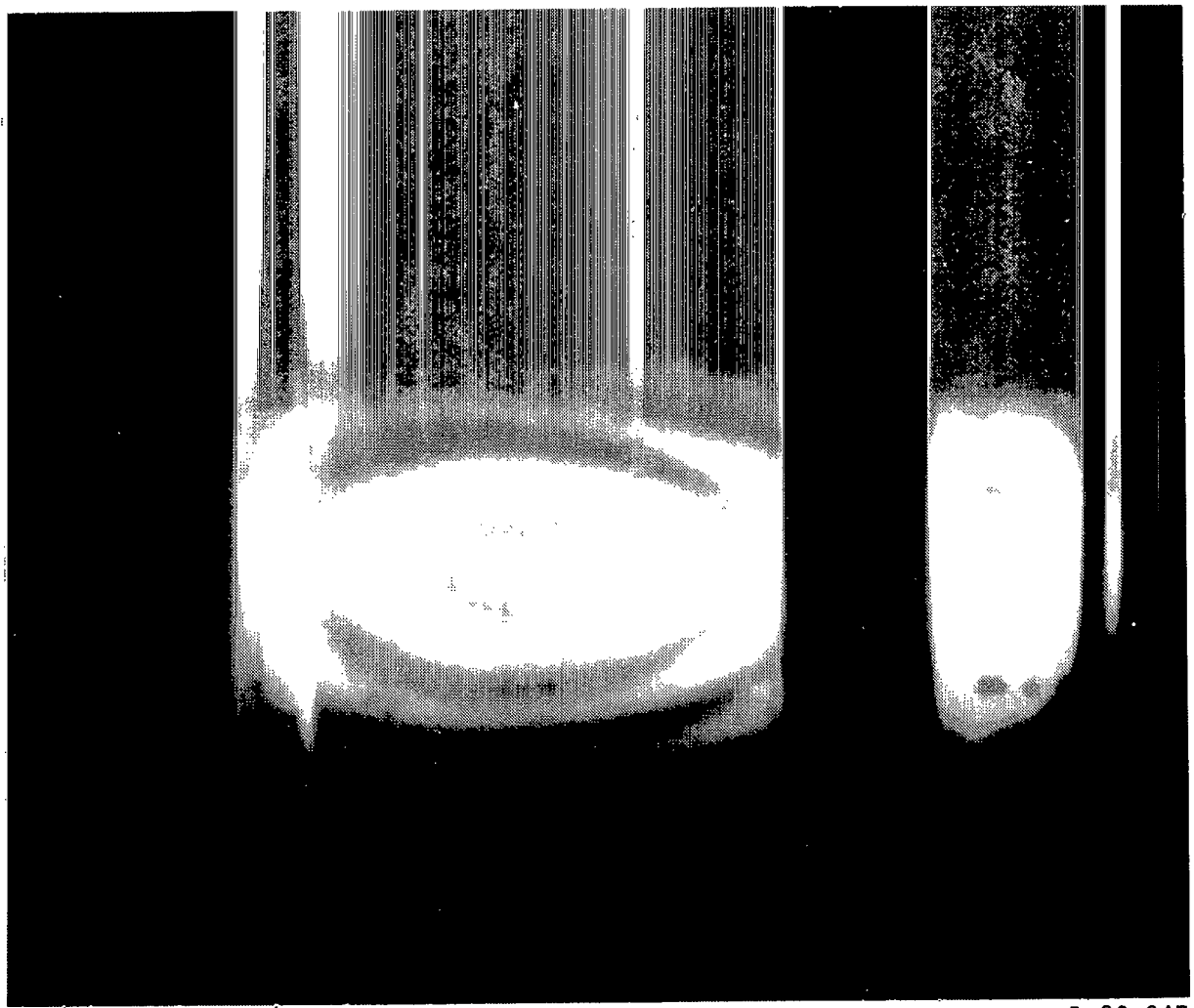

L-80-247

(a) $P/P_{ult} = 0.72$.

Figure 27.- Moire' fringe patterns of overall buckling specimen (typical).

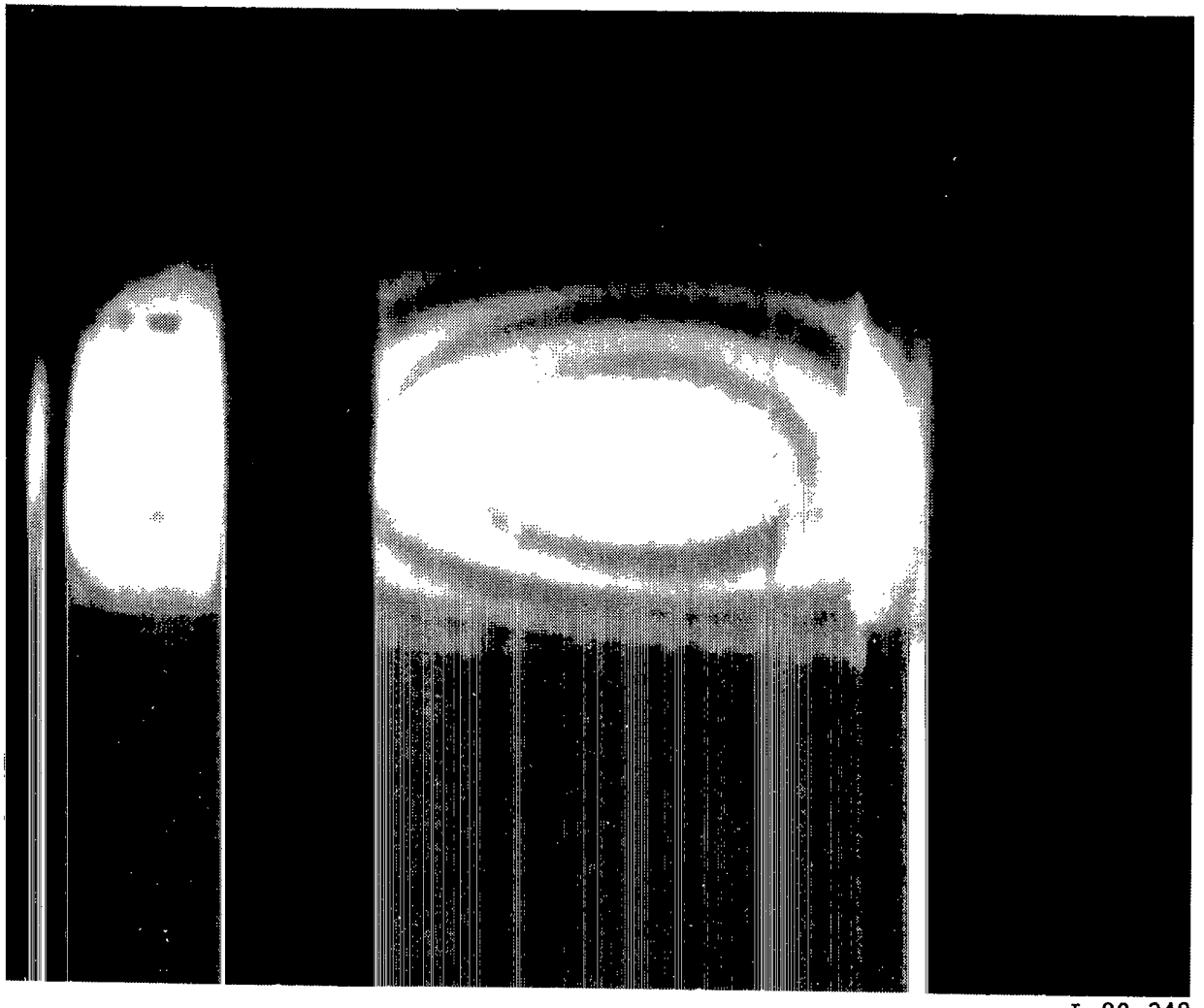

L-80-248

(b) $P/P_{ult} = 0.99$.

Figure 27.- Continued.

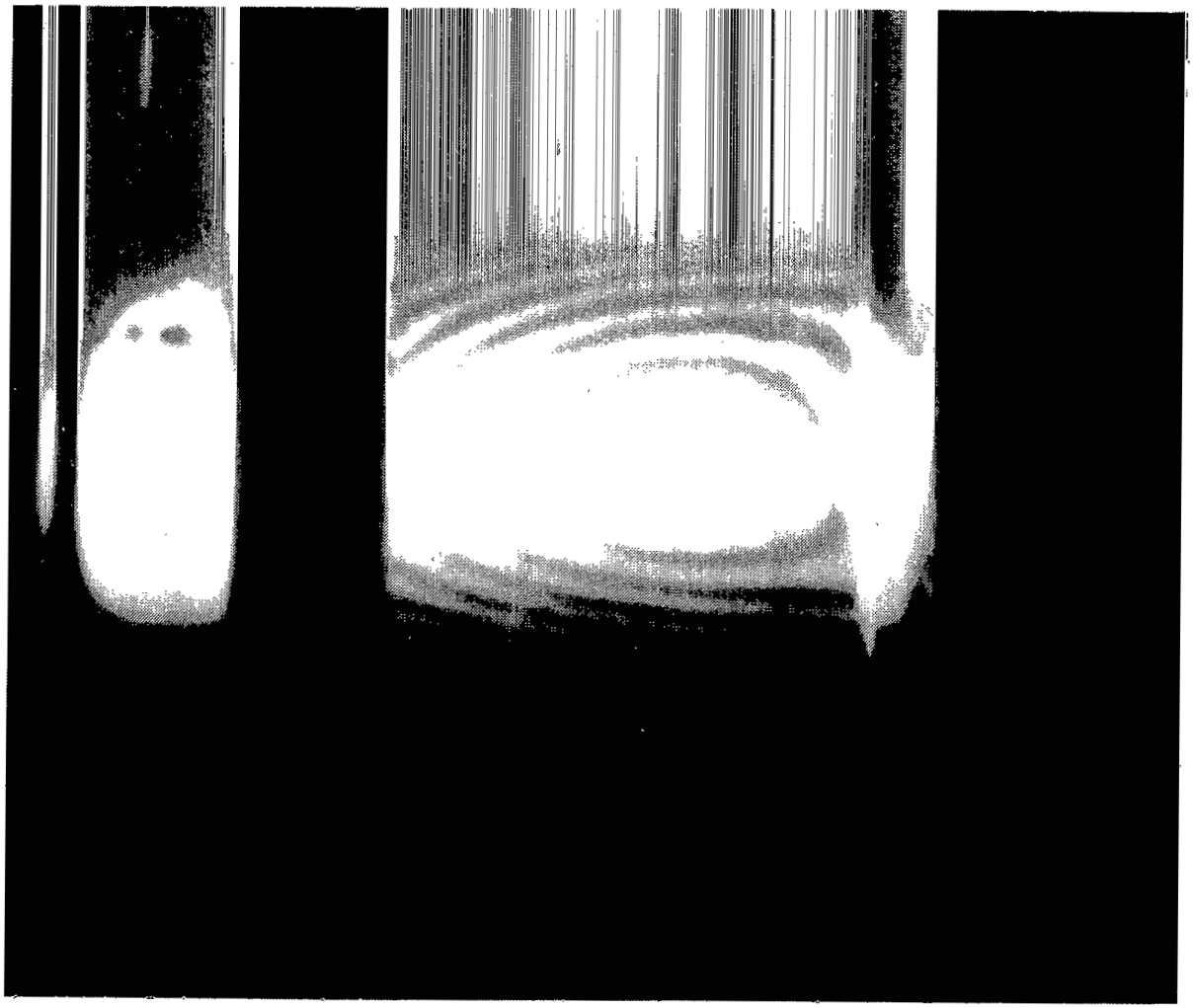

L-80-249

(c) $P/P_{ult} = 1.0$.

Figure 27.- Continued.

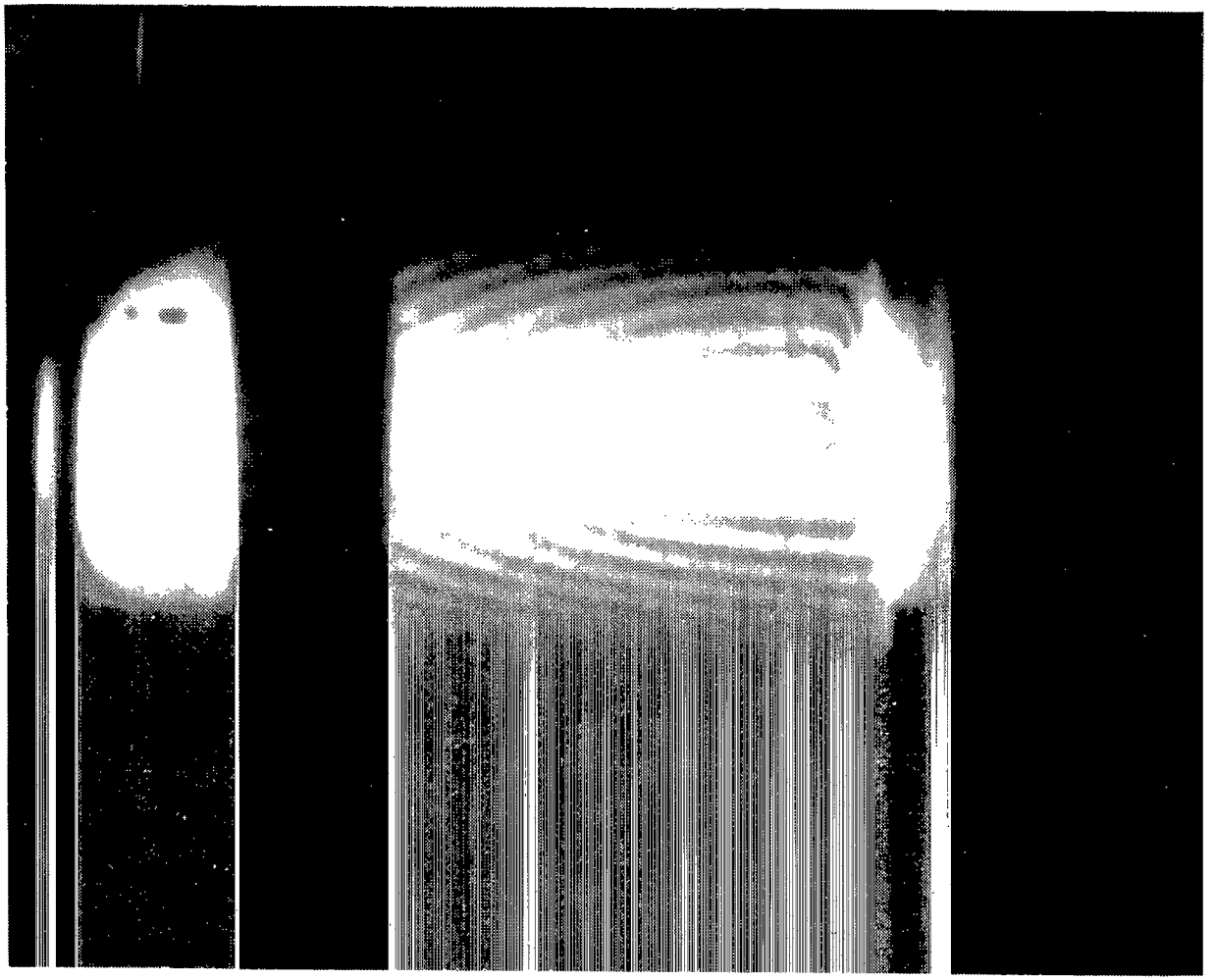

L-80-250

(d) P/P_{ult} = 0.99 (post buckling).

Figure 27.- Concluded.

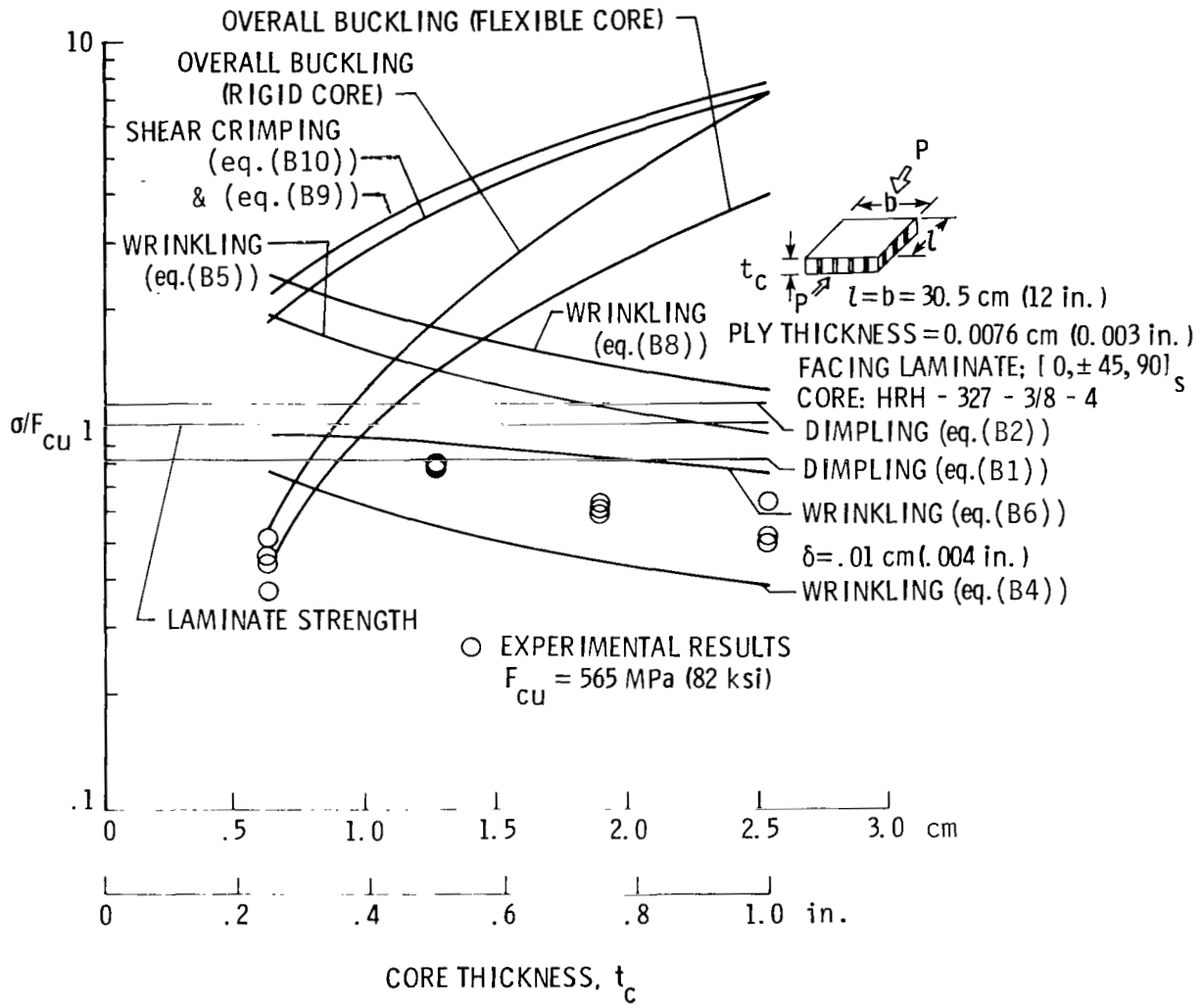

Figure 28.- Comparison of analytical and experimental results.

(a) Intracellular buckling.

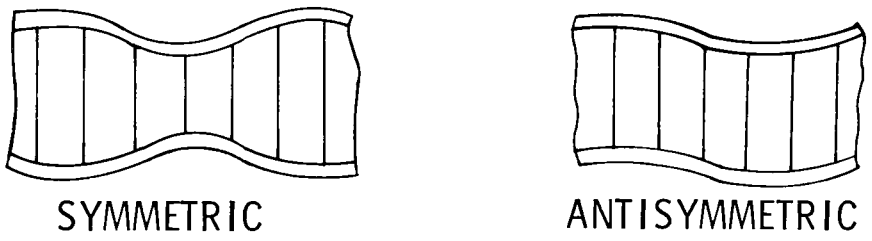

(b) Face wrinkling.

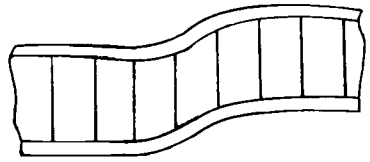

(c) Shear crimping.

Figure 29.- Local instability modes of failure of honeycomb sandwich structures.

1. Report No.	2. Government Accession No.	3. Recipient's Catalog No.
NASA TP-1785		

4. Title and Subtitle

TESTS OF GRAPHITE/POLYIMIDE SANDWICH PANELS IN UNIAXIAL EDGEWISE COMPRESSION

5. Report Date: December 1980

6. Performing Organization Code: 506-53-63-04

7. Author(s)

Charles J. Camarda

8. Performing Organization Report No.: L-13998

9. Performing Organization Name and Address

NASA Langley Research Center
Hampton, VA 23665

10. Work Unit No.

11. Contract or Grant No.

12. Sponsoring Agency Name and Address

National Aeronautics and Space Administration
Washington, DC 20546

13. Type of Report and Period Covered: Technical Paper

14. Sponsoring Agency Code

15. Supplementary Notes

16. Abstract

An experimental and analytical investigation has been made of the local and general buckling behavior of graphite/polimide (Gr/PI sandwich panels simply supported along all four edges and loaded in uniaxial edgewise compression. Material properties of sandwich panel constituents (adhesive and facings) were determined from flatwise-tension and sandwich-beam-flexure tests. Buckling specimens were 30.5 by 33 cm (12 by 13 in.), had quasi-isotropic, symmetric facings ($[0,\pm45,90]_s$), and a glass/polyimide honeycomb core (HRH-327®-3/8-4). Core thicknesses were varied (0.635, 1.27, 1.91, and 2.54 cm (0.25, 0.50, 0.75, and 1.00 in.)) and three panels of each thickness were tested at room temperature to investigate failure modes and corresponding buckling loads. Specimens 0.635 cm (0.25 in.) thick failed by overall buckling at loads close to the analytically predicted buckling load; all other panels failed by face wrinkling. Results of the wrinkling tests indicated that several buckling formulas were unconservative and therefore not suitable for design purposes; a recommended wrinkling equation is presented.

17. Key Words (Suggested by Author(s))	18. Distribution Statement
Buckling tests Composite materials Sandwich panels Graphite/polyimide High temperature tests	Unclassified - Unlimited Subject Category 24

19. Security Classif. (of this report)	20. Security Classif. (of this page)	21. No. of Pages	22. Price
Unclassified	Unclassified	76	A05

For sale by the National Technical Information Service, Springfield, Virginia 22161

NASA-Langley, 1980

6 1 1U,C, 011281 S00903DS
DEPT OF THE AIR FORCE
AF WEAPONS LABORATORY
ATTN: TECHNICAL LIBRARY (SUL)
KIRTLAND AFB NM 87117